NTNU – Trondheim
Norwegian University of
Science and Technology

Validation of material model for polypropylene (PP)

Kjetil Vange

Civil and Environmental Engineering
Submission date: June 2012
Supervisor: Arild Holm Clausen, KT
Co-supervisor: Marius Andersen, KT

Norwegian University of Science and Technology
Department of Structural Engineering

Department of Structural Engineering
Faculty of Engineering Science and Technology
NTNU- Norwegian University of Science and Technology

ACCESSIBILITY

OPEN

MASTER THESIS 2012

SUBJECT AREA:	DATE:	NO. OF PAGES:
Polymer engineering	7.6.2012	

TITLE:

Validation of material model for polypropylene (PP)
Validering av materialmodell for polypropylen (PP)

BY:

Kjetil Vange

SUMMARY:
Polymers are the up and coming engineering material. The number of possible applications is increasing fast and so is the need for a good polymer material model. The scientists at SIMLab at NTNU have developed such a material model. In this thesis is the material model calibrated to represent an impact modified polypropylene used by Toyota.

The validation started with the calibration. A review of the theoretical background of the material model and a detailed explanation of the calibration procedure are given to describe the derivation of the calibrated material model. The model is then applied in FE-simulations of the material tests and the two validation tests. The first validation test is a quasi-static tension test using a specimen with a centric hole. This test resembles the material tests but the centric hole makes the load response slightly more complex. The other test is an impact test using a drop tower. This test validates the material models ability to represent dynamic problems and also tests the representation of the strain rate dependency.

The material model proves that it is capable of representing all the tests in this thesis quite accurately.

RESPONSIBLE TEACHER: Professor Arild H. Clausen

SUPERVISOR(S) Marius Andersen, Anne Serine Ognedal

CARRIED OUT AT: SIMLab, NTNU

NORGES TEKNISK-NATURVITENSKAPELIGE UNIVERSITET
INSTITUTT FOR KONSTRUKSJONSTEKNIKK

MASTEROPPGAVE 2012

Kjetil Vange

Validation of material model for polypropylene (PP)

(Validering av materialmodell for polypropylen (PP))

As a part of the development of the finite element method, significant effort has been devoted to propose new material models which are able to represent the material behaviour at different conditions. Relevant parameters involve strain level, strain rate, temperature, and the material at hand may also exhibit anisotropy, viscoelasticity etc. Today, material models for metals are in general more accurate than models for e.g. polymers. This is a general tendency for all non-linear finite element programs, including Abaqus and LS-DYNA. SIMLab is involved in the development of improved models for thermoplastics. A model applicable for ductile polymers was ready in 2010, and the research work continues with other classes of models.

All new models need to be validated against experimental benchmark tests for different types of polymers. Validation involves also calibration, requiring material tests on the material at hand. This master thesis is concerned with a PP material provided by Toyota. The selected benchmark tests are tension of a plate with a hole and impact tests on small plates. Subsequently, the test results are to be compared with numerical predictions applying the material model for ductile thermoplastics.

Some keywords for activities related to this master thesis project are:

- Literature: Polymers in general, relevant test results, material models.
- Experimental tests: Material and component tests. Presentation of test results.
- Calibration: Identify the coefficients of the material model.
- Numerical modelling: Simulation of experimental tests. Evaluation of the model.

The candidate may agree with the supervisors to pay particular attention to specific parts of the investigation, or include other aspects than those already mentioned.

The thesis is to be organized as a research report, recognising the guidelines provided by Department of Structural Engineering.

Supervisors: Arild H. Clausen, Marius Andersen and Anne Serine Ognedal

The report is to be handed in at Department of Structural Engineering not later than 11 June 2012.

NTNU, 18 January 2012

Arild H. Clausen
faglærer

Sammendrag

Polymerer blir mer og mer brukt. Antallet bruksområder øker stadig og det samme gjør behovet for en numerisk materialmodell som kan representere polymerer. Forskerne ved SIMLab på NTNU har utviklet en materialmodell beregnet for polymerer. I denne masteroppgaven er materialmodellen kalibrert til å representere oppførselen til en utgave av polymeret polypropylen som er tilpasset bruk i støtfangere på Toyotas bilmodeller.

Valideringen startet med kalibreringen. Kalibreringen er utførlig beskrevet i oppgaven. Det vil si at den inneholder en beskrivelse av teorien bak materialmodellen og at den går gjennom kalibreringsprosedyren punkt for punkt. Deretter er den kalibrerte materialmodellen benyttet i elementmetodesimuleringer av materialtestene og av de to valideringstestene. Den første valideringstesten går ut på å strekke en plate med et sentrisk hull. Denne testen er mye lik materialtestene, men hullet bidrar til at lastresponsen blir mer kompleks. Den andre testen tar i bruk et fallverk og er med andre ord et dynamisk kontaktproblem som involverer store tøyningshastigheter. Med disse to testene får man testet materialmodellens evne til å representere ulike responser.

Resultatene viser at materialmodellen evner å representere testene svært tilfredsstillende.

Acknowledgements

I would like to express my gratitude to Professor Arild H. Clausen for his excellent guidance throughout the process of writing this thesis. I would also like to thank co-supervisor PhD student Marius Andersen and PhD student Anne Serine Ognedal for their contributions.

Tonje Hegni, Kristin Sælen and Torgrim Østen wrote similar theses. The meetings and discussions with this group have been decisive for the result.

A special thanks also goes to my fellow students for providing good input and feedback.

Trondheim, 7.6.2012

Contents

List of Figures

List of Tables

Chapter 1

Introduction

Polymers are the up and coming engineering material. The number of possible applications is increasing fast and so is the need for a good polymer material model. It is in the light of this that the Structural Impact Laboratory (SIMLab) at NTNU has developed a polymer material model for use in finite element simulations. This thesis will validate a calibrated version of this material model.

Polymers are versatile. This is because the polymer chains can be easily modified to achieve numerous properties. In addition is the mass density of polymers much lower than that of more classical engineering materials such as steel and aluminium. This makes polymers particularly interesting for the industry producing light weight structures such as cars and aeroplanes. Another reason for the interest from the automobile industry, is that polymers can be given good shock absorbing abilities. The material treated in this thesis is a version of such a polymer, namely a polypropylene (PP) optimized for use in car bumpers.

The objective of this thesis is to validate a calibrated version of the polymer material model. The material used for calibrating the material model is the PP mentioned above. The thesis starts with presenting some general theory regarding polymers. The next chapter then describes the material tests that make up the basis for the calibration. The next chapter then treats the calibration procedure in detail and derives the calibrated material model. The model is then applied to simulations of the material tests before being applied to the simulations of the validation tests. Two validation tests are carried out. An important point when choosing validation tests is to find tests that validate a wide spectre of properties. The first test chosen for this thesis is a tension test using a plate with a centric hole. This test is similar to the tests carried out when calibrating the material model, but the centric hole makes the load response a bit more complex. The

second test is an impact test using a machine known as drop tower. This is a test where a steel spear hits a plate with a given impact energy. The load response is dynamic and involves high strain rates. Through these two tests are both the quasi-static and the dynamic properties of the material model validated. All the analyses are carried out using the finite element code LS-DYNA.

The chapters are split into sections explaining the different parts of the process. In the chapters presenting results is the last section used to compare and discuss the presented result. The last chapter recapitulate the thesis in a conclusion and present suggestions for further work.

Chapter 2

Theory

The word polymer comes from Greek and means many particles [11]. And polymers are just that, chains of carbon based molecules packed tightly together. Polymers are becoming more and more important as an engineering material. It is a low-weight material that can be modified to achieve numerous properties. This thesis examines a version of the semi-crystalline thermoplast polypropylene, used by Toyota.

The three main categories of polymers are thermoplastics (amorphous and semi-crystalline), elastomers and duromers [12]. The main difference is the degree of cross-linking of the polymer chains, where the duromers have a high degree of cross linking, the elastomers a bit less and the thermoplasts none at all. The degree of cross-linking is important to the mechanical behaviour, which means that the three categories have quite different mechanical properties. Since the material treated in this thesis is a thermoplast, the chapter will only treat thermoplastics.

2.1 General chemical structure

The chemical structure of polymers differs quite a lot from the one found in many other engineering materials. The basic structure is an organic molecule, a monomer. A monomer can in its simplest form be an alkene or alkyne, where the double bond or triple bond is broken, making room for a connection to a neighbouring molecule on each side (see Figure 2.1). The process where these monomers connect and form a chain is called polymerization. When the monomer shown in Figure 2.1 is polymerized it becomes polyethylene, one of the most widely used polymers. This process is the process all polymers go through. By changing

the structure of the monomer or by mixing different monomers, a wide variety of characteristics can be achieved. A relevant example is to substitute one of the hydrogen atoms in the ethene monomer with a methyl group (CH_3). This results in th propylene monomer, which polymerizes to polypropylene (Figure 2.4).

The density of the polymer chains defines amorphous and crystalline regions. In crystalline regions the chains are more tightly packed than in amorphous regions. A short bond is stronger than a long bond, which means that the crystalline regions are stronger than the amorphous regions. This principle is especially important when dealing with semi-crystalline thermoplastic.

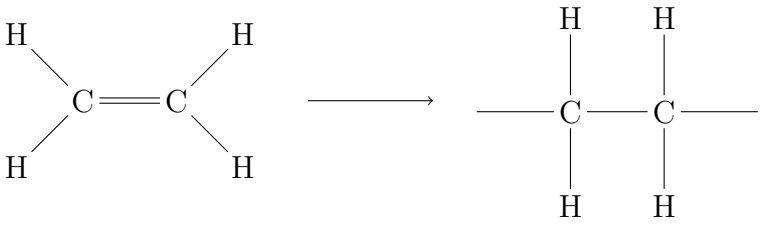

Figure 2.1: Connection between an independent molecule and a monomer

2.2 Mechanical properties

A certain combination of mechanical properties is often the objective when making a new or improving a polymer. The properties are easily modified, making it possible for a material to fit a certain application exactly. Thanks to this polymers have become preferable in many applications where more known engineering materials as steel and aluminium were used earlier.

The critical temperatures for polymers are often close to the service temperatures. The values of the critical temperatures also differ considerably from polymer to polymer. The critical temperature points are the glass temperature, T_g, and the melting temperature,T_m. None of them are exact temperatures, but rather a middle of a narrow range of temperatures. T_g applies only to the amorphous regions of the material. As the temperature rises the internal energy and the specific volume increases. When passing T_g the specific volume suddenly start to increase more than before. Making more room for the relative motion of the polymer chains. This affects the material stiffness, making it softer. Had it not been for the entangled structure of the polymer chains, the material would have lost all structure at this point. As the temperature closes T_m the volume continues to increase and the material becomes softer and softer. At the melting temperature the energy of the covalent bonds in the polymer chains is reached, and the bonds break. Since the

chains are dissolved, the material now becomes uniformly amorphous and liquid like. And it has lost all of its stiffness and usability. Most polymers are, however, manufactured so that they do not operate close to T_m.

Used at service temperature, thermoplasts have a similar material response as more common engineering materials like steel and concrete. The response is divided into an elastic and a plastic part. The transition between the two is often hard to identify, because it is gradual and not well defined. Both the elastic and the plastic response is time dependent, i.e. the material is viscoelastic and viscoplastic. This is easily seen in a load response diagram, where it is observed that the initial stiffness and the peak load are proportional to the strain rate. The importance of other time effects such as relaxation is proportional with the loading time, i.e. relaxation effects are more significant when the load works over a longer time span.

The bonds between the monomers in a polymer chain are strong covalent bonds, which make the chains a stable and strong chemical structure. The chains are connected to each other by Van der Waals bonds, dipole bonds or hydrogen bonds. These are much weaker than the internal covalent bonds of the molecule chains. This means that more or less all initial elastic deformation takes place in these weaker intermolecular bonds. The elasticity is split into two mechanisms, energy and entropy elasticity. The energy elasticity describes the reaction in the bonds between the chain molecules, and applies to both the amorphous and the crystalline regions of the material. When the polymer is exposed to loading, the bonds are elongated. Upon unloading the bonds retract to their initial positions of a lower energy level, hence energy elasticity. By returning to these positions the material also returns to its initial configuration. This behaviour is dominating when the material operates below T_g. As the operating temperature gets closer to T_g, the entropy elasticity becomes more and more important. It should be noted that because the entropy elasticity only applies to the amorphous regions, the influence of this mechanism will depend on the degree of polymerization. But when it occurs it is a more complex process than the energy elasticity. In order to fully understand the entropy elasticity one have to understand the concept of entropy. It is not within the scope of this thesis to explain entropy to its full extent. A simplified model is, however, to consider the entanglement of the polymer chains (not to be confused with cross-linking). In its unloaded form the polymer chains are entangled in an intricate mesh. When subjected to loading, the chains are straightened between the entanglement points allowing the material to deform. When unloaded the straightened chains return to a more entangled configuration, through this increasing the level of disorder, which is known as a simple explanation of entropy.

When the deformation potential of the elastic mechanisms are fully exploited the

material starts to deform plastically. Since all the weak bonds are deformed to their maximum, the only possibilities are a fracture or plastic deformation. The outcome strongly depends on the temperature. At a temperature far below T_g the material will fracture without deforming plastically. The closer the temperature gets to T_g the more plastic deformation can be endured by the material. This plastic deformation starts with the breakage of the intermolecular bonds between the polymer chains. This allows the chains to slide relative to each other. The only thing holding the chains together now is the intricate pattern in which they are packed. In order to move, the polymer chain must be able to slide pass its neighbours without being obstructed. Very often the chains obstruct each other, thus increasing the energy needed for further deformation. When the chains are finally able to slide, the plastic deformation has started. This deformation produces heat. If this heat is not able to escape it will speed up the plastic deformation by increasing the volume between the chains. When the yield stress is reached a neck will occur. As the necking process goes further and further the chains in the neck become more and more oriented in the direction of the load. The closer the chains are oriented to the load direction, the larger is the share of the load taken by the covalent bonds in the polymer chains. When the load is fully transferred to the covalent bonds, the strength increases significantly. This is seen as an increase in stress, i.e. hardening, in the stress-strain diagram. The increase is so significant that the neck becomes stronger than its surrounding material. The result is a neck that propagates along the material. In principle is this process able to continue until the neck meets a change in geometry that makes the surrounding material stronger. But a fracture will often occur prior to this due to the accumulation of imperfections. The reduction of the cross-section is also making the neck more exposed for such a fracture.

The mechanisms explained in the paragraph above take place in the amorphous regions of the material. For a semi-crystalline polymer the general behaviour is similar but the deformation is split into the deformation of the amorphous regions and the deformation of the crystalline regions (see Figure 2.2). The amorphous regions are the first do deform (Figure 2.2b). Then the orientation of the crystalline regions is shifted in the direction of the load (Figure 2.2c). When the material deforms further, the crystalline blocks split into smaller blocks (Figure 2.2d and 2.2e). When the deformation has come to the stage shown in Figure 2.2d and 2.2e a neck has occurred. The semi-crystalline material follows the same necking mechanism as explained for the amorphous material. It is worth mentioning that semi-crystalline polymers are more affected by impurities and imperfections than amorphous polymers. This is because the impurities and imperfections are pushed out of the regions that crystallize, locating them right outside the crystalline regions. This makes the transition between the amorphous and the crystalline regions a

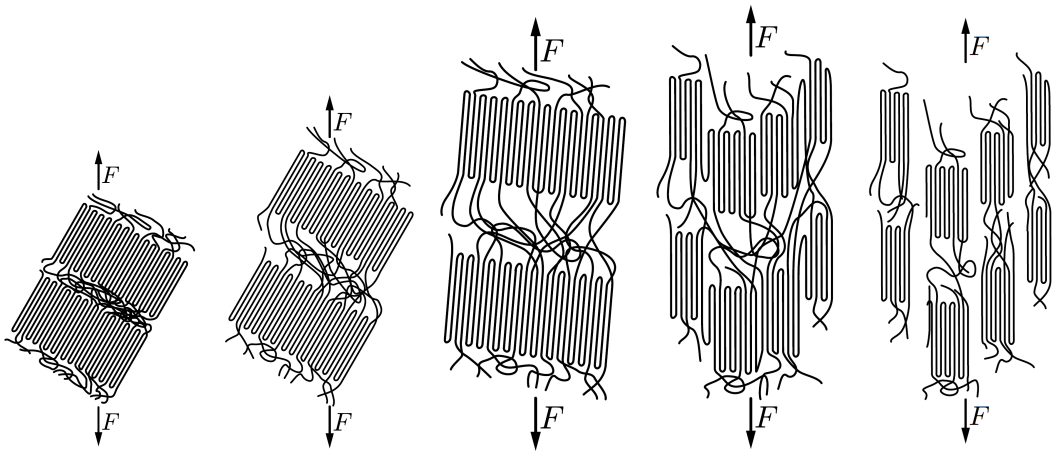

(a) Initial state (b) Deformation of amorphous regions (c) Changing the orentation of the crystalline regions (d) Splitting into blocks (e) Separated blocks

Figure 2.2: Plastic deformation in semi-crystalline polymers, after [12]

weak spot in the material.

The compression response of polymers is much less investigated than the tension response and this thesis will not try to reach any new conclusions on the matter. Some general considerations are that; as with tension, the response differs from polymer to polymer. Some polymers have a quite similar load response in tension and compression, distinguished mainly by a higher yield stress in compression than in tension. Others have a quite different response, e.g. softening in tension but not in compression. A higher yield stress in compression than in tension and also hardening effects are, however, seen in the load response of most polymers. A mechanism that is known to occur in compression, causing initially softening and later hardening, is the formation of shear bands. In this mechanism the response is determined by the polymer chain's response to the shear forces set up by the axial loading [12].

2.3 Introduction to the SIMlab polymer material model

Material models for steel and aluminium have been developed and perfected for many years. The same has not been the case for polymers, and especially not for thermoplastics. The model applied in this thesis is part of a developing process

lead by the scientists at SIMLab. SIMLab is a Centre for Research-based Innovation (SFI) located at the Department for Structural Engineering at the Norwegian University of Science and Technology (NTNU). SIMLab is in the process of developing a comprehensive material model for thermoplastics. The objective is a material model that can satisfactory describe the special properties of a wide range of thermoplastic polymers [1]. In addition the SIMlab group has focused on making the model attractive to the industry, i.e. making it fairly simple to use. This is mainly achieved by carefully examining each parameter of the material model. In other words; a property that has little influence on the response, but demands a complex calibration is left out. Next the chosen properties are incorporated into an easy-to-follow calibration procedure. In this chapter the model will just be briefly introduced, the main study is found in Chapter 4.

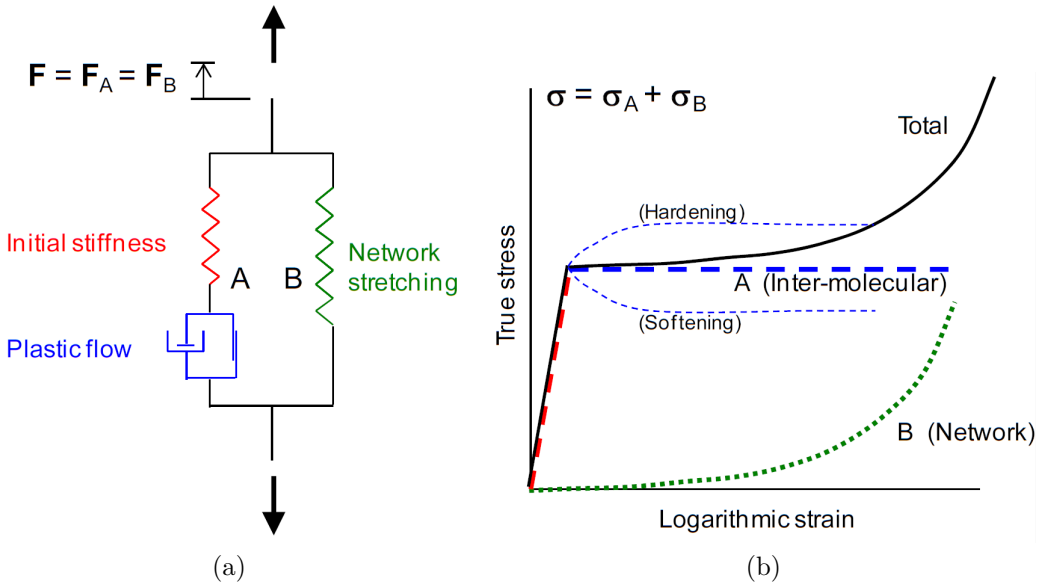

Figure 2.3: The rheological model and the resulting stress-strain diagram (after [2])

Figure 2.3 shows a graphical representation of the material model. It is split into two parts, Part A and Part B, which have the same deformation gradient $\mathbf{F} = \mathbf{F}_A = \mathbf{F}_B$. Part A describes the *inter*molecular resistance of the material, i.e. the stretching of the bonds in the molecules. First the weak and then the strong, as explained in the previous section. When the yield stress is reached Part A goes into a state of plastic flow, which is seen in Figure 2.3b as plastic deformation without increase of stress. The rheological model describes these mechanisms with a Neo-Hookean spring and a plastic flow element coupled in series. The plastic flow element consists of a friction element and a viscous damper coupled in parallel (see Figure 2.3a). Part B describes the *intra*molecular resistance, which is the

1	E_0	Young's modulus. Often given by manufacturer
2	ν_0	Poisson's ratio. Determined from the transverse strains
3	σ_T	The yield stress at a fictitious "zero strain rate" (detailed explanation in Chapter 4)
4	σ_s	The saturation stress at a fictitious "zero strain rate" (detailed explanation in Chapter 4). A parameter used to describe the softening.
5	H	A rate independent hardening parameter
6	α	The ratio between the yield stress in compression and tension
7	β	A parameter controlling the plastic dilatation. • $\beta \geq 1$ • $\beta = 1.0$ = Isochoric (volume preserving) conditions
8	$\dot{\varepsilon}_{0A}$	The reference strain rate
9	C	A strain rate sensitivity parameter
10	C_R	Initial elastic modulus
11	λ_L	Locking stretch

Table 2.1: The eleven coefficients of the material model. The colour coding shows the relation to the rheological model in Figure 2.3a

resistance set up by the adhesion and entanglement of the polymer chains, i.e. the mechanism of polymer chains sliding along each other and the mechanism in which polymer chains are stretched between entanglement points. This corresponds to the entropy driven mechanisms in the polymer (described in more detail in the previous section). The rheological model describes this with a hyperelastic spring which is controlled by an initial stiffness and a locking stretch. It should also be noticed that the two parts can be superpositioned, making the Cauchy stress tensor equal to:

$$\boldsymbol{\sigma} = \boldsymbol{\sigma_A} + \boldsymbol{\sigma_B} \tag{2.1}$$

Experiments show that polymers dilate during plastic flow [9]. This means that it is possible to describe the plastic flow using a pressure-dependent yield criterion and an associated flow rule. A typical choice for a polymer material is Raghava's yield criterion (details in Chapter 4). It is, however, shown that this assumption predicts unrealistically large volumetric strains (too much dilatation). A non-associative flow rule is thus needed. The solution is to apply a modified Raghava criterion where the parameter β is introduced in order to control the dilatation (Table 2.1, row 7).

The material model is implemented as an user-defined material in LS-DYNA[6] and works for solid and shell elements. The model assumes isothermal and isotropic conditions and does not include any fracture criterion [1].

2.4 Polypropylene

The material treated in this thesis is a polypropylene used by Toyota. Toyota has given limited information about the chemical structure of the material. They have stated that it is injection moulded, is to be used for bumper applications, that the talc filling is 10-15% and that the elastomer content is unknown. On the basis of this limited knowledge, the considerations done in this section are quite general, and based on the chemical structure found in polypropylene versions with similar specifications.

Polypropylene (PP) is also known as polypropene. The latter name reveals that the base molecule, or monomer, of polypropylene is propene with chemical formula C_3H_6 (Figure 2.4). Propene is propane based and therefore part of the second most basic group of mers, only beaten by the ethane based mers.

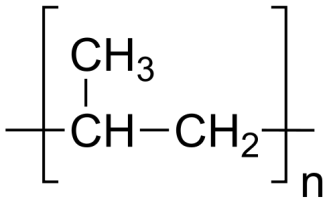

Figure 2.4: The monomer of polypropylene

The methyl group seen in Figure 2.4 can be placed in different order around the backbone of the polymer chain. This is referred to as the tacticity of the polymer. PP is in most cases isotactic, meaning that the methyl group is placed on the same side of the backbone (see Figure 2.5a). Other possible tacticities for PP are syndiotactic (Figure 2.5b), where the side group alternates from side to side regularly, and atactic, where the side group is placed randomly (not shown). The tacticity is closely linked to the mechanical properties because it directly affects the polymer's ability to crystallize. In order to crystallize the material must be either iso- or syndiotactic. Since the PP in question is semi-crystalline, it is most probably isotactic.

Polypropylene is separated into three different categories: Homopolymer, consisting of only propylene based molecules. Random copolymer, a propylene-ethylene

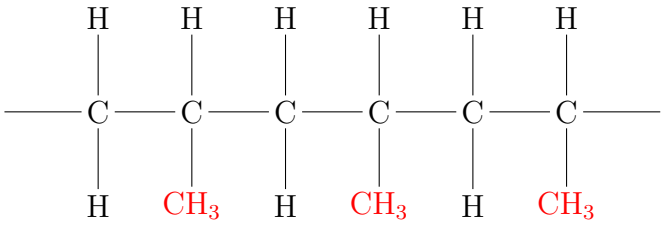

(a) Isotactic polymer structure

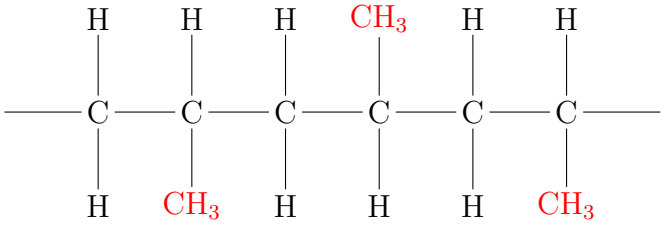

(b) Syndiotactic polymer structure

Figure 2.5: Two of the possible tacticities of PP

copolymer containing mainly propylene. And heterophasic copolymer, also referred to as high-impact PP or impact-modified PP. The latter is in most cases based on a homopolymer blended with an ethylene-propylene random copolymer (EPR) and block copolymers of different sequence lengths. For exterior use it is normal to add talc to stabilize the thermal and mechanical properties [3]. Given the information about the material (see the introduction to the section), it is reasonable to assume that the material at hand has a similar chemical structure as the heterophasic copolymer.

The material is injection moulded. The process is shown in Figure 2.6. First the plastic granulates are put into the cylinder. The granulates melt in the cylinder due to the heat produced by the heaters and the friction that occurs when the granulate is forced ahead by the screw. When a dose is ready for injection in the end of the cylinder, the melt is injected into the mould. The melt cools in the mould and is then ejected. Some of the advantages of injection moulding is low unit cost, high production rate and the ability to produce complex geometries. A main disadvantage is that the machine is very expensive [3].

The most critical part of the injection moulding process is called the holding pressure stage. In this stage the molten material is already injected into the mould. As it cools, the volume decreases (this especially applies to crystalline and semi-crystalline polymers). Since the mould is still pressurized the reduction is compensated by more melt from the cylinder, thus filling the mould completely. The applied holding pressure directly affects the properties of the finished product.

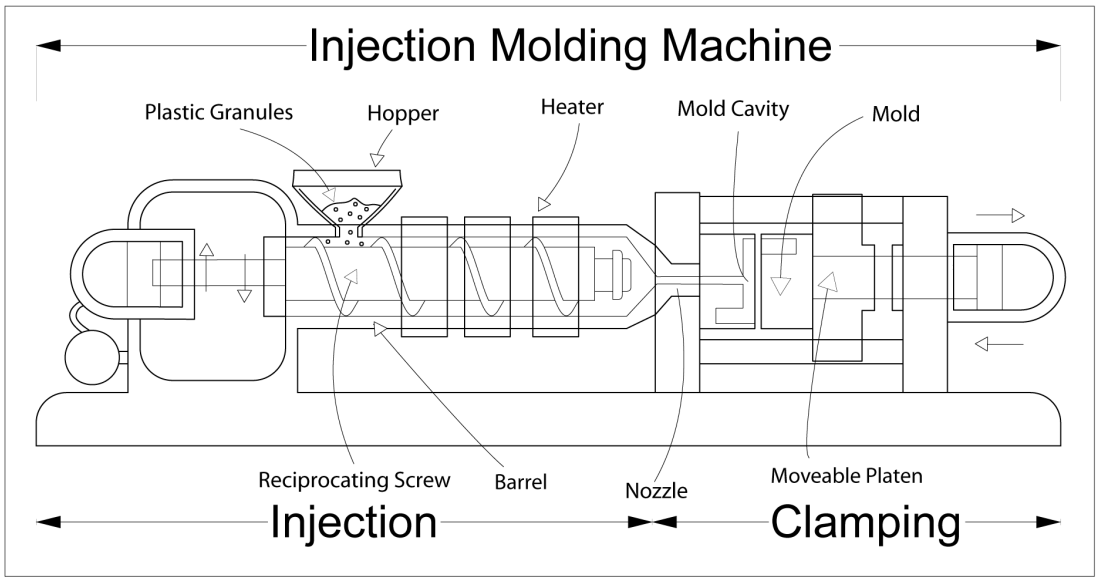

Figure 2.6: An injection moulding machine (Created by Brendan Rockey, University of Alberta Industrial Design, for a Wikipedia article about injection moulding)

The pressure must therefore be carefully adjusted so that the wanted properties are achieved and unwanted imperfections are avoided. In addition the material properties depend on how fast the melt is cooled. This again depends on the environment in the mould and the temperature of the melt that enters the mould.

The injection moulding process may leave some characteristics in the finished material. Whether this happens or not depends on the injected material, the mould geometry and the mould environment (as explained in the previous paragraph). The material at and closest to the surface is often subjected to very high shear rates and rapid cooling. This leads to a highly oriented and low-crystallinity microstructure which can be observed as a ”skin” covering the material. This skin-like structure is easily observed on the PP treated in this thesis (see Figure 3.4). The shear effects that occur during the injection process also lead to a orientation of the material in the flow direction, i.e. the material has an anisotropic structure and will have a direction dependent load response [3].

Chapter 3

Material tests

A total of 17 calibration tests were carried out. 14 of them were tension tests and 3 were in compression. The results of these tests are used to find many central material parameters needed for the calibration such as Young's modulus, the yield stress in tension and compression and the strain rate dependency. The machine used was a Dartec M1000 RK with a 20 kN load cell linked to an Instron controller. A camera was rigged in order to be able to use digital image correlation (DIC) in the post-processing. The respective instrument rigs will be commented in more detail in later sections. All tests were done at room temperature, which was somewhere between $22 - 25\,^{\circ}\mathrm{C}$.

The specimens were machined from two different rectangular plates into the geometry shown in Figure 3.2a. Of the 14 tension tests, 3 were taken from the transversal direction of the second plate. The rest were machined from the longitudinal direction and from both plates. Since the plates were only about 3.1 millimetres thick they were used with their original thickness. Before a specimen was cleared for testing the cross-section was measured on three different places along the gauge-length (the initial dimensions for each test are found in Appendix A) and then painted as shown in Figure 3.1. In order to eliminate any irregular specimens and minimize the scatter, each test was run twice. This meant that if two tests at the same configuration gave similar results, the results were declared valid. The tests were deformation-controlled, i.e. the test machine was set to a certain deformation speed, measured in mm/s. This speed had to be calculated so that the wanted strain rate was achieved in the specimen. The strain rates used in the calibration tests are $\dot{\varepsilon} = 10^{-3}\ \mathrm{s}^{-1}$, $\dot{\varepsilon} = 10^{-2}\ \mathrm{s}^{-1}$ and $\dot{\varepsilon} = 10^{-1}\ \mathrm{s}^{-1}$.

The test specimens had to be pre-treated in a special way. A prepared and tested specimen can be seen in Figure 3.1. The speckled pattern consists of an undercoat

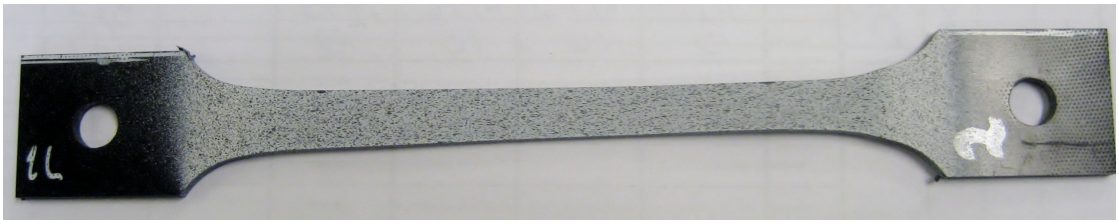

Figure 3.1: Painted specimen after testing

of white spray paint randomly speckled with black spray paint. To ensure that the paint would not become dry and crack up during the test, the paint was applied shortly before testing. The camera rig then photographed the specimens at a rate adapted to the strain rate. The rates used were 0.1 Hz for the slowest tests, 1 Hz for the middle rate and 10 Hz for the highest rate. The pattern created by the two layers of paint could then be read by a image correlation program, in this case a program named 7D. The program puts the pictures in succession, sorted by name. Then the user places a mesh on the images to mark the area from where information should be gathered. The program then uses the speckled pattern to correlate the physical deformation with the deformation shown in the pictures. By treating these correlated data the program can produce matrices containing different types of deformation data, e.g. deformations in x- or y-direction or maximum and minimum logarithmic strain. The latter matrices combined with the force data from the Instron controller were used to create the stress-strain diagrams shown in this chapter. In order to use the matrices from 7D they had to exported. This can be done in either text (.txt) format or in a Matlab format named .mat. Since Matlab was used for post-processing, the logarithmic strain matrices were exported in .mat format. The .mat-file contains a matrix for every picture taken by the camera. The dimension of the matrix is defined by the mesh that was placed by the user prior to the correlation process. In the meshes used in this chapter, the columns are placed along the transversal direction of the specimen and the rows along the longitudinal, i.e. a cross-section along the longitudinal axis of the specimen is described by a row. The strain was found to be constant over the cross-section. The mean strain value in each row can thus be used. Another reason for using mean values is that numerical noise that occur in the correlation process is reduced. By finding the row with the highest mean strain value, the cross-section of maximal deformation was located. The mean value of the longitudinal and transversal strain in this row was then gathered from each matrix. The final result being two vectors, one for the longitudinal strain and one for the transversal strain, showing the increase of strain through the deformation history(the MatLab scripts are found in Appendix B).

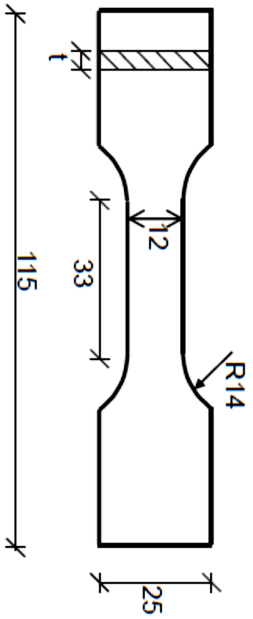

(a) The tension specimen geometry

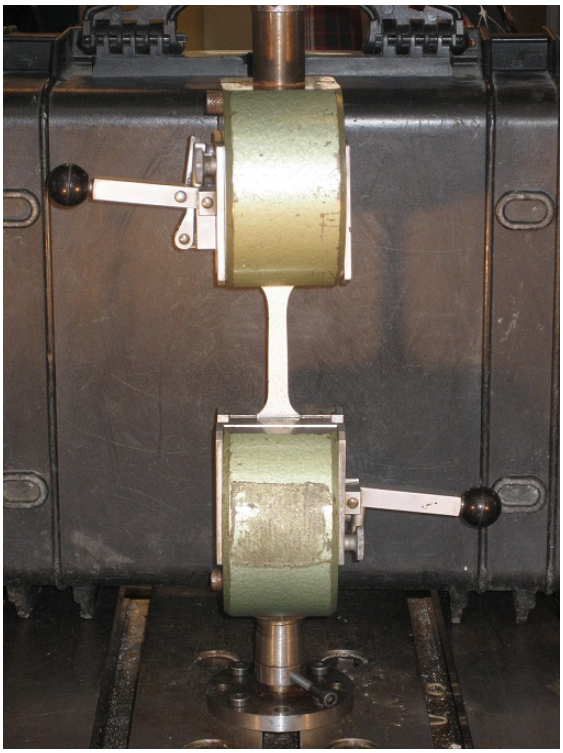

(b) The tension specimen mounted in the rig

Figure 3.2: Tension specimen geometry and tension test rig

3.1 Uniaxial tension tests

The uniaxial tension tests were the first ones to be executed. The specimen geometry is shown in detail in Figure 3.2a. After the specimens had been prepared as described earlier they were placed in the rig as shown in Figure 3.2b. Because the strain rate dependency of polymers is much greater than for most metals the tests were run at three different strain rates, ranging from $\dot{\varepsilon} = 10^{-3}$ s^{-1} to $\dot{\varepsilon} = 10^{-1}$ s^{-1}. The tests are labelled on the form "Tension (T)/Compression (C)""Test number" - "Direction of test""Plate number", i.e. the second tension test taken from the longitudinal direction of plate one is named "T2-L1".

The stress-strain relations shown in this section consist of true stress and logarithmic strain. To calculate the true stress the strain in all three material directions are needed. Earlier studies ([5], [7]) have, however, shown that the transversal strains are isotropic, i.e. if $\varepsilon_{longitudinal} = \varepsilon_x$ then $\varepsilon_y = \varepsilon_z$. This is also assumed in this thesis which yields the following expression for the stress;

$$\sigma_{True} = \frac{F}{A} = \frac{F}{A_0 \cdot exp(2\varepsilon_2)} \tag{3.1}$$

where F is the force logged by the Instron controller, A_0 is the cross-sectional area at t=0 and ε_2 the transversal strain. As explained in the opening paragraphs, the strain was read from the cross-section of maximal strain, the stress is thus calculated in this cross-section.

3.1.1 Low strain rate, $\dot{\varepsilon} = 10^{-3}$ s^{-1}

With the gauge length of 33 mm the deformation speed was 0.033 mm/s. This is close to a quasi static loading, and the tests had a duration of about 45 minutes. This strain rate is chosen as the reference strain rate for the calibration.

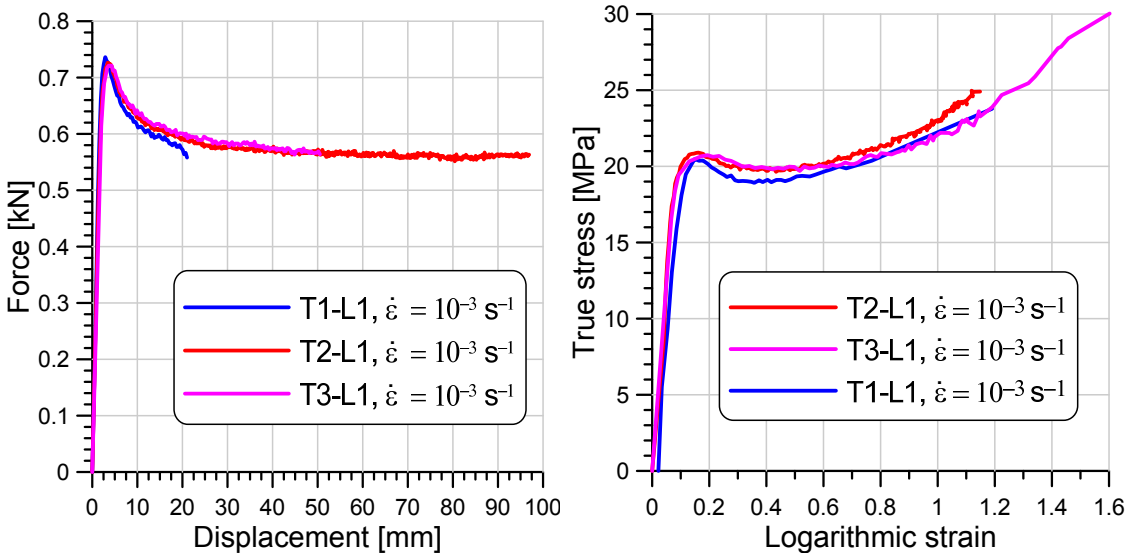

(a) Force vs displacement, $\dot{\varepsilon} = 10^{-3}$ s^{-1} (b) Stress vs strain, $\dot{\varepsilon} = 10^{-3}$ s^{-1}

Figure 3.3: Test results, $\dot{\varepsilon} = 10^{-3}$ s^{-1}

Figure 3.3 shows the results of the three tests made at this strain rate. The test T1-L1 failed the validity check and was rejected. Figure 3.3a shows that the polypropylene has a distinct peak load. Note also the low load capacity and high ductility compared to most other engineering materials.

Now looking at the stress-strain diagram in Figure 3.3b. It is seen that the material slightly softens before hardening is initiated. There is also a small difference in

the plastic response of the two tests. Test T3-L1 softens a bit more gradually than T2-L1 and also hardens somewhat less. Another difference between the two is that one of them developed a fracture and the other did not (T2-L1, see Figure 3.1). Exactly why this was the case is hard to point out exactly, but may be linked to the dispersion of imperfections in the specimens.

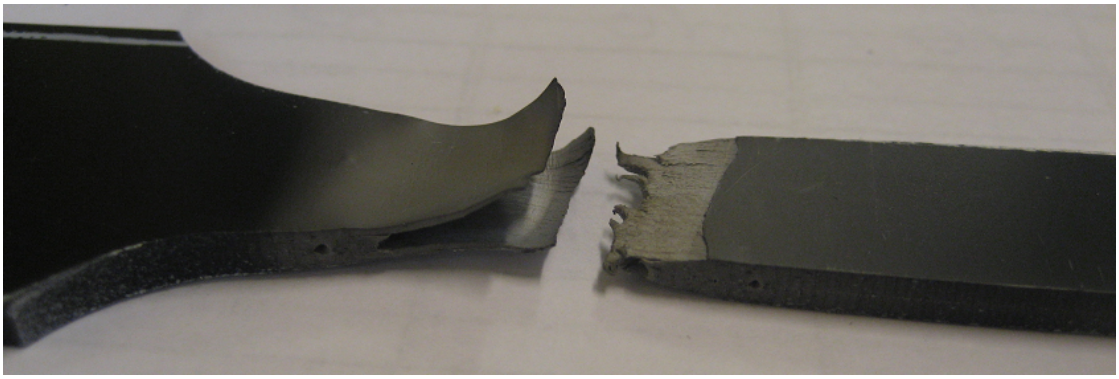

Figure 3.4: The external layer after fracture

In the fracture zone of test 3 (similar to the one in Figure 3.4) the external layer of the material is easily observed. It seems more elastic than the core material and deforms with the material until the core has completely fractured. Then it quickly breaks and folds, exposing the plastically deformed outer layer. This effect can also be observed at tests done at higher strain rates, but is most evident in these tests.

All in all the first test series did not bring many surprises. The validity check proved necessary through the rejection of test T1-L1. All the logging equipment also worked as expected, something it also did during the rest of the testing.

3.1.2 Average strain rate, $\dot{\varepsilon} = 10^{-2}$ s^{-1}

These tests provide the first possibility to observe the strain rate dependency. Since these tests have a much shorter duration than the previous, this is the strain rate used in the majority of the tests. In this series specimens from both plates and from both the longitudinal and the transverse direction are tested.

In Figure 3.5 a selection of diagrams can be seen. The test T8-L1 is similar to the ones tested at $\dot{\varepsilon} = 10^{-3}$ s^{-1}, only now with $\dot{\varepsilon} = 10^{-2}$ s^{-1}. T7-L2 is oriented in the same direction as T8-L1, but is taken from plate two. The tests at this strain rate show a similar response as with $\dot{\varepsilon} = 10^{-3}$ s^{-1} (the response curves of all the tests are found in Appendix A). They have a distinct yield point and after some plastic

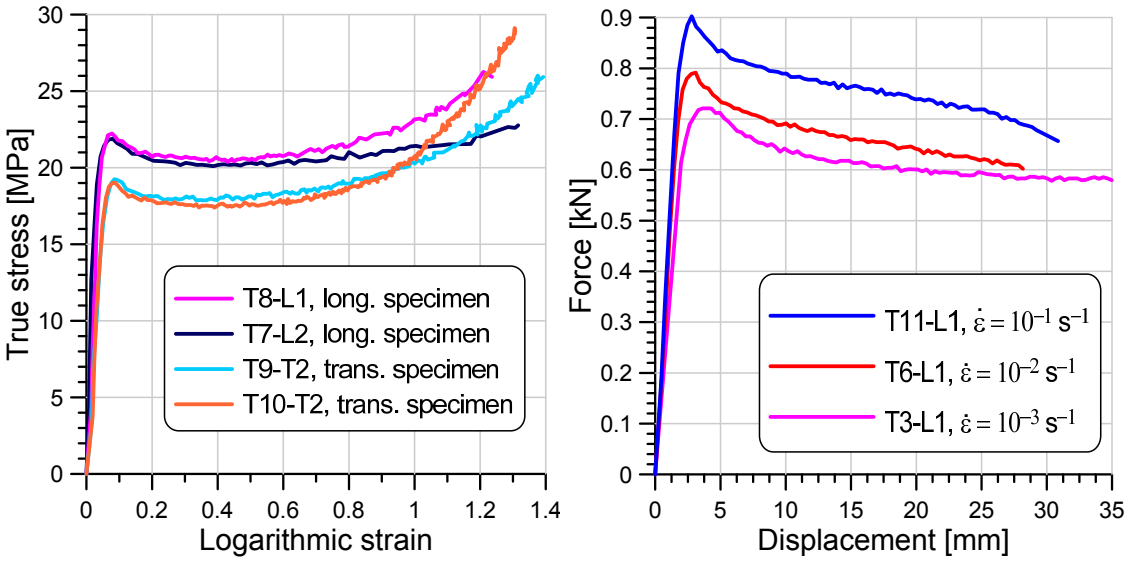

(a) Illustraion of the anisotropy (b) Illustration of the strain rate dependency

Figure 3.5: Selected force-displacement curves , $\dot{\varepsilon} = 10^{-2}$ s^{-1}

deformation they start to harden. The expected increase in Young's modulus and the yield stress is observed. The last two tests, T9-T2 and T10-T2, are taken from the transverse direction of plate 2. As the figure shows, the results are quite dependent on the location. The yield stress and the peak load are 10-15% lower for the specimen from the transverse direction. The hardening also differs from the longitudinal specimens by being more evident in the transverse specimens. The directional dependent response is not unusual in injection moulded polymers and is most probably a result of the shear effects that occurred during the moulding (see [3] for further details). The non-uniform material structure is also observed in the somewhat special fracture surfaces and in the fact that some specimens break and others do not. Anisotropy and fracture mechanics are, however, not implemented in the material model and will not be represented in the numeric analyses.

Figure 3.5b shows the strain rate dependency. To better illustrate the phenomenon this plot also includes a curve from the tests where $\dot{\varepsilon} = 10^{-1}$ s^{-1}. As the curve shows, the peak load increases with the strain rate. It is also seen that the increase from $\dot{\varepsilon} = 10^{-2}$ s^{-1} to $\dot{\varepsilon} = 10^{-1}$ s^{-1} is larger than the increase from $\dot{\varepsilon} = 10^{-3}$ s^{-1} to $\dot{\varepsilon} = 10^{-2}$ s^{-1}. A similar behaviour is observed for the yield stress. The increase in load capacity with strain rate is a result of the non-Newtonian nature of polymers. This is included in the numerical model, and the implementation will be explained in Chapter 4.

3.1.3 High strain rate, $\dot{\varepsilon} = 10^{-1}$ s^{-1}

At this strain rate the material starts to behave quite differently from the earlier tests. The peak load and yield stress increases and the total deformation is reduced. The fracture surface becomes more "cut-off", i.e. the outer layer is not stretched as much before fracture and becomes less visible. At this speed all tests end with fracture. Heat effects can also be of a magnitude worth considering, but these are not part of the material model and thus not reviewed in any extent in this thesis.

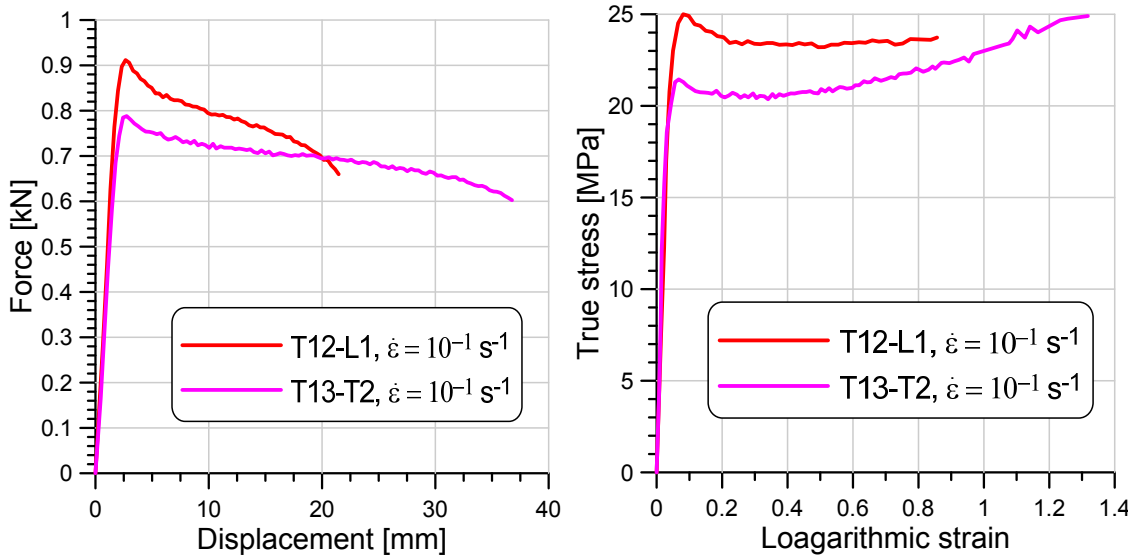

(a) Force-displacement curves, $\dot{\varepsilon} = 10^{-1}$ s^{-1} (b) Stress-strain curves, $\dot{\varepsilon} = 10^{-1}$ s^{-1}

Figure 3.6: Results from tests done with $\dot{\varepsilon} = 10^{-1}$ s^{-1}

The graphs in Figure 3.6 show some results from the testing. Two transversal specimens were tested also at this speed, the figures repeating the point of anisotropy. The initial response resembles that of the other strain rates, but after the yield point there are some differences. These tests do not harden as much as the others and they also fracture faster. These effects are most probably the result of the mentioned heat effects. The transverse specimens show a bit different behaviour. They have lower load levels and are able to deform more before fracturing. The reason for this is probably the lowered load level, which makes the heat effects less significant, thus allowing more deformation.

3.2 Uniaxial compression tests

The test rig used for the compression tests is shown in Figure 3.7a. The compression test specimens were only 3.2 millimetres thick and 6 millimetres in diameter and were machined using a belt puncher. Note that these were measured to 3.2 millimetre thickness instead of 3.1 millimetre even though they were taken from the same plate as the tension specimens. The exact reason for this is not known, it is probably a wrong measurement or some swelling mechanism caused by the machining with the belt puncher. The speckled pattern was applied onto the specimens and the camera was adapted to the small dimensions. To minimize the friction between the machine and the specimen, a 0.08 millimetre thick greased tape was applied (clearly visible at the contact surfaces shown in Figure 3.7a). Force was then applied until 1.5 millimetre (approximately 50% of the thickness) displacement was reached.

(a) The test rig prepared for compression testing

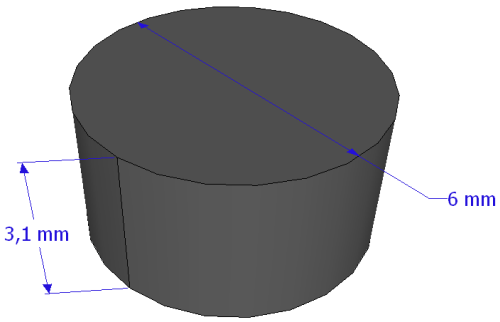

(b) The compression test specimen

Figure 3.7: Compression test set-up and specimen geometry

In the post-processing it became obvious that the specimen was too small to be processed with 7D. This made it a bit more challenging to gather the needed information. Since the vertical displacement was logged by the Instron controller, the challenge consisted of finding the horizontal displacement, i.e. the elongation of the diameter. This displacement has to be known in order to calculate the area

of the deformed cross-section which again is needed to calculate the true strain. A Matlab script became the solution. The script read all the images taken by the camera, turned them into large matrices of ones and zeroes and then found the first and the last "one" in a row located at some cross-section along the thickness direction of the specimen (the script can be found in Appendix B). Since the greased tape removed much of the friction, the deformation was quite uniform and the deformation could be taken from the cross-section located at the mid-point of the specimen.

With all the needed deformation data at hand, the stress could be calculated quite easily:

$$\sigma_{True} = \frac{F}{A} = \frac{F}{\left(\frac{\pi}{4}\right)d^2} \tag{3.2}$$

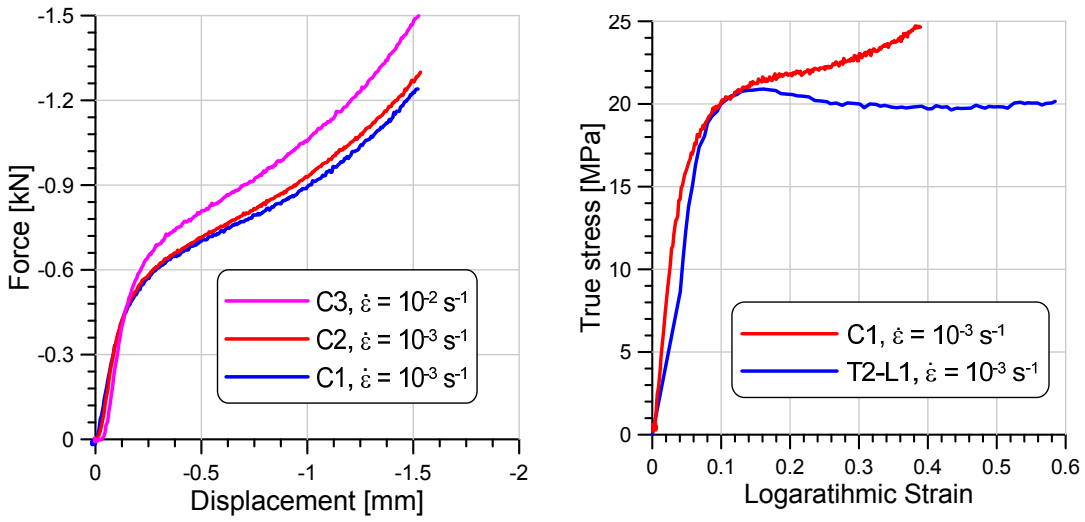

(a) Force displacement curves for the compression tests

(b) Force-displacement curves for tension and compression, $\dot{\varepsilon} = 10^{-3}\ s^{-1}$

Figure 3.8: The results of the compression tests

Figure 3.8a shows the force-displacement diagrams of the three compression tests. It is seen that the strain rate dependency also applies to compression loading and that, unlike the tension tests, no unloading occurs. The main reason for doing the compression tests is to find the ratio between the yield stress in tension and compression (α). This can be found from Figure 3.8b, which shows the stress-strain curve for both a tension and a compression specimen. The reason for the higher yield stress is the polymer chains reaction to compressive loading.

3.3 Summary

The test procedure described in this chapter provides the basis needed to fully calibrate the material model. The observations can be summed up in the following points:

- The results were not scattered. Only one of 17 tests was rejected.
- The material was found to be anisotropic
- The strain-rate dependency is obvious, being relatively near a log-linear pattern
- The yield stress in tension and compression are quite alike
- Softening is observed in tension but not in compression
- Hardening is observed both in tension and compression

In Chapter 4 it is shown how these parameters are analysed to define the different parameters of the material model.

Chapter 4

Calibration

This chapter explains and exemplifies the calibration of the material model. This process consists of identifying 11 non-zero coefficients that describe different parts of the material behaviour. The chapter starts with a review of the constitutive model. Then it is shown how the basic parameters, like stress-strain diagrams, yield stresses and forces are found from the results of Chapter 3. The next section will then show how to use this information to find the numbers, ratios and relations (the 11 coefficients) that can be understood by the LS-DYNA solver. The chapter is concluded with simulations of the material tests from Chapter 3, applying a calibrated version of the topical material model.

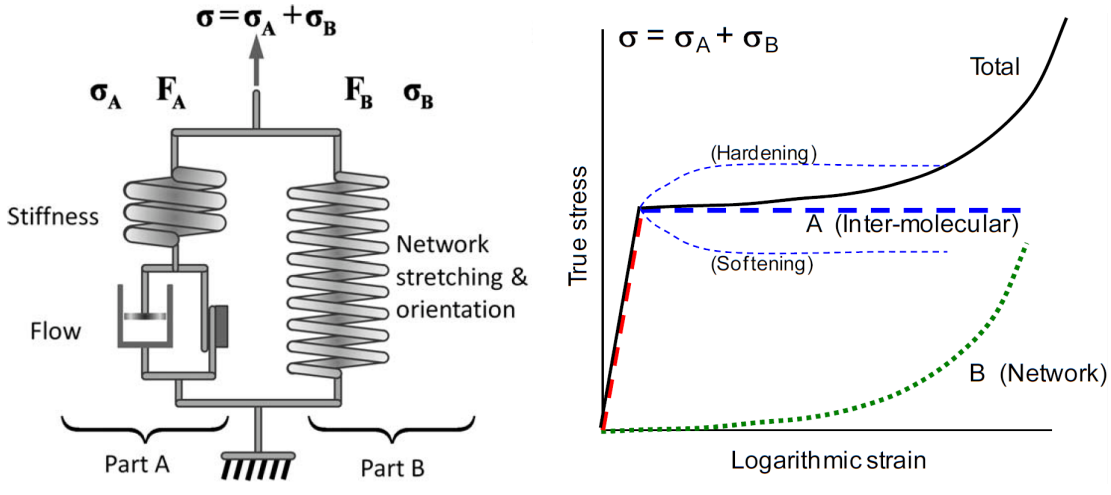

(a) (b)

Figure 4.1: The constitutive model and the resulting stress-strain diagram (after [2] and [8])

4.1 The constitutive model

Figure 4.1 (similar to Figure 2.3) shows an overview of the material model. In the following sections the derivation of the equations belonging to the different elements of the rheological model is shown. The theory is based on the following references [1], [9] and [2]. These documents and publications are produced by the team that created the material model and contains the theory behind it. This section contains only a representation of their work.

Polymers are both viscoelastic and viscoplastic. The material model, however, represents only the viscoplastic behaviour. This is because the model is designed for structural impact and crashworthiness simulations [9]. The material model also assumes constant temperature and an isotropic material structure [1].

The model is split into two main parts. This principle was introduced by Haward and Thackray in 1968 [4] and makes up the basis for most polymer material models today. The two parts describe; (i) the initial energy-elasticity followed by plastic flow and (ii) evolving entropy elasticity with increasing deformation. As mentioned in Section 2.3, these two parts have been named Part A and Part B in the material model. They have the same deformation gradient $\mathbf{F} = \mathbf{F}_A = \mathbf{F}_B$. This can be related to Figure 4.1a by imagining that the horizontal lines linking the Part A and Part B element will remain horizontal when the material deforms, thus deforming both parts equally. The change in volume is expressed by the Jacobian determinant of the deformation gradient. This means that Part A and Part B experience the same change of volume, since:

$$J = det\boldsymbol{F} = J_A = J_B \tag{4.1}$$

The resistance contributions from the two parts can be summed. The Cauchy stress tensor is thus:

$$\boldsymbol{\sigma} = \boldsymbol{\sigma}_A + \boldsymbol{\sigma}_B \tag{4.2}$$

4.1.1 Part A - Intermolecular resistance

Part A describes the intermolecular resistance using an elastic spring, a friction element and a viscous damper (see Figure 4.1a). The deformation is described by the gradient $\mathbf{F}_A$ which is decomposed into an elastic and a plastic part, $\mathbf{F}_A =$

$\mathbf{F}_A^e \cdot \mathbf{F}_A^p$. This also applies to the Jacobian of the deformation gradient, and thus to the volume change.

The spring element is modelled as a Neo-Hookean spring. The spring is described by the well known elastic parameters Young's modulus (E_0) and Poisson's ratio (ν). The Neo-Hookean formulation allows for large elastic deformations and yields the Kirchhoff stress tensor;

$$\boldsymbol{\tau}_A = \lambda_0 \ln J_A^e \boldsymbol{I} + \mu_0 (\boldsymbol{B}_A^e - \boldsymbol{I}) \tag{4.3}$$

where λ_0 and μ_0 are the Lamé constants of linearised theory. These are linked to E_0 and ν through;

$$\mu_0 = G = \frac{E_0}{2(1+\nu)} \tag{4.4}$$

$$\lambda_0 = \frac{E_0 \nu}{(1+\nu)(1-2\nu)} \tag{4.5}$$

The viscoplastic behaviour of the material model is represented by the friction element and the viscous damper. The friction element is defined by the parameters in Table 4.1.

σ_s	The saturation stress	β	The dilatation parameter
σ_T	The yield stress in uniaxial tension	H	Ramping parameter
α	The yield stress ratio		

Table 4.1: The parameters of the friction element

The parameters are implemented in the following yield criterion;

$$f_a = \bar{\sigma}_A - \sigma_T - R \tag{4.6}$$

where σ_T is the yield stress in uniaxial tension and R is an isotropic variable representing hardening or softening. If the material at hand had been structural steel or aluminium, the equivalent stress ($\bar{\sigma}_A$) would most probably have been calculated using the von Mises or Tresca criterion. This yield criterion is mean stress independent and assumes equal yield stress in tension and compression, properties which do not fit polymers very well. Another yield criterion is therefore assumed. It was first formulated by Raghava et al. [10]

$$(\sigma_1-\sigma_2)^2+(\sigma_2-\sigma_3)^2+(\sigma_3-\sigma_1)^2+2(|\sigma_C|-|\sigma_T|)(\sigma_1+\sigma_2+\sigma_3)=2|\sigma_C\sigma_T| \quad (4.7)$$

where σ_1, σ_2 and σ_3 are the principal stresses, σ_C and σ_T the yield stress in compression and tension, respectively. By introducing the first principal invariant I_1 and the deviatoric stress invariant J_2;

$$I_1=\sigma_1+\sigma_2+\sigma_3 \quad (4.8)$$

$$J_2=\frac{1}{6}[(\sigma_1-\sigma_2)^2+(\sigma_2-\sigma_3)^2+(\sigma_3-\sigma_1)^2] \quad (4.9)$$

plus the parameter α;

$$\alpha=\mid\frac{\sigma_C}{\sigma_T}\mid\geq 0 \quad (4.10)$$

the Raghava criterion can be formulated as [5]:

$$f(I_1,J_2)=(\alpha-1)\sigma_T I_1+3J_2-\alpha\sigma_T^2=0 \quad (4.11)$$

The uniaxial yield stress can be made separate in Equation (4.11) yielding:

$$f(I_1,J_2)=\bar{\sigma}-\sigma_T \quad (4.12)$$

$\bar{\sigma}$ is then the Raghava equivalent stress:

$$\bar{\sigma}=\frac{(\alpha-1)I_1+\sqrt{(\alpha-1)^2\ I_1^2+12\alpha J_2}}{2\alpha} \quad (4.13)$$

If $\sigma_C=\sigma_T$, i.e. $\alpha=1$, the pressure dependence is removed from Equation (4.13) and it becomes equal to the von Mises criterion:

$$\alpha=1\Rightarrow\bar{\sigma}=\sqrt{3J_2} \quad (4.14)$$

Now the last term, namely R, will be explained. This term is added to include hardening or softening after yield (illustrated as dotted blue lines in Figure 4.1b). R is a function of the accumulated plastic strain $\bar{\varepsilon}_A^p$ and takes the form;

$$R(\bar{\varepsilon}_A^p) = (\sigma_s - \sigma_T)[1 - exp(-H\bar{\varepsilon}_A^p)] \tag{4.15}$$

where σ_s is the saturation stress, i.e. the stress at the end of the Part A contribution, and H is a ramping parameter used to optimize the fit of the stress-strain curve between the yield stress and the saturation stress. Introducing (4.15) into (4.6) yields:

$$f_a = \bar{\sigma}_A - \sigma_T - (\sigma_s - \sigma_T)[1 - exp(-H\bar{\varepsilon}_A^p)] \tag{4.16}$$

When put in the yield criterion (Equation (4.16)) and compared to Figure 4.1b it is seen that R represents hardening when positive, i.e. $\sigma_s > \sigma_T$, and softening when negative ($\sigma_s < \sigma_T$).

The viscous damper in Figure 4.1a is described by the parameters C and $\dot{\varepsilon}_{0A}$. C is found by using the relation between yield stresses at different strain rates in tension, as will be described in Section 4.2. $\dot{\varepsilon}_{0A}$ is the reference strain rate chosen by the user, typically $10^{-4} - 10^{-3}$ s^{-1}. The next paragraphs show where these and the β parameter from the friction element belong in the material model.

Experiments have shown that an associated flow rule, i.e. a flow rule associated with the yield function (see Equation (4.17)), predicts too large volumetric plastic strains.

$$\dot{\varepsilon}_A^p = \dot{\bar{\varepsilon}}_A^p \frac{\partial f}{\partial \boldsymbol{\sigma_A}} \tag{4.17}$$

Associated flow rule

$$\dot{\varepsilon}_A^p = \dot{\bar{\varepsilon}}_A^p \frac{\partial g}{\partial \boldsymbol{\sigma_A}} \tag{4.18}$$

Non-associated flow rule

This is solved by introducing a new, non-associated relation for the plastic potential. In this case a Raghava-like plastic potential function g_A;

$$g_A = \frac{(\beta - 1)I_{1A} + \sqrt{(\beta - 1)^2 I_{1A}^2 + 12\beta J_{2A}}}{2\beta} \geq 0 \tag{4.19}$$

where the β parameter is introduced to control the volumetric plastic strains (confront row 7 of Table 2.1). The multiplier in the flow rule, $\dot{\bar{\varepsilon}}_A^p$, is strain rate dependent and described by the constitutive relation (see [9] for more details):

$$\dot{\bar{\varepsilon}}_A^p = \begin{cases} 0 & \text{if } f_A \leq 0 \\ \dot{\varepsilon}_{0A} exp\Big[\frac{1}{C}\Big(\frac{\bar{\sigma}_A}{\sigma_T + R}\Big) - 1\Big] - 1 & \text{if } f_A > 0 \end{cases} \tag{4.20}$$

Note the location of the parameters C and $\dot{\varepsilon}_{0A}$ in Equation (4.20).

4.1.2 Part B - Network resistance

Part B describes the network resistance with a hyperelastic spring. The spring needs the two input parameters C_R and $\bar{\lambda}_L$. C_R represents the initial elastic modulus of Part B and $\bar{\lambda}_L$ represents the locking stretch which is related to the maximum attainable deformation of the material [9]. They are both identified in the Part B contribution of the Cauchy stress tensor:

$$\boldsymbol{\sigma}_B = \frac{1}{J_B}\frac{C_R}{3}\frac{\bar{\lambda}_L}{\bar{\lambda}} L^{-1}\Big(\frac{\bar{\lambda}}{\bar{\lambda}_L}\Big)(\boldsymbol{B}_B^* - \bar{\lambda}^2 \boldsymbol{I}) \tag{4.21}$$

In Equation (4.21) J_B represents the Jacobian = J = det (**F**) and $L^{-1}(\circ)$ the inverse function of the Langevin function $L(x) \equiv \coth x - \frac{1}{x}$. The kinematic variables $\bar{\lambda}$ and $\boldsymbol{B}_B^*$ are defined as:

$$\bar{\lambda} = \sqrt{\tfrac{1}{3} tr(\boldsymbol{B}_B^*)} \quad , \quad \boldsymbol{B}_B^* = \boldsymbol{F}_B^* \cdot (\boldsymbol{F}_B^*)^T \tag{4.22}$$

They represent the distortional stretch and the distortional left Cauchy-Green deformation tensor, respectively. $\boldsymbol{F}_B^* = J_B^{-1/3}\boldsymbol{F}_B$ is the distortional part of $\mathbf{F}_B$.

4.2 The calibration procedure

In this section it is shown how the data from the material tests are utilized to identify the parameters defining the material model. The parameters are determined from three categories of material data; the transverse deformation, the yield stresses and the stress-strain diagram of the baseline test. The representation of the procedure is mainly based on an unpublished guideline document for the material model written by Clausen et al. [1].

The first point of the calibration procedure is to decide which of the tests that should be the reference test. Based on the results found in Chapter 3, T3-L1

was chosen as the reference test. In this case both the two slowest tests were good candidates, and the results of both tests were put through the calibration procedure. The calibration of T3-L1, however, gave the most optimal response curve and was thus chosen over the other option.

4.2.1 Parameters based on transverse deformations

The parameters identified from the transverse strains are the dilatation parameter β and Poisson's ratio ν_0. Both are based on the reference test T3-L1. The strain relations are seen in Figure 4.2.

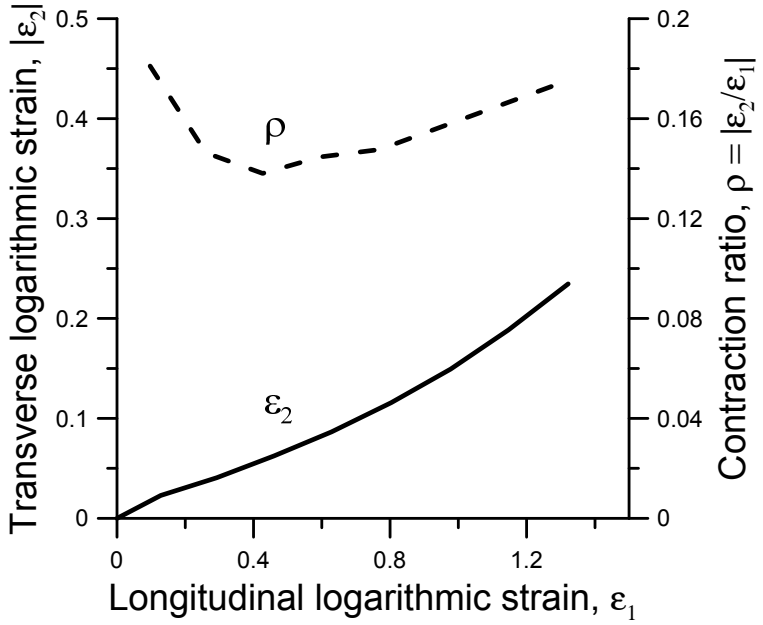

Figure 4.2: Transverse vs. longitudinal strain and contraction ratio vs. longitudinal strain for the reference test $\dot{\varepsilon} = 10^{-3}$ s^{-1}

The left y-axis and the x-axis show the transverse strain, ε_2, as a function of the longitudinal strain, ε_1. Possion's ratio is set to the slope of this curve for $\varepsilon_1 <\sim 0.1$. The value found is $\nu_0 = 0.24$, which is a rather low value compared to 0.4 in HDPE and 0.3 in PVC [5].

The contraction ratio ρ indicates in which degree the volume changes. It is inversely proportional to the change of volume, i.e. a small ρ means a large change in volume. The range of the ratio is $0 < \rho \leq 0.5$, where $\rho = 0.5$ corresponds to no change of volume. From Figure 4.2 it is seen that the topical contraction ratio

is about 0.165, which is a low value. This means that the material dilates (the volume expands) considerably.

In order to derive the β parameter the gradient of the plastic potential function have to be introduced. Equation (4.23a) is similar to the plastic potential function in Equation (4.18). The gradient of this function is shown in Equation (4.23b) [1].

$$\bar{\boldsymbol{L}}_A^p = \dot{\bar{\varepsilon}}_A^p \frac{\partial g_A}{\partial \overline{\boldsymbol{\Sigma}}_A} \tag{4.23a}$$

$$\frac{\partial g_A}{\partial \overline{\boldsymbol{\Sigma}}_A} = f_1 \frac{\partial I_{1A}}{\partial \overline{\boldsymbol{\Sigma}}_A} + f_2 \frac{\partial J_2 A}{\partial \overline{\boldsymbol{\Sigma}}_A} = f_1 \boldsymbol{I} + f_2 \, \partial \overline{\boldsymbol{\Sigma}}_A^{dev} \tag{4.23b}$$

where the functions f_1 and f_2 read

$$f_1 = \frac{\partial g_A}{\partial I_{1A}} = \frac{\beta - 1}{2\beta} + \frac{(\beta-1)^2 I_{1A}}{2\beta\sqrt{(\beta-1)^2 I_{1A}^2 + 12\beta J_{2A}}} \tag{4.24a}$$

$$f_2 = \frac{\partial g_A}{\partial I_{2A}} = \frac{3}{\sqrt{(\beta-1)^2 I_{1A}^2 + 12\beta J_{2A}}} \tag{4.24b}$$

The dilatation yields that both f_1 and f_2 are non-zero. Since the stress state in the material tests is uniaxial, the first and second invariant of the Cauchy stress tensor read $I_{1A} = \sigma$ and $J_{2A} = (1/3)\sigma^2$. When these invariants are inserted into the non-zero f_1 and f_2 the result is

$$f_1 = \frac{\beta - 1}{2\beta} + \frac{(\beta-1)^2 \sigma}{2\beta\sqrt{(\beta-1)^2\sigma^2 + 4\beta\sigma^2}} = \frac{\beta - 1}{\beta + 1} \tag{4.25a}$$

$$f_2 = \frac{3}{\sqrt{(\beta-1)^2\sigma^2 + 4\beta\sigma^2}} = \frac{3}{\beta+1}\frac{1}{\sigma} \tag{4.25b}$$

The last step is now to formulate the rate of deformation for plastic flow, $\boldsymbol{D}_A^p$. It is defined by the current stress and strain state of the material. The current stress state is as mentioned uniaxial stress, the current strain state is defined by the assumptions of isotropic transverse strains, a constant ρ value and proportional deformation.

$$\boldsymbol{D}_A^p = \begin{pmatrix} \dot{\varepsilon}_1^p & 0 & 0 \\ 0 & \dot{\varepsilon}_2^p & 0 \\ 0 & 0 & \dot{\varepsilon}_3^p \end{pmatrix} = \dot{\varepsilon}_1^p \begin{pmatrix} 1 & 0 & 0 \\ 0 & -\rho & 0 \\ 0 & 0 & -\rho \end{pmatrix} = \dot{\bar{\varepsilon}}_A^p \frac{\partial g_A}{\partial \overline{\boldsymbol{\Sigma}}_A} \tag{4.26}$$

The latter part of Equation (4.26) shows that this rate is equal to the rate of deformation shown in Equation (4.23a). By assuming $\dot{\varepsilon}_1^p = \dot{\bar{\varepsilon}}_A^p$, i.e. shortening the equivalent strain rate, and inserting the Equations in (4.25) into Equation (4.26) the following equations are derived:

$$\begin{pmatrix} 1 & 0 & 0 \\ 0 & -\rho & 0 \\ 0 & 0 & -\rho \end{pmatrix} = \frac{\beta - 1}{\beta + 1} \begin{pmatrix} 1 & 0 & 0 \\ 0 & 1 & 0 \\ 0 & 0 & 1 \end{pmatrix} + \frac{3}{\beta + 1} \frac{1}{\sigma} \begin{pmatrix} (2/3)\sigma & 0 & 0 \\ 0 & -(1/3)\sigma & 0 \\ 0 & 0 & -(1/3)\sigma \end{pmatrix} \tag{4.27}$$

Solving the system of equations yields

$$\beta = \frac{2 - \rho}{1 + \rho} \tag{4.28}$$

ρ is set to 0.17. The ρ value is rounded up because the other possible reference test (T2-L1) had slightly higher ρ than the chosen reference test. The chosen value for ρ gives $\beta = 1.56$

4.2.2 Parameters based on the yield stresses

In contrast to most metals, the yield stress for polymers is different in tension and compression, and it increases considerably with increasing strain rate. This behaviour is described using the ratios and relations explained in this section.

In order to use the relation between the yield stresses they have to be identified using the same principle. In this thesis the yield stresses were identified using the Considère criterion:

$$\frac{d\sigma_t}{d\varepsilon_t} = \sigma_t \tag{4.29}$$

where σ_t and ε_t are the true stress and the longitudinal logarithmic strain, respectively. Figure 4.3a shows how this relation appears graphically. The yield stress is defined as the point where the two curves intersect. The method was implemented

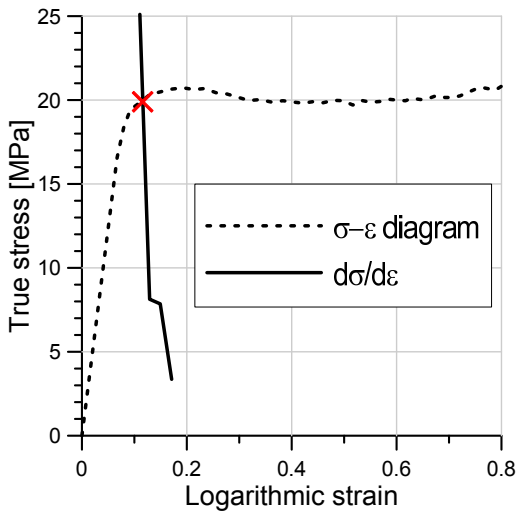

(a) The yield stress calculation of test T3-L1

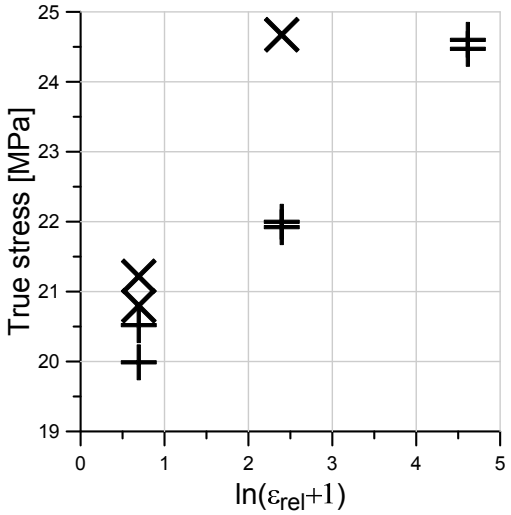

(b) The relation between the yield stresses and the strain rate. (+) are tension tests and (×) are compression tests

Figure 4.3: The method used to identify the yield stresses and the yield stresses in relation to the strain rate

in a Matlab code which calculated the yield stress for all the material tests (the script can be found in Appendix B.3).

The first and easiest parameter to identify from the yield stresses is α. This is the ratio between the yield stress in compression and tension, i.e. $\alpha = \sigma_{yC}/\sigma_{yT}$. As seen in Figure 4.3b is α not independent of the strain rate. The calibration procedure states that the two yield stresses are to be taken from a test done at the reference strain rate $\dot{\varepsilon}_{0A} = 10^{-3}$ s^{-1}. Even though the yield stress at the intermediate strain rate is much higher, it is the best solution to use the result of the reference test. The reason is that the test from the intermediate strain rate is not verified by a second test, and thus less valid. For this particular PP the α value is found to be $\alpha = 1.062$, which indicates that the yield stress is only slightly higher in compression than in tension.

The next parameters are central in describing the strain rate dependency. These are the yield stress in tension, σ_T, the reference strain rate, $\dot{\varepsilon}_{0A}$, and a slope ratio C. They are connected as shown in Equation (4.30):

$$\bar{\sigma}_A = \sigma_T \left(1 + C\, ln\left(\frac{\dot{\bar{\varepsilon}}^p_A}{\dot{\varepsilon}^0_A} + 1\right)\right) \tag{4.30}$$

$\dot{\varepsilon}_A^0$ is the first to be identified. This is the reference strain rate and is defined as [1];

... the local logarithmic strain rate $\dot{\varepsilon}$ in the section experiencing the onset of necking and thereby the initial yielding.

For this particular PP this corresponds to a strain rate of $\dot{\varepsilon}_A^0 = 10^{-3}$ s^{-1}. This parameter is incorporated into a variable called the relative strain rate. This is the ratio between the Part A plastic strain rate and the reference strain rate:

$$\dot{\varepsilon}_{rel} = \frac{\dot{\bar{\varepsilon}}_A^p}{\dot{\varepsilon}_A^0} \tag{4.31}$$

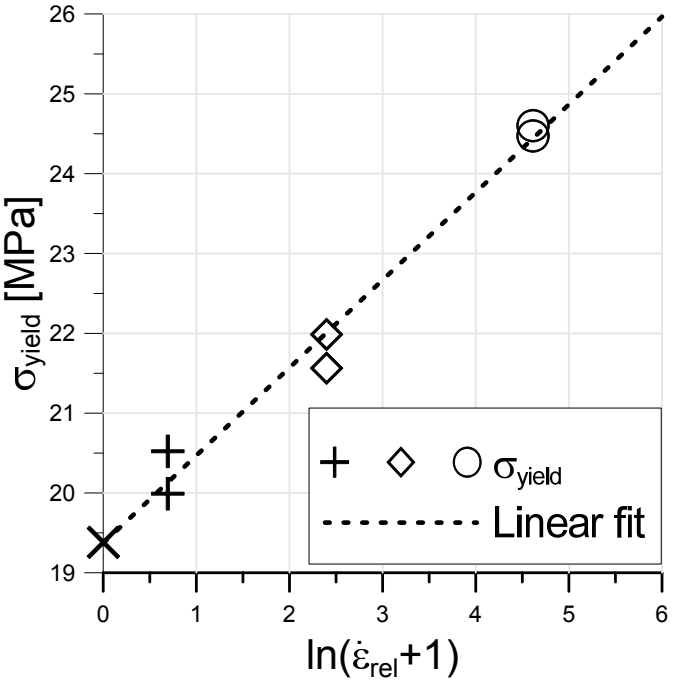

Figure 4.4: The yield stresses and the linear fit used for extrapolation

Now moving on to σ_T and C. A problem with $\bar{\sigma}_A$ in Equation (4.30), i.e. the Raghava equivalent stress, is that it describes a point at the stress curve in which both Part A and Part B contribute. This means that if the yield stress from the reference test (σ_T) is applied as shown in Equation (4.30), the Part B contribution to the yield stress is left out. The result being that when the model sums the Part A and Part B contributions to the stress it ends up with $\bar{\sigma}_A > \sigma_{yield}$. To overcome this transitional problem, a static yield stress σ_0 is introduced. Figure 4.4 illustrates the concept. The figure shows the yield stress at the three strain rates

applied in the material testing (see Chapter 3) as function of $ln(\dot{\varepsilon}_{rel}+1)$. The dotted line represents a linear regression (Equation (4.32)) between these six points. This have to be done in order to identify both the newly introduced σ_0 and C.

$$y = ax + b \tag{4.32}$$

σ_0 is shown as the X on the y-axis and thus corresponds to "b" in Equation (4.32). Since the x-axis shows a strain rate relation this placement indicates that σ_0 is the yield stress at a fictitious static or "zero" strain rate:

$$\dot{\varepsilon}_{rel} = 0 \Rightarrow ln(\dot{\varepsilon}_{rel} + 1) = ln(1) = 0 \tag{4.33}$$

By doing this the Part B contribution is removed and the correct Part A equivalent stress can be formulated as:

$$\bar{\sigma}_A = \sigma_0 + \sigma_0 C \cdot ln(\dot{\varepsilon}_{rel} + 1) \tag{4.34}$$

The C parameter can now be derived;

$$C = \frac{\bar{\sigma}_A - \sigma_0}{\sigma_0 ln(\dot{\varepsilon}_{rel} + 1)} = \frac{a}{\sigma_0} \tag{4.35}$$

where "a" corresponds to a in Equation (4.32), i.e. representing the gradient of the linear regression curve. For the PP in this thesis σ_0 and a are found to be $\sigma_0 = 19.4$ MPa (derived in the next section) and $a = 1.1$ which gives $C = 0.057$.

4.2.3 Parameters found from the stress-strain curve of the reference test

This section will identify the remaining Part A parameters E_0, σ_T, σ_s and H and the two Part B parameters C_R and $\bar{\lambda}_L$. They are all found from a stress-strain diagram based on the chosen reference test, T3-L1.

Young's modulus increases with increasing strain rate, i.e. polypropylene is viscoelastic. This is, as mentioned earlier, not incorporated in the material model and Young's modulus, E_0, is to be found from the elastic response of the reference test. It is, however, well known that data from Digital Image Correlation (DIC) are subjected to noise for small strain values, thus making an Young's modulus

provided by the material manufacturer preferable. The manufacturer has, however, not provided any value for Young's modulus and the modulus used in this thesis may therefore be a major source of error in the representation of the elastic behaviour. That said, it should be noted that the elastic behaviour has not been the primary focus in developing this material model and the elastic response makes up only a small part of the total response. Given the above conditions, E_0 has been identified using the stress-strain curves from the DIC. In the initial phases E_0 was found by fitting the DIC based stress-strain curve of the reference test exactly, resulting in $E_0 = 250$ MPa. This is a very low value and numerical simulations indicated that the correct value was more in the range of 400-500 MPa, which resulted in choosing $E_0 = 400$ MPa. This value also represents a mean of Young's modulus over the three strain rates applied. This deviates a bit from the guidelines [1], but it has proved a reasonable estimation in the numerical simulations.

The parameters not yet derived depend on the dilatation and whether the material softens or hardens. The topical PP shows a significant dilation and a slight softening. The softening means that $R(\dot{\varepsilon}_A^p)$ in Equation (4.6) is negative and that the stress-strain curve has a local maximum quite early in the response. It is assumed that the material behaviour is elastic up to this maximum point, i.e. the yield stress σ_T is equal to the stress value at this point. This assumption is more correct the more distinct the softening is, i.e. a material experiencing a softening of low gradient may have a more gradual transition to plastic behaviour than assumed. The assumption, however, does not exempt σ_T from being adjusted down to σ_0 as explained earlier, rendering:

$$\sigma_T = \sigma_0 = 19.4 \text{ MPa} \tag{4.36}$$

Now to the saturation stress, σ_s. This parameter describes the stress in the material at the end of the transition described by the R parameter. For the PP this means that σ_s is the stress at the point where the softening ends, i.e. lower than σ_T. It has proved more challenging to find this stress value for materials that softens, than for the ones that do not. This is because this and the three other remaining parameters, H, C_R and $\bar{\lambda}_L$, are not independent of each other. Making a direct addition of the individual curve fits inaccurate. The solution is to incorporate all four parameters into a function describing the entire stress-strain curve.

Some additional information is required in order to derive the function describing the complete stress-strain curve. The main objective is to describe the total stress through the contributions of Part A and Part B:

$$\sigma_{target} = \sigma_A + \sigma_B = \sigma_{total} \tag{4.37}$$

Equation (4.21) shows the stress contribution of Part B, $\boldsymbol{\sigma}_B$. The latter part of this equation is

$$(\boldsymbol{B}_B^* - \bar{\lambda}^2) \tag{4.38}$$

where $\boldsymbol{B}_B^*$ is

$$\boldsymbol{B}_B^* = J^{-2/3}\boldsymbol{F}_B(\boldsymbol{F}_B)T = J^{-2/3}\begin{pmatrix}\lambda_1^2 & 0 & \\ 0 & \lambda_2^2 & 0 \\ 0 & 0 & \lambda_3^2\end{pmatrix} \tag{4.39}$$

and the parameter $\bar{\lambda}$, also shown in Equation 4.22 on page 30, is equal to

$$\bar{\lambda} = \sqrt{\frac{1}{3}tr(\boldsymbol{B}_B^*)} = \sqrt{\frac{1}{3}J^{-2/3}(\lambda_1^2 + 2\lambda_2^2)} \tag{4.40}$$

where the volume change is $J = J_B = det(\boldsymbol{F}) = \lambda_1\lambda_2^2$. By putting Equation (4.39) and (4.40) into Equation 4.21 on page 30 the Part B stress contribution is derived:

$$\boldsymbol{\sigma}_B = \begin{pmatrix}\sigma_{B1} & 0 & 0 \\ 0 & \sigma_{B2} & 0 \\ 0 & 0 & \sigma_{B2}\end{pmatrix} = J^{-5/3}\frac{C_R}{3}\frac{\bar{\lambda}_L}{\bar{\lambda}}L^{-1}\left(\frac{\bar{\lambda}}{\bar{\lambda}_L}\right)\begin{pmatrix}\frac{2}{3}(\lambda_1^2 - \lambda_2^2) & 0 & 0 \\ 0 & \frac{1}{3}(\lambda_2^2 - \lambda_1^2) & 0 \\ 0 & 0 & \frac{1}{3}(\lambda_2^2 - \lambda_1^2)\end{pmatrix} \tag{4.41}$$

From Equation (4.41) it is seen that $\boldsymbol{\sigma}_B$ represents a deviatoric stress state. This means that in order to make the total stress (cf. Equation (4.37)) define an uniaxial stress state the stress component $\sigma_{A2}(= \sigma_{A3})$ must fulfil:

$$\sigma_{A2} = -\sigma_{B2} = \frac{1}{2}\sigma_{B1} \tag{4.42}$$

Equation (4.41) shows that σ_{B1} contains the inverse of the Langevin function. The nature of this function makes it complicated to use in regression. This is solved by using a Padé approximation to $L^{-1}(\circ)$ [1]. This yields the following expression for σ_{B1}

$$\sigma_{B1} = \frac{2}{9} C_R J^{-5/3} \frac{3\bar{\lambda}_L^2 - \bar{\lambda}^2}{\bar{\lambda}_L^2 - \bar{\lambda}^2} \left(\lambda_1^2 - \lambda_2^2\right) \tag{4.43}$$

The next step is to use the Raghava yield criterion to formulate an expression for the stress in Part A. Based on the above assumptions I_{1A} and J_{2A} read:

$$I_{1A} = (\sigma_{A1} + 2\sigma_{A2}) \tag{4.44a}$$

$$J_{2A} = \frac{1}{3}(\sigma_{A1} - \sigma_{A2}) \tag{4.44b}$$

By introducing this into the Raghava yield criterion (cf. Equation (4.19)) and then applying some algebra, the stress contribution of Part A can be formulated as:

$$\sigma_{A1} = \frac{1}{k_1}\sigma_{A,ua} + \frac{1}{2}\frac{k_2}{k_1}\sigma_{B1} \tag{4.45}$$

where $k_1(\alpha)$ and $k_2(\alpha)$ are constants derived through the algebra, extracting α (the yield stress ratio) into constants. $\sigma_{A,ua}$ in the above equation describes the uniaxial Part A stress. Since the majority of the response is plastic $\sigma_{A,ua}$ is set equal to

$$\sigma_{A,ua} = \sigma_T + (\sigma_s - \sigma_T)[1 - exp(-H\bar{\varepsilon}_1^p)] \tag{4.46}$$

Equation (4.46) and (4.43) are introduced into Equation (4.37) and the result is:

$$\sigma_{target} = \sigma_{A1} + \sigma_{B1} = \left(\frac{1}{k_1}\sigma_{A,ua} + \frac{1}{2}\frac{k_2}{k_1}\sigma_{B1}\right) + \sigma_{B1} \tag{4.47a}$$

$$\sigma_{target} = \frac{1}{k_1}\Big(\sigma_T + \Big(\sigma_s - \sigma_T\Big)\Big[1 - exp(-H\bar{\varepsilon}_l^p)\Big]\Big) + \left(\frac{1}{2}\frac{k_2}{k_1}\right)\frac{2}{9}C_R J^{-5/3}\frac{3\bar{\lambda}_L^2 - \bar{\lambda}^2}{\bar{\lambda}_L^2 - \bar{\lambda}^2}\left(\lambda_1^2 - \lambda_2^2\right) \tag{4.47b}$$

This equation has been implemented into a worksheet in Microsoft Excel by Clausen et al. The regression gave the following values; $\sigma_s = 12.5$ MPa, $H = 2.19$, $C_R = 3.79$ MPa and $\bar{\lambda}_L = 50.43$.

The parameters are summarized in Table 3.2. The fit of the calibrated stress-strain curve to the one of T3-L1 is shown in Figure 4.5.

1	E_0	400 MPa
2	ν_0	0.24
3	σ_T	19.4 MPa
4	σ_s	12.5 MPa
5	H	2.19
6	α	1.062
7	β	1.56
8	$\dot{\varepsilon}_{0A}$	0.001 s^{-1}
9	C	0.05716
10	C_R	3.79 MPa
11	$\tilde{\lambda}_L$	50.43

Table 3.2: The eleven calibrated parameters (colour coded with Figure 2.3a on page 10)

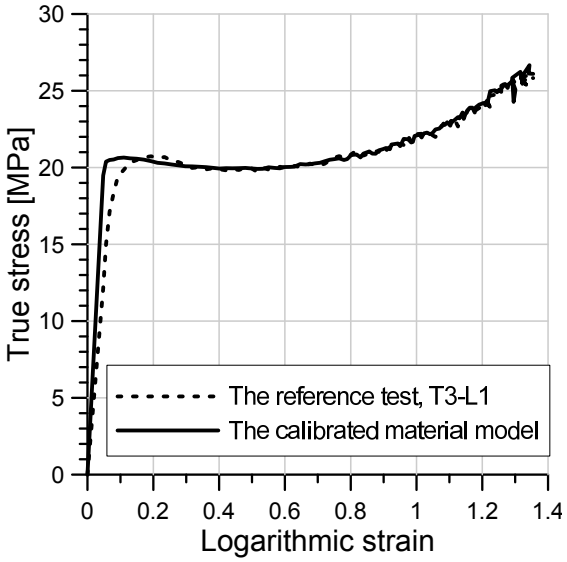

Figure 4.5: Stress-strain curves for the reference test and the calibrated material model

4.3 Application of the calibrated material model

In this section the material model is applied in the finite element code LS-DYNA [6]. The uniaxial tension and uniaxial compression tests will be treated in this chapter. Each subsection starts with a short review of the modelling process. This is followed by a presentation of the results, split into a subsection for each strain rate. The results shown in these first subsections are all from simulations with a reference material model, i.e. a material model where the parameters are strictly based on the calibration derived in this chapter. At the end of the section the results are compared and discussed and some parameters are treated in a brief parameter study. The material cards and the input files can be found in Appendix C.

4.3.1 Uniaxial tension

The specimen was modelled both as full-size and as only the gauge length. In order to get the best representation of the strain rate, the full-size model was used. For the medium and low strain rate tests the full-sized model became very time consuming. A version of the full-size model with symmetry about the longitudinal axis was therefore used to reduce the time of the calculations. Since the specimen was only three millimetres thick, a thickness symmetry was considered unnecessary.

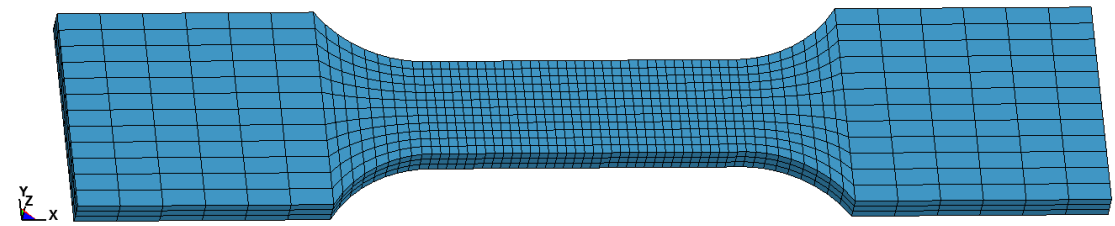

(a) The full-size meshed geometry

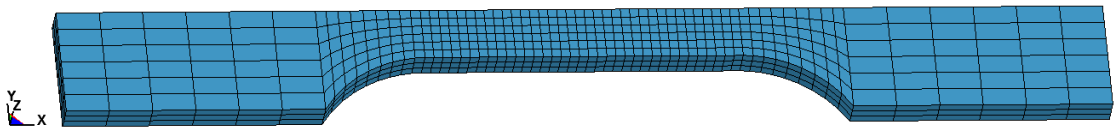

(b) The half meshed geometry

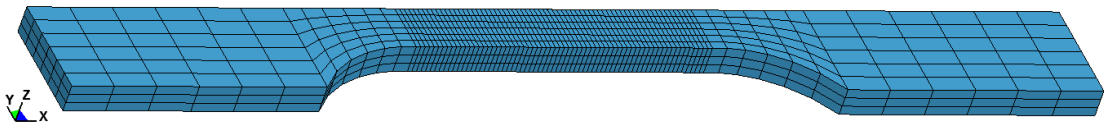

(c) The mesh used in the low-strain-rate tests

Figure 4.6: The applied geometries

The applied geometries are shown in Figure 4.6. Fully integrated solid elements were used (element formulation 2 in LS-DYNA [6]). In the gauge length the elements measure approximately $1mm \times 1mm \times 1mm$, which correspond to 33 elements along the longitudinal axis of the gauge, 12 along the transversal and 3 in the thickness direction. Except from the simulation of the low-strain-rate test, this mesh has proved the most optimal with regard to accuracy and computational expense. For the lowest strain rate a finer mesh had to be applied in the gauge length to avoid numerical error. The refinement was done by doubling the number of elements in the longitudinal direction (see Figure 4.6c), thus making the elements more and more cubic as they deform

The first five longitudinal elements at each end were defined in node sets representing the clamps of the test machine. The node set in one end was defined as fixed and the set in the other end was prescribed a constant deformation in mm/s.

Strains and stresses were collected from the elements defining the mid-point of the modelled specimen, i.e. in the mid-point of the gauge. This is also the section that experiences the initial yielding thus corresponding to the section used for collecting data from the material tests.

Mass scaling of 10^5 was applied. The mass density of the material was found to

be approximately $\rho = 1000$ kg/m^3. With the applied units and the mass scaling of 10^5 the effective weight in the analysis was $\rho = 1.00 \cdot 10^{-5}$ tonne/mm^3. As long as the problem is close to static the mass scaling can be applied without affecting the results in any extent. Other levels of mass scaling have been applied but they have been found less optimal than the one chosen.

Low strain rate, $\dot{\varepsilon} = 10^{-3}$ s^{-1}

This is the reference strain rate. Three material tests were done at this speed, where of one was rejected. Of the two remaining, the test T3-L1 was chosen as the reference model and is thus the basis of the applied material model.

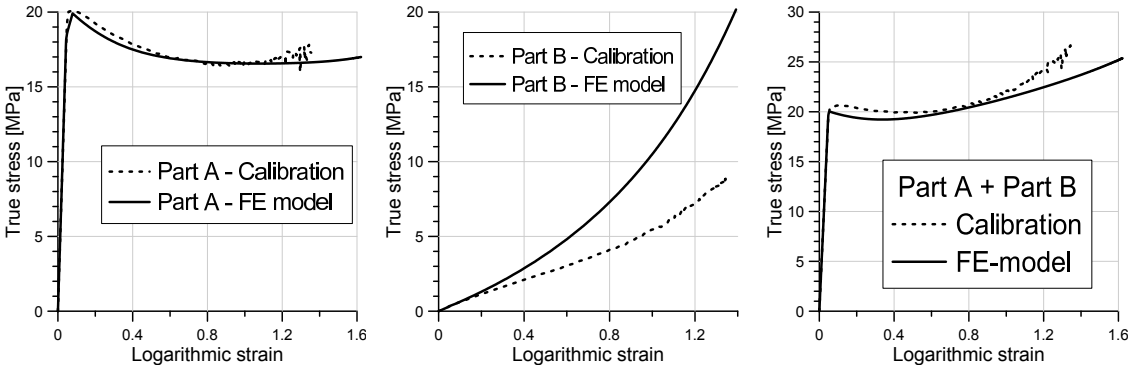

(a) Comparison of Part A (b) Comparison of Part B (c) Part A and Part B combined

Figure 4.7: The contribution of the two parts separate and combined

Figure 4.7 shows the results of a finite element simulation where $\dot{\varepsilon} = 10^{-3}$ s^{-1}. The results are split into Part A and Part B and compared with the same parts of the calibrated response curve, see Figure 4.5. In Figure 4.7a it is seen that Part A of the simulation and the calibration agree quite well. The opposite is seen in Figure 4.7b. The initial response is similar, but the deviation increases with increasing strain. The sum of the two, however, is not too bad. This indicates that part of the error in the Part B contribution is counterbalanced by Part A. This error allocation can indicate that the degree of agreement between the material tests and the simulations lies in how well Part B fits to the response of the topical material test.

Figure 4.8 shows the results of the simulation of the tests with the lowest strain rate. The force-displacement diagram in Figure 4.8a shows that the model matches quite well with the force-displacement curves of the material tests. But on the other hand shows Figure 4.8b that the model deviates quite a bit from the stress-strain response of the same tests. This is because the two diagrams display a

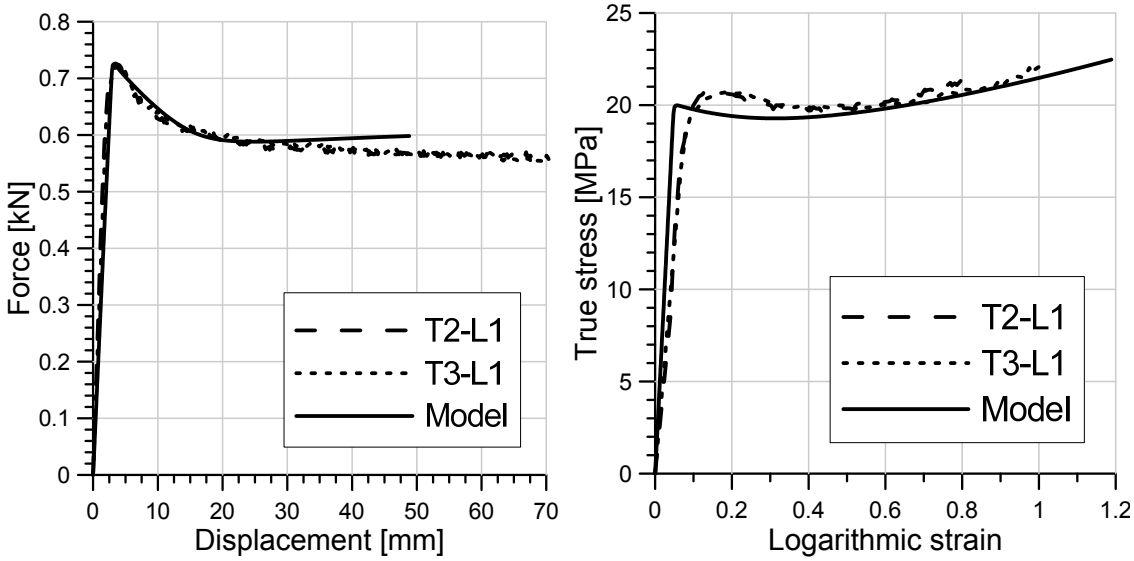

(a) Force-displacement diagram

(b) Stress-strain diagram

Figure 4.8: Diagrams comparing the results of the model and the tests

global response and a local response, respectively, and it appears that the global response is well represented by the model, but the local is not. This is also seen when comparing the deformed shape of the test specimens and the model. The necking is less evident in the specimens than in the model. The diffuse necking might indicate that the resistance mechanisms are a bit more complex than the ones represented by the model.

Intermediate strain rate, $\dot{\varepsilon} = 10^{-2}$ s^{-1}

At this strain rate the parameters describing the strain rate dependency are tested for the first time. It seems that the result of the response is satisfactory.

In contrast to the low-strain-rate modelling, the finite element model fits nearly perfect to the tests at this rate. The maximum force fits very well and the response continues to agree all the way until the force stabilizes. In the stress-strain diagram the assumed E_0 of 400 MPa seems to fit very well and so does the yield stress and the plastic material behaviour. It is challenging to find an exact reason for why this simulation agrees better with the test results than the low-strain-rate tests. One point contributing to the agreement is that this is the strain rate defining the mid-point of the linear strain rate regression line (cf. Figure 4.4), something which calls for a good estimate of the yield stress. The assumptions regarding the elastic behaviour also agree very well.

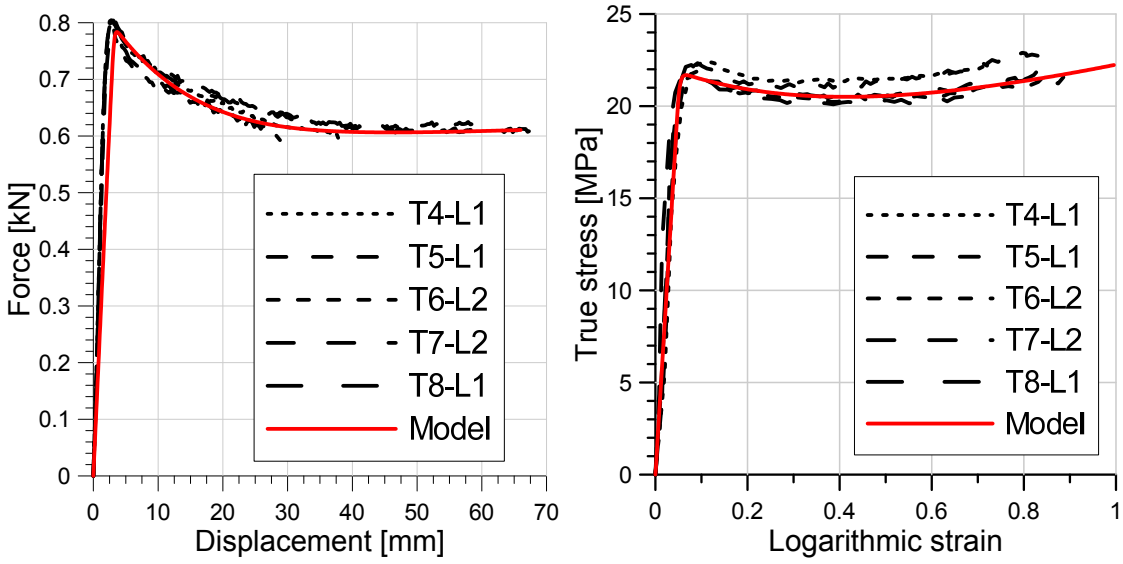

(a) Force-displacement diagram

(b) Stress-strain diagram

Figure 4.9: Diagrams comparing the model and the tests

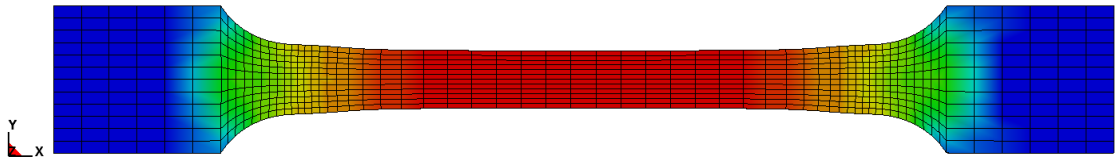

Figure 4.10: The deformed finite element model applied a fringe plot showing the maximum principle stress ($\dot{\varepsilon} = 10^{-2}\, s^{-1}$)

Figure 4.10 shows the deformed mesh applied a fringe plot of the maximum principle stress. The red colour indicates maximum values and blue minimum. In each end of the gauge (in the transition from orange to yellow) can the end points of the propagating neck be observed. It is seen that the entire neck is exposed to high stresses. The gradual transition from high to low stresses at the end of the gauges indicates that the transitions from the gauge to the clamping areas are well represented by the applied mesh.

High strain rate, $\dot{\varepsilon} = 10^{-1}\ \mathbf{s}^{-1}$

The high-strain-rate tests were over in seconds. At strain rates this high there might be significant heat effects that are not represented by the numerical model.

Figure 4.11 shows the response curves for the high-strain-rate tests. In Figure 4.11a

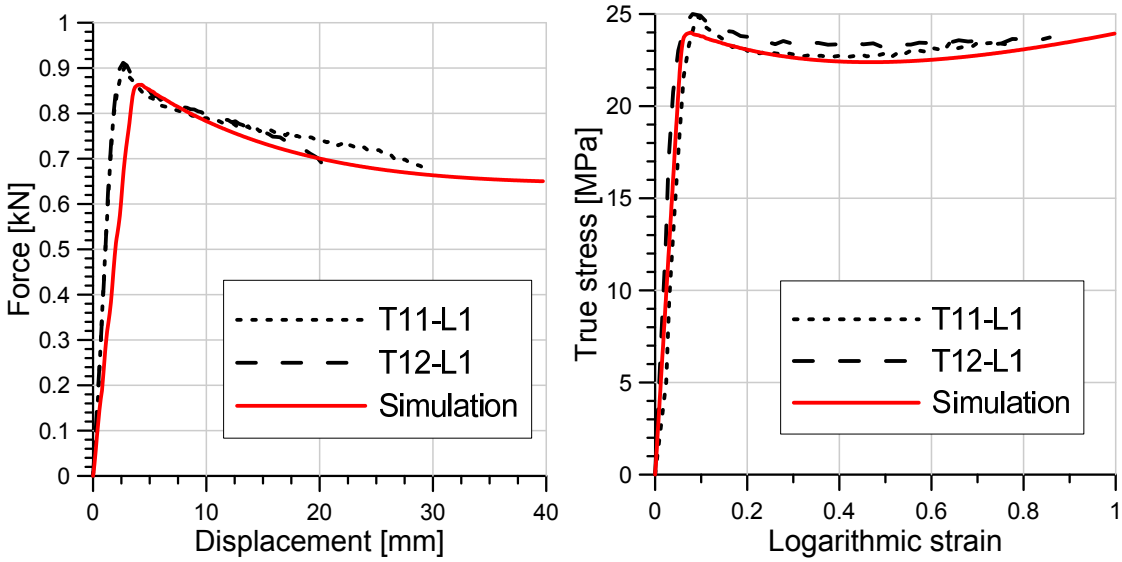

(a) Force-displacement diagram

(b) Stress-strain diagram

Figure 4.11: Diagrams comparing the model and the tests

a deviation in both peak load and unloading is observed. The peak load of the finite element model is a bit low. The gradient of the unloading is also too low compared to the material tests. Another difference is that the material test fractured before a stable load level was reached(seen for the intermediate strain rate in Figure 4.9a). This is not captured in the finite element analysis because the material model does not contain any fracture criterion. Figure 4.11b shows the stress-strain diagram. For these high-strain-rate tests the stress-strain curve is closer than the force-displacement curve. But there are some differences around the yield point; first the yield stress is a little low, then there is a slight difference in the softening, where the model predicts a too low gradient. The assumed Young's modulus, however, fits rather well, implying that the viscoelastic effects are more present when going from $\dot{\varepsilon} = 10^{-3}$ s^{-1} to $\dot{\varepsilon} = 10^{-2}$ s^{-1} than from $\dot{\varepsilon} = 10^{-2}$ s^{-1} to $\dot{\varepsilon} = 10^{-1}$ s^{-1}. The flat plastic response shown by the material tests in Figure 4.11b indicates that there might be heat effects impeding the hardening of the material.

4.3.2 Uniaxial compression

Three material tests were carried out in compression. Of these were two made at the lowest strain rate and one at the intermediate. The main objective of the compression testing was to find the α parameter. The mechanisms that decide the response to compression loading have been subject to less research than the

tension response. To define and compare these mechanisms is outside the scope of this thesis and the compression tests have thus been given less attention than the tension tests.

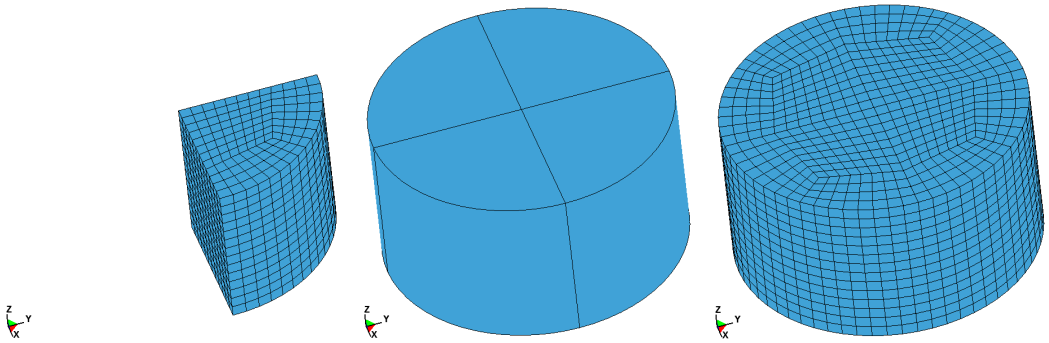

(a) The symmtric part used in the simulations

(b) The symmtric part mirrored

(c) The mirrored part with mesh

Figure 4.12: The symmetric part used in the simulations. And the same part mirrored to show the full geometry (no analysis was carried out using the geometry shown in Figure 4.12c)

The full-sized specimen had the dimensions; diameter, $D = 6$ mm and thickness, $t = 3.2$ mm (see Figure 3.7b). The finite element analyses were carried out using the geometry shown in Figure 4.12a. It has a boundary condition along both the surfaces facing inwards. This is defined to allow movement in the in-plane directions and no movement in the direction perpendicular to the surface. Any rotation at these surfaces was also prohibited. The top and bottom surfaces are defined in separate node sets. The top is defined to move with constant speed in mm/s. The bottom is locked in the thickness direction and allows movement in the radial direction. With these boundary conditions the near-frictionless situation from the material tests is captured and the specimen deforms uniformly

The mesh is made with approximately 4 elements per millimetre in both the radial and thickness direction. The strains and stresses are read from the same location as in the material test, i.e. a cross-section at the midpoint of the specimen.

Low strain rate, $\dot{\varepsilon} = 10^{-1}$ s^{-1}

Figure 4.13 shows the results of the low-strain-rate compression simulation. The force displacement diagram is closest to the response of the test. The transition from elastic to plastic behaviour happens for a load approximately 50 N higher in the finite element analysis than in the test. After this point the model represents the plastic behaviour quite well before it starts to deviate with a significant

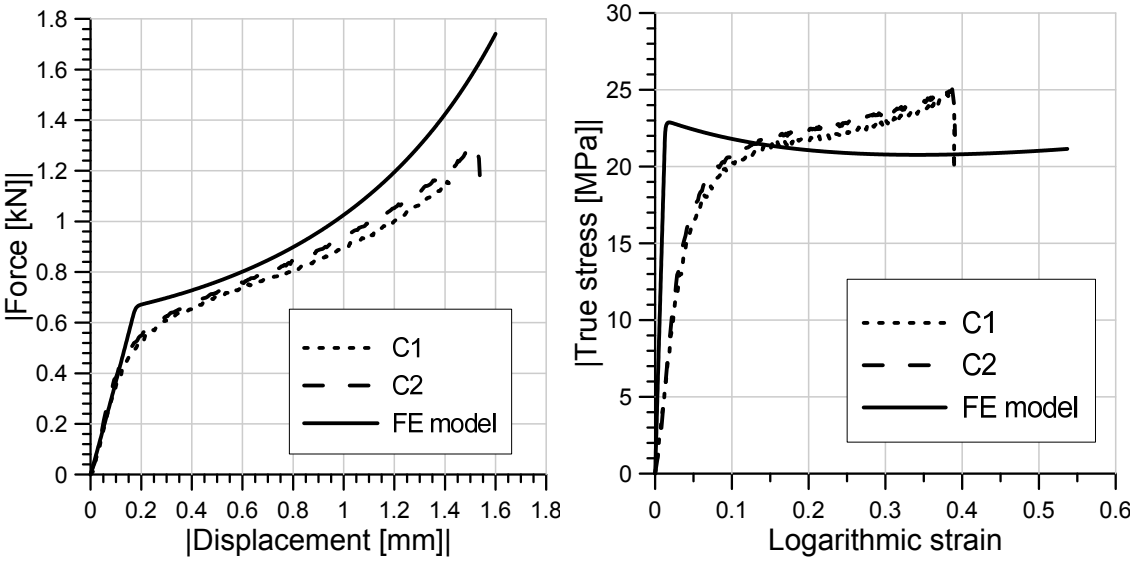

(a) Force-displacement diagrams of the tests and the FE model at $\dot{\varepsilon} = 10^{-3}\, s^{-1}$

(b) The stress-strain diagrams of the tests and the FE model at $\dot{\varepsilon} = 10^{-3}\, s^{-1}$

Figure 4.13: The results of the finite element model of the uniaxial compression test at $\dot{\varepsilon} = 10^{-3}$ s^{-1}

load increase. The stress-strain diagram will not be correctly represented for this material. This is because the numerical model represents the same stress-strain behaviour in tension and compression, i.e. a yield point followed by softening and then hardening. The only difference is the α value that defines how much higher the yield stress is in compression than in tension. When the material has a compression response with a gradual transition to plastic behaviour and then hardening directly afterwards (as shown in Figure 4.13b), the material model will have problems representing it.

Intermediate strain rate, $\dot{\varepsilon} = 10^{-2}$ s^{-1}

The finite element model describes more or less the same at this strain rate as for the previous. The main difference is that the increased strain rate makes the yield stress a little higher

It is seen from Figure 4.14 that the response deviates quite a bit. The global force-displacement response (seen in Figure 4.14a) is not completely off. It misses the transition from elastic to plastic behaviour and ends up on a higher maximum load. The stress-strain curve on the other hand is much less accurate. The reason for this is as explained for the low strain rate. The elastic behaviour, however, is

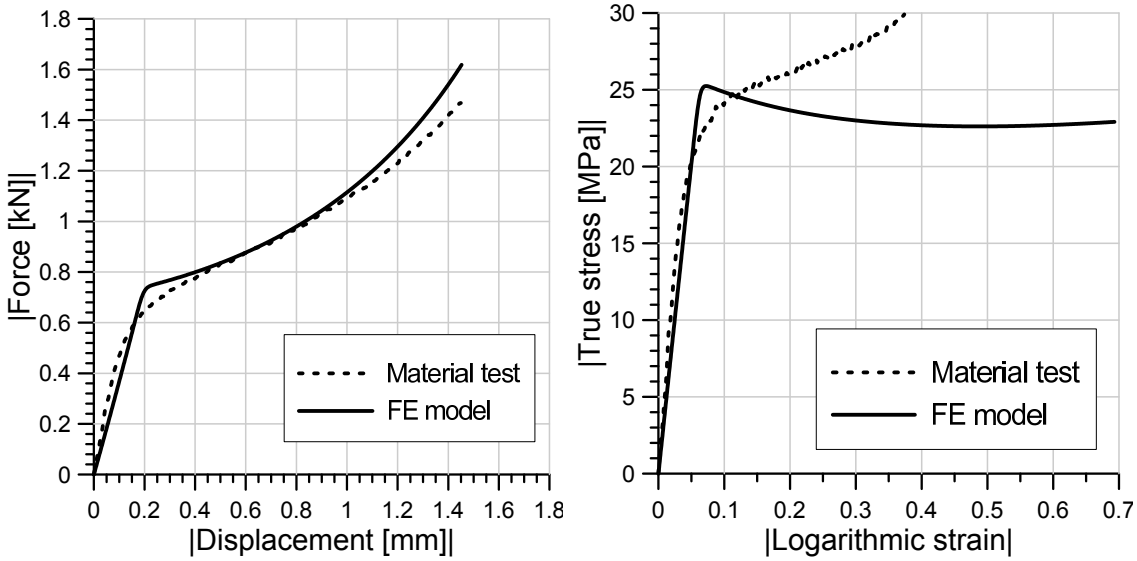

(a) Force-displacement diagrams of the test and the FE model at $\dot{\varepsilon} = 10^{-2}\, s^{-1}$

(b) The stress-strain diagrams of the test and the FE model at $\dot{\varepsilon} = 10^{-2}\, s^{-1}$

Figure 4.14: The results of the finite element model of the uniaxial compression test at $\dot{\varepsilon} = 10^{-2}$ s^{-1}

almost correct at this strain rate. This is because the applied Young's modulus is more correct for this intermediate strain rate than for the low strain rate (also seen for the unaxial tension tests).

4.3.3 Comparison and discussion

In general, the material model manages to represent the topical polypropylene well. There are, however, some major and minor deviations. In this section the results are compared and discussed.

The strain rate dependency is challenging to represent. This is especially true for this material because it has a larger difference in the yield stress between the highest and the intermediate strain rate than between the intermediate and the low. This makes the strain-rate relation less log-linear (cf. Figure 4.4). In addition the shape of the curves vary with the strain rate.

The strain rate dependency is shown in Figure 4.15. An obvious deviation is the viscoelastic behaviour. On the other hand shows Figure 4.15a that the strain-rate dependency of the yield stress is quite well represented by the simulations. When examining the yield points in Figure 4.15a it is seen that it is approximately 2

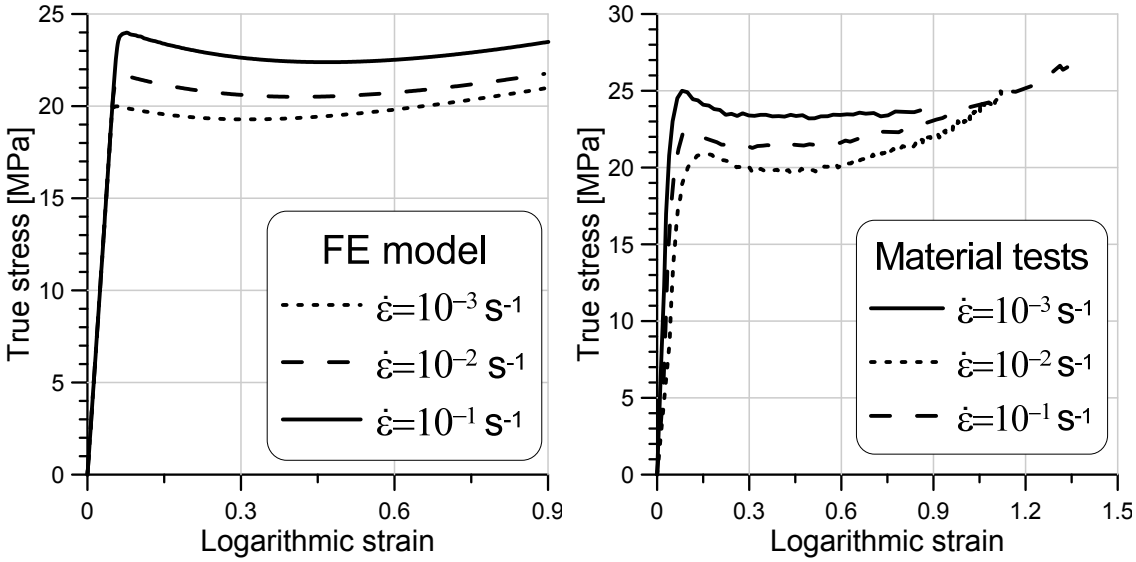

(a) The stress-strain relation for the finite element model

(b) The stress-strain relation for three different strain rates

Figure 4.15: Comparison of the strain-rate dependency of the finite element model and the material tests

MPa difference in the yield stress from strain rate to strain rate. Examination of Figure 4.15b reveals that the difference is approximately 1.5 from the low to the intermediate strain rate and 2.5 from the intermediate to the high strain rate, i.e. the mean difference over the spans is the same.

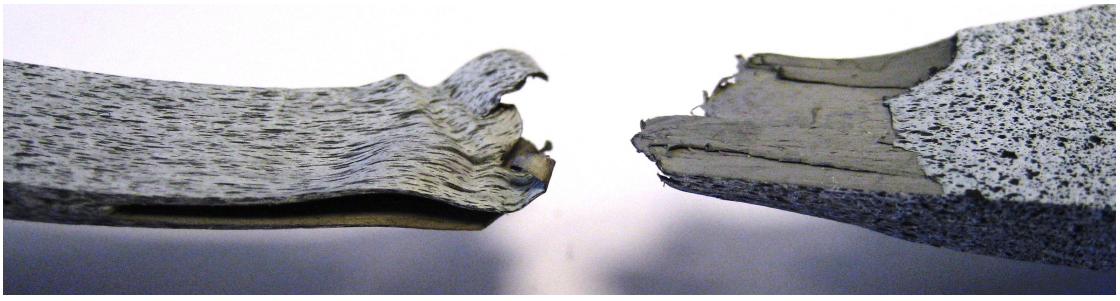

Figure 4.16: The fracture surface of test T5-L1

The graphs in Figure 4.15 also show that the representation of the softening does not fit perfectly, especially not for the lowest strain rate. The material tests in Figure 4.15b show a linear elastic behaviour almost all the way up to the yield point. But close to this point the behaviour becomes less linear. Figure 4.15a shows that this gradual transition is not represented by the material model. The

especially gradual softening seen in the slowest material test in Figure 4.15b is partly linked to the outer layer of the material (see Figure 4.16). This layer is, as mentioned in Chapter 2, the part of the material that has been in direct contact with the mould surface during the cooling phase of the manufacturing. It has therefore been cooled more rapidly than the rest of the material and may possess other mechanical properties. The skin on the topical PP shows a more ductile behaviour than the core material and is often intact even though the core material has fractured. The question is then; how is the adhesion between this layer and the core? If there is a distinct transition between the core and the outer skin, it might lead to a material behaviour that resembles the behaviour of a composite material. Such a transition may also mislead the Digital Image Correlation software into giving only the strains of the outer skin and not of the core material. It has also been observed that the outer skin becomes less distinct with increasing strain rate. Which might be part of the explanation to why the curves fit better with increasing strain rate.

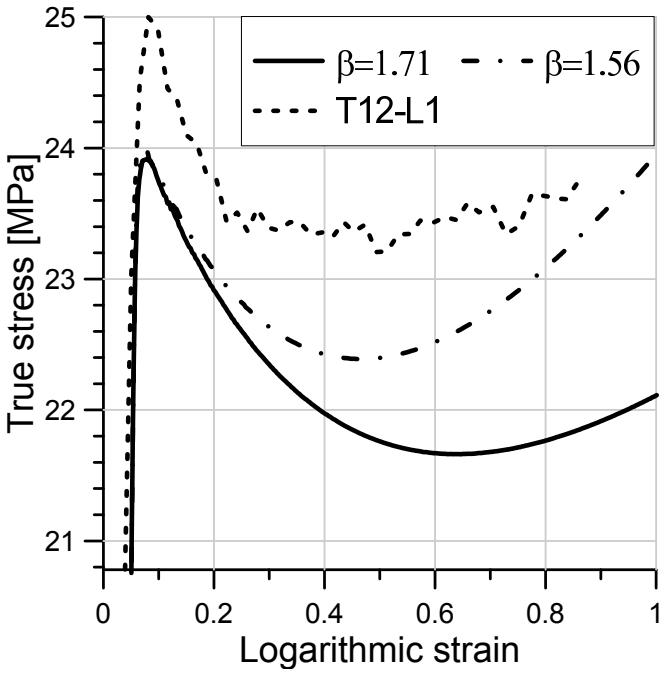

Figure 4.17: Comparison of hardening. T12-L1 is a high-strain-rate test. The two other curves are FE models with β as in the calibration ($\beta = 1.56$) and with β based on the high-strain-rate tests ($\beta = 1.71$)

The material model predicts more strain hardening than the material tests show. The main reason for this is assumed to be the heat effects that occur during high-strain-rate plastic deformation. These are, as mentioned earlier, not incorporated

in the material model. Another source of error linked to this is the dilatation parameter β. In the topical PP this parameter also varies quite a bit with the strain rate. This variation is not represented by the material model.

A short recapitulation of the effect of β (see Section 4.1 for details); β is directly dependent on the contraction ratio ρ (not the mass density) found from the material tests. The smaller the ρ value, the larger the value of β. A higher β value means that the dilation (increase of volume) is larger. When the volume increase is high the neck becomes less evident. The difference in β between the baseline test and the fastest tests is close to 0.15, which corresponds to a difference in ρ of about 0.07. Since the range of ρ is only $0 < \rho < 0.5$ this difference could have a significant effect. An assumption regarding the effect of β is that; due to the increase in volume the polymer chains are less oriented in the direction of the load, hence less hardening effect. Figure 4.17 shows the effect of β on the stress-strain relation. The lower curve is the FE model with $\beta = 1.71$, which is the β value found in the fastest material tests. The middle line represents the baseline model ($\beta = 1.56$) and the upper line is one of the high-strain-rate tests, T12-L1. The hardening in the lower curve ($\beta = 1.71$) is significantly less than in the baseline model and fits better with the hardening of the material test. On the other hand is the softening more correct for the baseline test. It is not certain that the effect shown in Figure 4.17 is solely because of ρ, but the variation of this parameter certainly has some effect.

The material is anisotropic (cf. Chapter 3). Since anisotropy is not included in the material model, the material calibration is dependent on the direction of the loading. For the topical PP the difference between the longitudinal and transversal response seems to correspond quite nearly to the difference between two strain rates in the longitudinal direction. This relation is most probably a coincidence, but still worth noticing. The graphical representation is seen in Figure 4.18. The agreement is quite good, especially for the tests done at the high strain rate and the finite element simulation at the intermediate strain rate. Here the maximum load, the yield stress and the strain hardening agrees nearly perfect. Some unevenness is observed in the unloading of the material test in Figure 4.18a and none of the two tests reach a stable load before fracture. For the comparison of the intermediate material tests and the slow finite element model, the accordance is slightly less. The strain hardening seen in the material tests in Figure 4.18d is the most prominent strain hardening of all the 14 tests. If it had not been this prominent, the agreement with the FE simulation would have been even better.

There are some sources of error related to the calibration procedure. The first is the input data from the DIC. If for example the camera frequency is set too low, the result can become too coarse, i.e. contain too few data points to correctly

describe the deformation. Some additional uncertainty is connected to the speckled pattern painted on the specimens (more in Chapter 3). The next thing is the decision regarding the baseline test. There might be properties that could be described better by choosing one of the other material tests as basis. Even though the calibration guidelines state that the baseline test should be a test from the lowest strain rate, this is not an absolute demand. In this thesis a test from the intermediate material tests was considered, but the calibration did not turn out more optimal than the calibration based on the low-strain-rate test. After choosing the baseline model and starting the calibration the next uncertainty is, as mentioned in earlier sections, Young's modulus. Here the DIC makes up a mediocre foundation for a certain decision, and the best thing is to find it from tests designed for deciding this parameter. When evaluating the yield stresses the main uncertainty is connected to describing the strain rate dependency. As will be seen in the numerical validation of the material model, the strain-rate dependency is not necessarily log-linear for large strain rates. This might be solved by adding a high strain rate test to the linear regression, thus adjusting the fit to this kind of response. The cost of this being reduced accuracy in modelling of the low strain rate response. The macroscopic approach to the microstructure of the material [9] can also be a source of error. The microstructure varies quite a bit from polymer to polymer, and some structures might be easier to fit to the material model than others. And as closure, some human error might be present in treating the experimental data. This source of error is of course endeavoured minimized by the author.

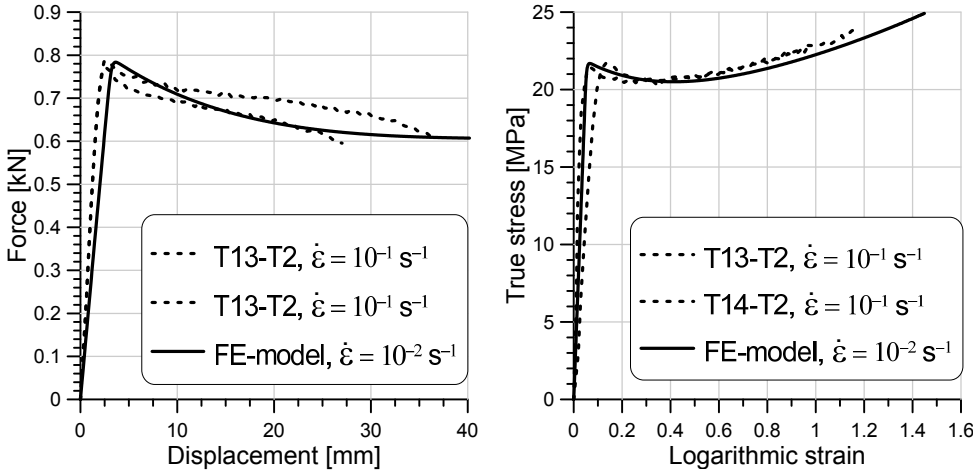

(a) Force-displacement diagram

(b) Stress-strain diagram

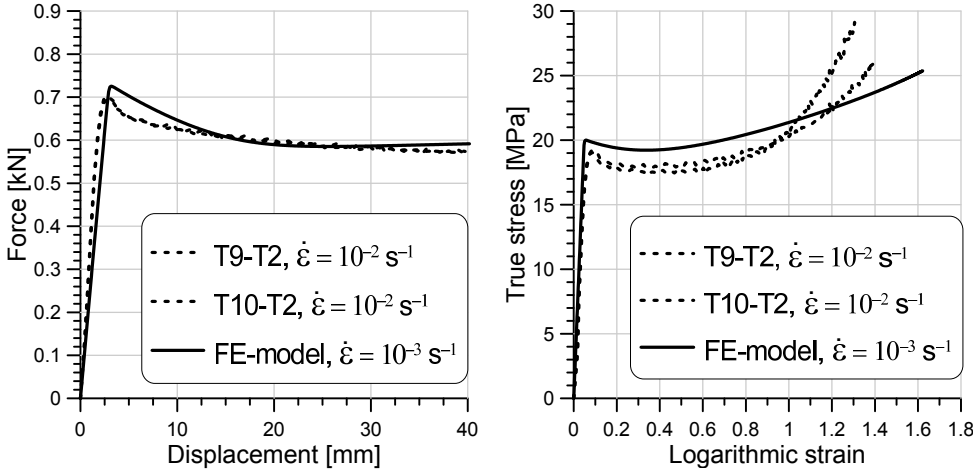

(c) Force-displacement diagram

(d) Stress-strain diagram

Figure 4.18: Comparison of the response of the high strain rate and intermediate strain rate transversal material tests and the intermediate and slow strain rate FE simulations, respectively

Chapter 5

Validation

Two different validation tests were carried out. The first is a tension test using a plate with a centric hole and the other is a high-strain-rate test using a machine known as drop tower. The main objective of the validation is to test a wide range of the properties of the calibrated material model. The chapter is divided into one section for each test. Each section is divided into the following four parts; the test set up, the numerical discretization, the results and the conclusion. In the conclusion, the results are compared and discussed.

5.1 Plate with centric hole

This test was chosen because of its pure and simple loading. In spite of the simple loading the load response is more complex and gives good information about how the material model manages to represent more complex deformations than those found in the calibration tests.

5.1.1 The material test

The specimen is a 3.1 millimetre thick rectangular plate with a centric hole. The force is applied in the longitudinal direction, which is oriented along the axis parallel to the side that measures 160 millimetres (see Figure 5.1). The point of making the hole is that it creates two similar gauges, one at each side of the hole. By varying the strain rate it is possible to evaluate how the model manages to represent the strain rate dependency for more complex load responses than in the

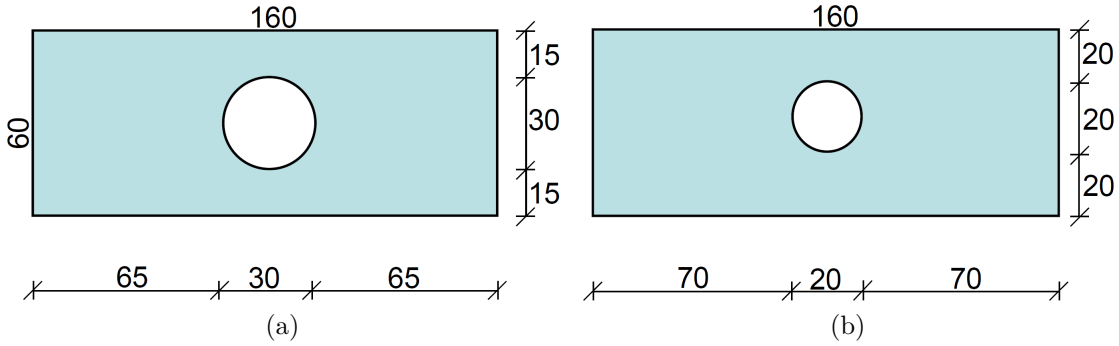

Figure 5.1: The specimens used. The large hole to the left and the small to the right

calibration tests. Two hole diameters at two different deformation velocities were tested. The tests are summarized in Table 5.1.

Test number	Test name	Deformation speed [mm/s]	Hole diameter [mm]	Gauge length [mm]	
				Gauge 1	Gauge 2
1	D1V1	0.05	30	15.39	15.19
2	D2V1	0.05	20	20.09	20.44
3	D1V2	0.5	30	15.07	15.33
4	D2V2	0.5	20	20.54	19.8

Table 5.1: The specifications of the four validation tests

The gauge lengths in Table 5.1 were supposed to be equal (see Figure 5.1) but a slight difference in the placement of the hole was detected. This deviation results in a slightly unsymmetrical response in some of the tests.

The tests were named as shown in Table 5.1. The principle is that D"number" gives the diameter, where D=30 mm is named 1 and D=20 mm is named 2. The V"number" gives whether the deformation speed is 1 = 0.05 mm/s or 2 = 0.5 mm/s.

The specimens were tested in the same machine as the material tests, namely a Dartec M1000 RK with a 20 kN load cell connected to an Instron controller. The clamps were mounted approximately 30 millimetres from the edge of the plate making the effective specimen length 100 millimetres. Digital image correlation was used to capture the deformation. Two cameras were applied; one was fixed at the surface with the hole, the other was fixed at the surface perpendicular to the surface with the hole, i.e. monitoring the thickness. To be able to process the pictures with 7D, the specimens were painted with the same speckled pattern as

the material tests (see Figure 5.2).

The speed was set in millimetres per second. The velocities of 0.05 mm/s and 0.5 mm/s were set to give strain rates in the gauge areas of approximately 0.0025 s^{-1} and 0.025 s^{-1}, respectively.

$U_{l,25}$	The longitudinal displacement found 25 millimetres above the hole. Shown as the upper red dot in the figure to the right
$U_{l,C}$	The longitudinal displacement at the "top" of the circle. Seen as the lower red dot in Figure 5.3a
$U_{t,1}$	The transversal deformation of gauge 1. Shown as U1 in the figure to the right
$U_{t,2}$	The transversal deformation of gauge 2. Shown as U2 in the figure to the right
F	The force needed to needed to deform the specimen. It is the top clamp that moves, making this the point where the load is applied

Table 5.2: The parameters that are to be compared

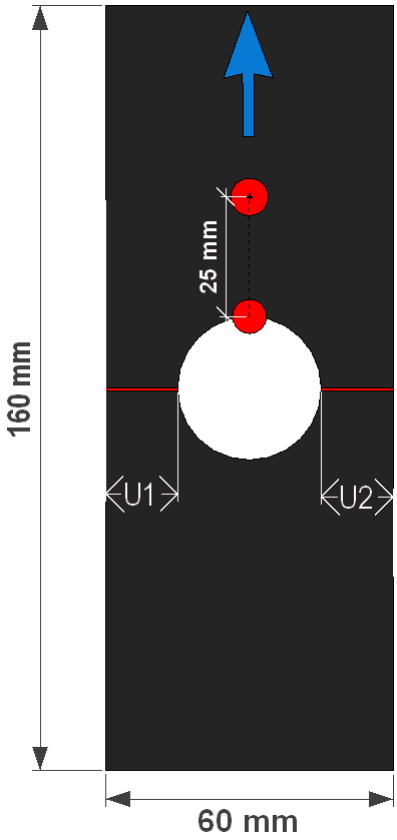

The post-processing was mainly carried out using 7D and Matlab. The main interest in these tests was to see how the longitudinal and transverse deformation and the force-displacement relation were represented by the finite element model. On this basis a collection of parameters were chosen for the comparison of the tests and the finite element analyses. The parameters and their location are shown in Table 5.2. In order to compare these displacements, they had to be taken from the same location in both the test specimen and the finite element model. The process of collecting the deformation data started with 7D. The pictures taken during the test were processed in the same way as the material tests in Chapter 3. The difference was that the displacements were added to the output. The matrices constructed by 7D containing the strain and displacement data were loaded into Matlab. A Matlab script was then used to define the points from where the deformation was to be gathered. The same script also output the needed

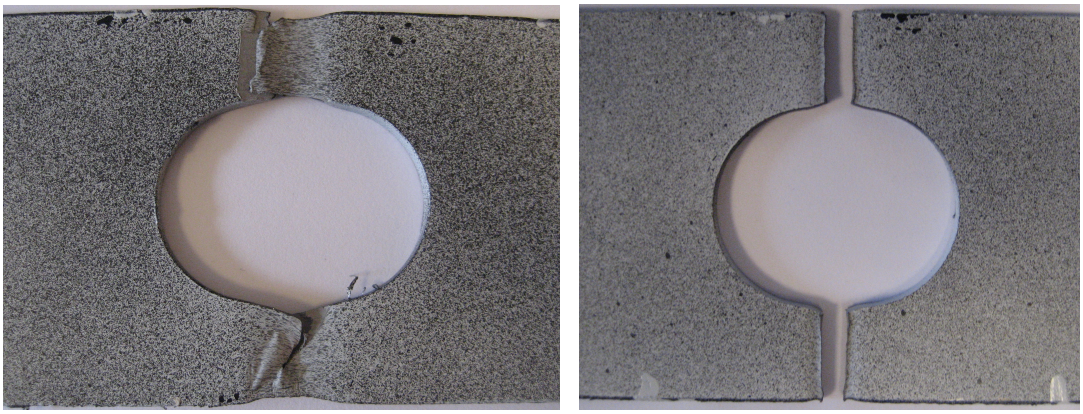

(a) The specimen used in test D1V1 (b) The specimen used in test D1V2

Figure 5.2: The specimens used in the two tests where D=30 mm. The same behaviour was seen for the specimens with D=20 mm

deformation vectors. An additional script was made to find $U_{t,1}$ and $U_{t,2}$. The script was similar to the one used for treating the test data from the compression tests. It used the pictures directly from the camera, made them into black and white and found the first and last white point at each gauge. The difference between these points in each gauge was stored for every picture, resulting in two displacement vectors describing the displacement $U_{t,1}$ and $U_{t,2}$ (the scripts can be found in Appendix B). $U_{t,1}$ and $U_{t,2}$ were stored until a fracture occurred in the gauge, which in some cases was a bit earlier than the end of the test.

The load response was much as expected for the four tests. The load level was inversely proportional to the hole size, the peak load increased with increasing strain rate and the fast tests fractured faster than the slow ones. Yet again the fracture surfaces were subject to some extra examination. These were very different in the slow and the fast tests. The two specimens with D=30 mm are shown in Figure 5.2. In Figure 5.2a it is seen that the external skin becomes clearly visible in the tests at the lowest speed. Since the strain data from the gauge is only used indirectly in these analyses, there should be minimal effect of the layer on the load response. Apart from this it is seen that the cross-section of the slow test is significantly reduced in the gauges. At the highest speed the fracture was much more sudden, something that is also shown in Figure 5.2b. The gauge cross-sections are only reduced very locally. Much of the deformation is no longer visible because the material retracted a bit after fracturing. All the results can be found in Appendix A.2.

5.1.2 The finite element model

This test was chosen for its simple yet complicated nature. The complicated part of the problem became clearer in the process of creating a good finite element model.

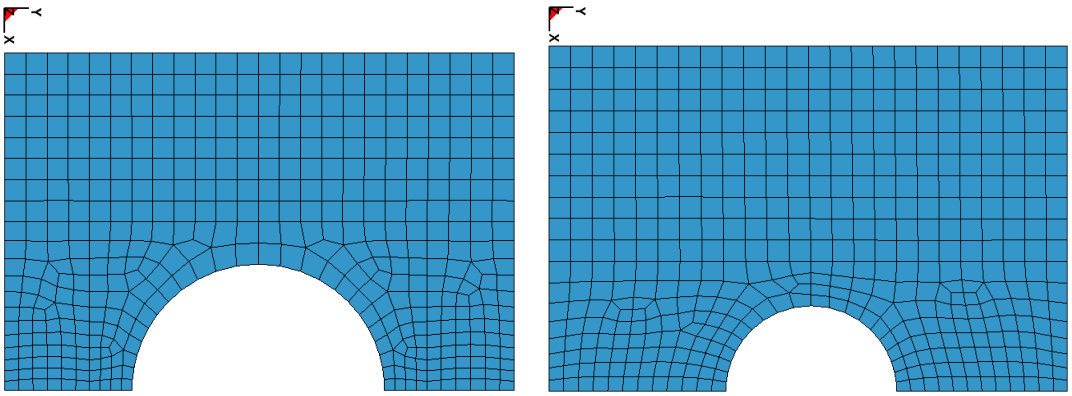

(a) The geometry with D=30 mm (b) The geometry with D=20 mm

Figure 5.3: The meshed geometry used in the finite element analyses (D1V2 and D2V2)

Figure 5.3 shows two of the applied meshed geometries. Symmetry about the mid-transversal axis was applied resulting in a model representing 40 mm of the total 160 mm. Since the holes were not placed entirely symmetric, there was no symmetry about the longitudinal axis. This asymmetry also meant that four separate models (one for each test) had to be made in order to attain the wanted level of accuracy. The mesh is graded so that it is finest near the gauge and coarser further away from the gauge. Four elements were used in the thickness direction. In spite of looking a bit untidy, the mesh performed well with the fully integrated element formulation "2" of LS-DYNA [6]. Part of the reason for the untidy impression is the unsymmetrical placement of the hole. This makes the refinement of the mesh close to the gauge more challenging.

A boundary condition restraining the longitudinal displacement and allowing transversal displacements was applied in the gauge. The deformation was applied to the model using a boundary condition defining a prescribed motion. This was applied along the edge opposite the hole. Other mesh geometries and boundary conditions were tried, but were all less optimal than the solution presented above.

The correct strain rate was found from the DIC data. First the critical cross-section had to be found. This was done using a similar script as for the material tests, i.e. a script using the mean values of the longitudinal strain to locate the

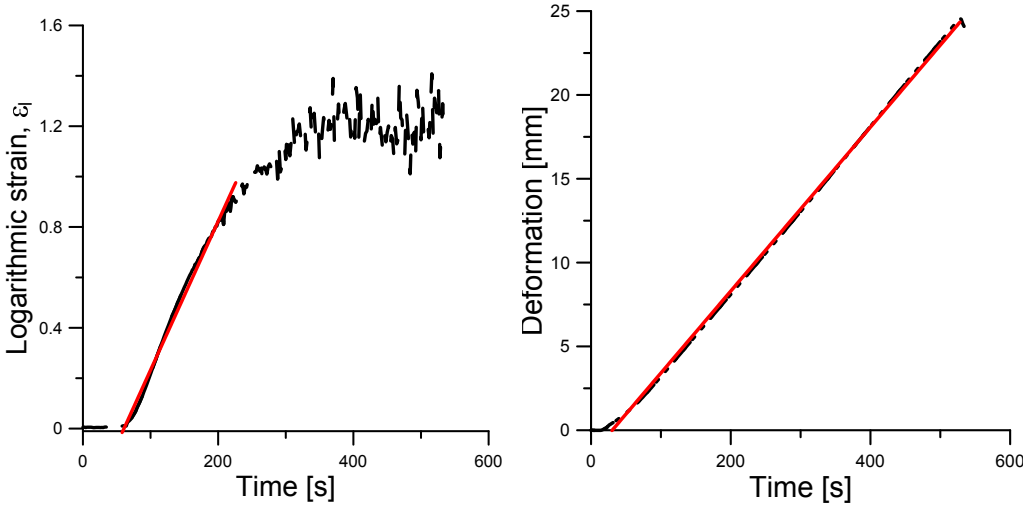

(a) Regression of the longitudinal strain. The gradient of the red line corresponds to the strain rate measured in the gauge of the material test

(b) Regression of the longitudinal deformation. The gradient of the red line corresponds to the deformation speed experienced in the gauge of the material test

Figure 5.4: Calculation of the strain rate and the deformation rate of test D2V1

critical cross-section. The script found that the critical cross-section was located at the mid-point of the gauge. Then a strain-time diagram (seen in Figure 5.4a) was plotted and a linear regression was fitted to the linear part of the resulting diagram (the red line in Figure 5.4a). As a validation of this, the same was done for the longitudinal deformation. The longitudinal displacements were output from the wanted locations as defined in 7D. Both operations were carried out using Matlab and the scripts are added in Appendix B.4.

The analyses went well after preparing the model as described above. When they were finished the results were gathered from points in the model corresponding to those defined on the specimen.

5.1.3 Results

In this section the results of both the material tests and the finite element analyses are presented. The finite element analyses will consequently be shown as full lines in the plots, the model consequently with dashed lines. The presentation will start with the tests done with v=0.05 mm/s and then move on to the ones where v=0.5 mm/s. There will be a short discussion for each test and a finishing comparison and discussion at the end.

D1V1

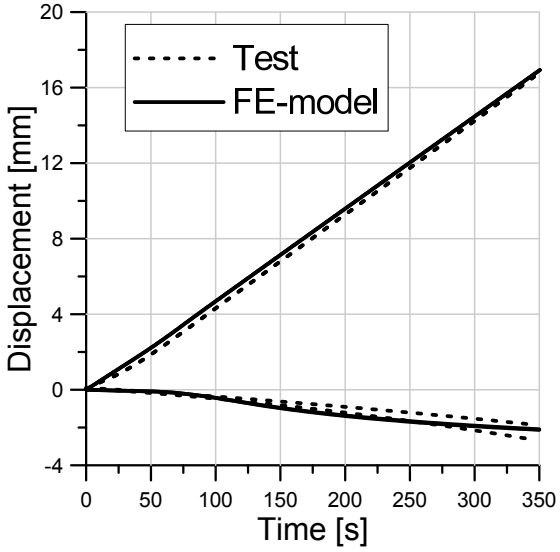

(a) The displacements. The upper curves represents the longitudinal displacements ($U_{l,25}$, $U_{l,25}$ $U_{l,C}$). The lower curves represent the transversal displacements ($U_{t,1}$, $U_{t,2}$)

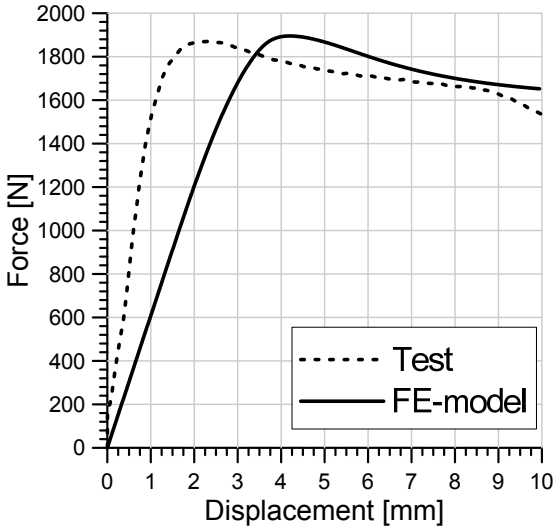

(b) The force plotted against the displacement

Figure 5.5: The results of the test and the FE-simulation of D1V1

Figure 5.5 shows the results of the test and analysis of D1V1, i.e. the test where D=30 mm and v=0.05 mm/s. It is seen from Figure 5.5a that the displacements are quite well represented. A slight difference in the gradients is observed. This difference occurs because the deformation speed in the physical test is not constant. It is a bit lower in the beginning and then it stabilizes at a speed similar to that of the analysis. The analysis, however, is defined to be constant from the start until the end.

The force displacement diagram in Figure 5.5b agrees less with the material tests than Figure 5.5a. It is seen that the modelled peak load and plastic response is more or less correct. This means that the main deviation is found in the stiffness, which is too low. This can be corrected by adjusting Young's modulus. The cost of this being that the peak load becomes slightly higher, and thus less correct.

Figure 5.6 shows the force-displacement response for a higher value of Young's modulus. The correction makes the stiffness nearly correct and yields only a minor increase in the peak load. In this test the strain rate in the gauges is approximately 0.0025 s^{-1}. If the calibration results are taken as reference, Young's modulus should be somewhere between 300 and 400 MPa for this strain rate. The

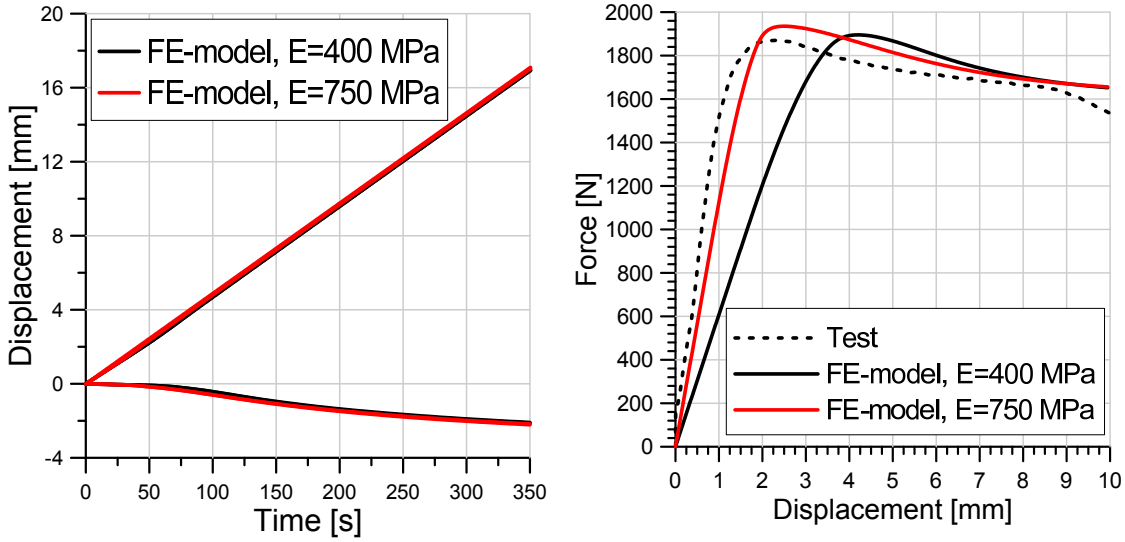

(a) The displacements

(b) Force-displacment diagram

Figure 5.6: Similar diagrams as in 5.5. The red curves represent the analysis where E is increased in order to make the initial stiffness match better with the test

most correct analysis result is, however, attained with a modulus as high as 750 MPa. The exact reason for this is not clear. The increase in Young's modulus causes a negligible decrease in the deformations (seen in Figure 5.6a).

D2V1

The results of this test is in many ways similar to the first. An important difference is the load level. Since this hole is only 2/3 the size of the largest, the forces are significantly larger.

Figure 5.7a shows that the deformation fits even better for this test than the previous. The variation in the longitudinal displacement is captured by the model and is seen as the second curve from the top. This curve represents $U_{l,C}$, i.e. the displacement at the top of the circle. This variation is, however, not captured by the model in the displacement 25 millimetres above the circle, $U_{l,25}$, which has a constant gradient. The gauge displacements fit very well, and represent the displacement more or less exact.

A similar behaviour as for D1V1 is observed in Figure 5.7b. The stiffness is too low, but the peak load and the plastic behaviour fit better with the test. The curve representing the test where E=750 MPa is also added to Figure 5.7. The

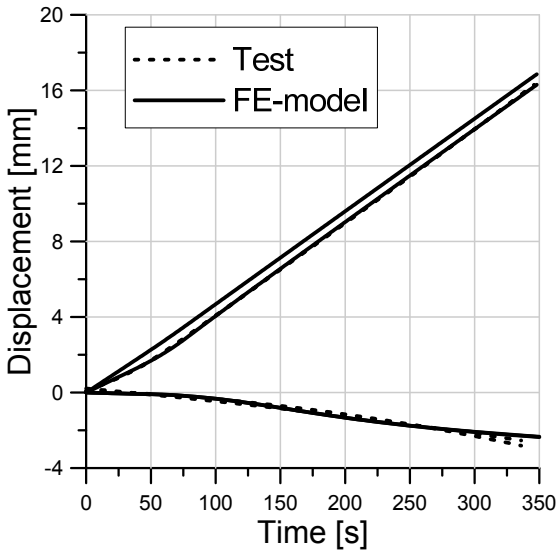

(a) The displacements. The upper curve represents the longitudinal displacement $U_{l,25}$. The curve parallel to this is $U_{l,C}$. The lower curves represent the transversal displacements ($U_{t,1}$, $U_{t,2}$)

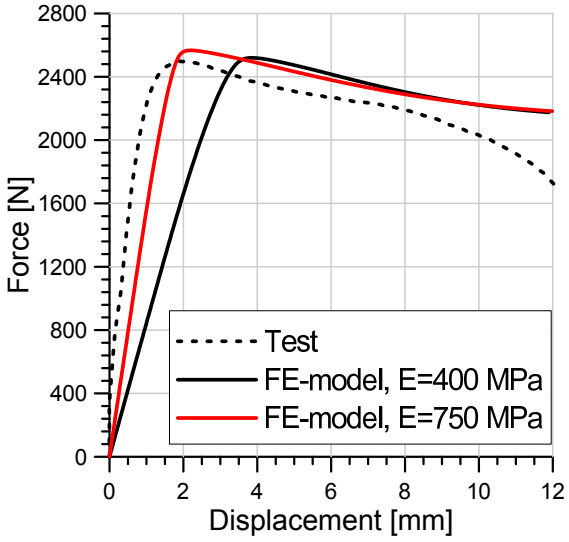

(b) The force plotted against the displacement $U_{l,25}$

Figure 5.7: The results of the test and the FE-simulations of D2V1

agreement becomes significantly better, again reducing the accuracy of the peak load. The difference in displacements is not shown because it was so small that it could be neglected.

D1V2

This was the first test at the high deformation speed. The main difference between the velocities was the gauge deformation, which was much more local for this and the next test than for the two previous. In addition some differences were observed in the plastic response and the longitudinal displacements.

Figure 5.8 sums up the results. The difference in timespan should be noted. These tests were through in about 20 seconds, while the slower ones took between 5 and 10 minutes. The displacements are described quite accurately. Figure 5.8a shows that the gradient of the longitudinal deformation in the material test (the upper dotted line in Figure 5.8a) is varying. It has an initial gradient slightly lower than that of the model, then it gradually approaches the model, before it ends up with a higher gradient than the model. The longitudinal displacements $U_{l,25}$ and $U_{l,C}$ from the model are different from each other in this test too. $U_{l,C}$ (the second full

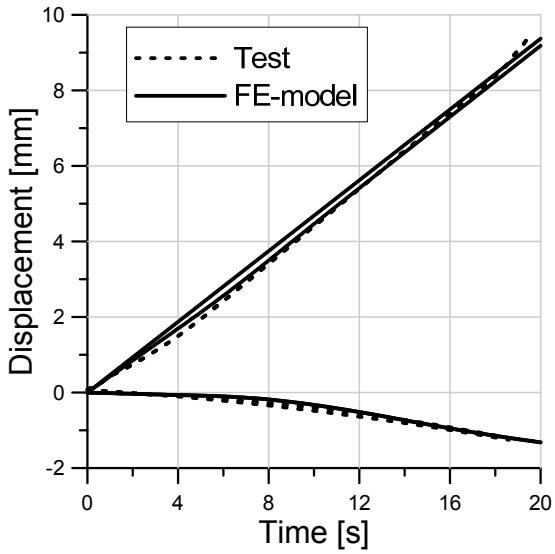

(a) The displacements. The upper curve represents the longitudinal displacement $U_{l,25}$. The curve parallel to this is $U_{l,C}$. The lower curves represent the transversal displacements ($U_{t,1}$, $U_{t,2}$)

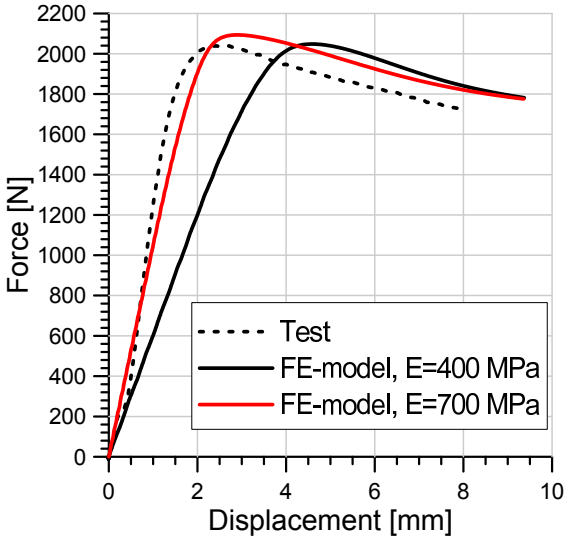

(b) The force plotted against the displacement $U_{l,25}$

Figure 5.8: The results of the test and the FE-simulations of D1V2

line from the top) is closer to the deformation of the test than $U_{l,25}$. None of them capture the last gradient increase seen in the model.

The force-displacement diagram is shown in Figure 5.8b. The peak force agrees almost perfectly for E=400 MPa and is only slightly off for the adjusted Young's modulus. The transition from elastic to plastic behaviour is a bit different. The model where E=700 MPa has a more sudden transition. The test and the simulation where E=400 MPa has a more gradual transition. The difference in the load level at the end of the test indicates that the gradient of the model's plastic behaviour is a little low.

D2V2

This specimen was the one with the highest difference in gauge size. Gauge 1 is 0.74 millimetres wider than gauge 2. This results in a slightly unsymmetrical response. Because of the small hole and the high deformation rate, this is also the test where the highest load level occurs. The results of this test are shown in four instead of two plots, this to avoid plots containing too many curves.

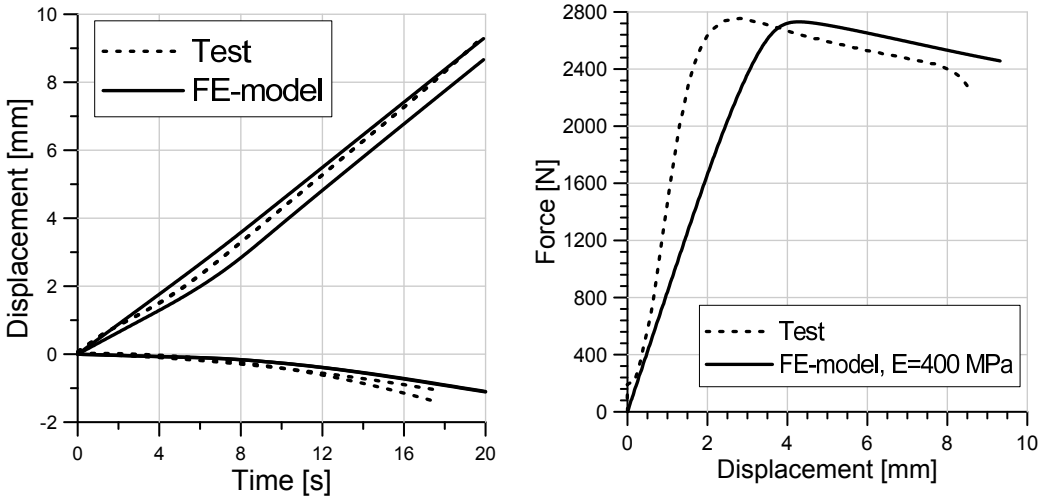

(a) The displacements. The upper curve represents the longitudinal displacement $U_{l,25}$. The curve parallel to this is $U_{l,C}$. The lower curves represent the transversal displacements ($U_{t,1}$, $U_{t,2}$)

(b) The force plotted against the displacement $U_{l,25}$

Figure 5.9: The results of the test and the FE-simulations of D2V2

Figure 5.9 shows the results of D2V2. The longitudinal displacements of the model are more scattered in this test than in the previous tests. The test result is now located between the two curves instead of corresponding to one of them. It is still only $U_{l,C}$ from the model that has a changing gradient. A slight scattering is also seen in the test's transversal gauge displacements. The corresponding displacements from the finite element model deviate a bit but end up at approximately the same displacement.

The force-displacement diagram shows similar results as the previous. The differences are a higher and more correct peak load and a slightly better agreement in the stiffness. If the stiffness is adjusted the results become as shown in Figure 5.10.

The adjustment of Young's modulus results in changes in both the displacement and the force-displacement diagram. The longitudinal displacement $U_{l,C}$ of the model now corresponds better to the longitudinal displacement of the test. In addition, the transversal deformations have moved down a notch, which results in a better fit with the transversal deformations of the test.

The force-displacement relation is very well represented. In this case both the stiffness and the peak load are correct. The deviation is now located at the transition from elastic to plastic material behaviour, where the test turns and becomes just slightly steeper than the simulation.

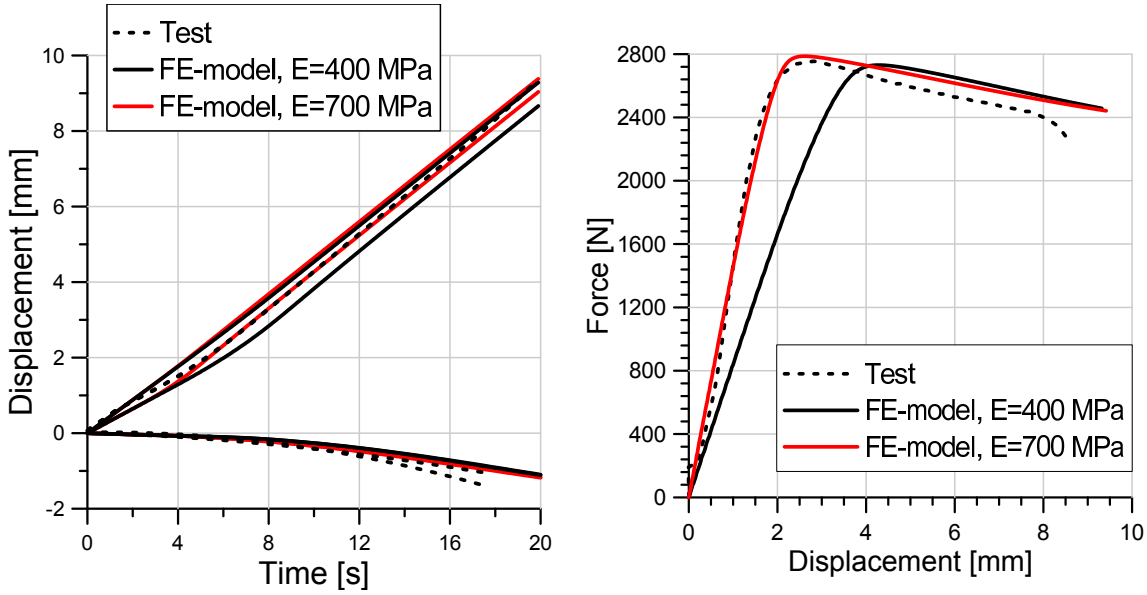

(a) The displacements. The upper curve represents the longitudinal displacement $U_{l,25}$. The curve parallel to this is $U_{l,C}$. The lower curves represent the transversal displacements ($U_{t,1}$, $U_{t,2}$)

(b) The force plotted against the displacement $U_{l,25}$

Figure 5.10: The results of the test and the FE-simulations of D2V2

5.1.4 Comparison and discussion

The four tests have proved that the material model is capable of describing quite complicated deformations.

Figure 5.11 shows the strain-rate dependency of the tests and the finite element simulations. The tests show a minimal increase in Young's modulus with increasing strain rate, indicating that modelling of the viscoelastic behaviour can be left out without losing much accuracy. When examining the strain rate dependence, it is seen that this is very well represented by the model. The transition from elastic to plastic behaviour is quite gradual in the tests. In the simulations this gradual transition is only captured by the geometry with the largest hole. The geometry with D=20 mm has a much more distinct transition. For the plastic deformation of the tests it is seen that the slowest tests almost stabilize at a constant load level before the fracture occurs. This is not the case for the faster tests, which descend constantly until the fracture occurs at about 8 millimetres of longitudinal displacement. The simulations vary a bit in their representation of this plastic behaviour. The two geometries where D=30 mm display the same stabilizing

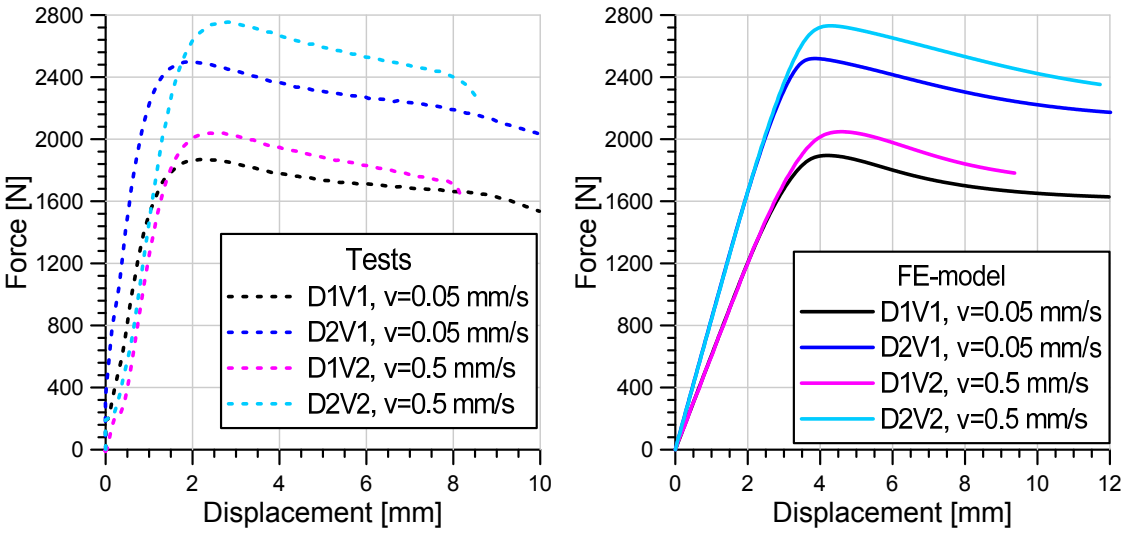

(a) The strain-rate dependency observed in the tests

(b) The strain-rate dependency observed in the FE-simulations

Figure 5.11: The strain-rate dependency

trend as the tests for both deformation rates. The tests with the smaller hole has a behaviour resembling that of the fastest tests, i.e. a constant decrease of capacity. The slowest of these two (D2V1) stabilizes gradually, but much slower than the test.

These tests bring new information regarding Young's modulus. Since a major part of the deformation was elastic, the response was quite dependent on this parameter. In the calibration tests the fastest tests deformed with $E \simeq 600$ MPa and the slowest with $E \simeq 350$ MPa. In these validation tests the lowest strain rate was only slightly higher than the lowest strain rate applied in the calibration testing, but still $E = 750$ MPa gave good results. It is also a bit strange that Young's modulus had to be slightly lowered in order to attain the best fit with the fastest test. The logic assumption would be the opposite. This indicates that Young's modulus may vary a bit, not only with the strain rate but also with other factors linked to the geometry and the load application.

The sources of uncertainty are always present. An obvious source of error introduced quite early in this testing is the unsymmetrical placement of the holes. Digital image correlation also has its known weaknesses. The process of defining the points from where the deformations were to be found is also a significant source of inaccuracy. This was done with the measurement tools in 7D, which resulted in approximative distances. The method used to find the transversal deformation of the gauges utilizes pictures with a wide spectre of grey scales. These were con-

verted into pictures containing only black or white by defining a limit for where white ended and black started. The number of white pixels will vary with where this limit is set, thus introducing an inaccuracy in the measuring of the gauge widths.

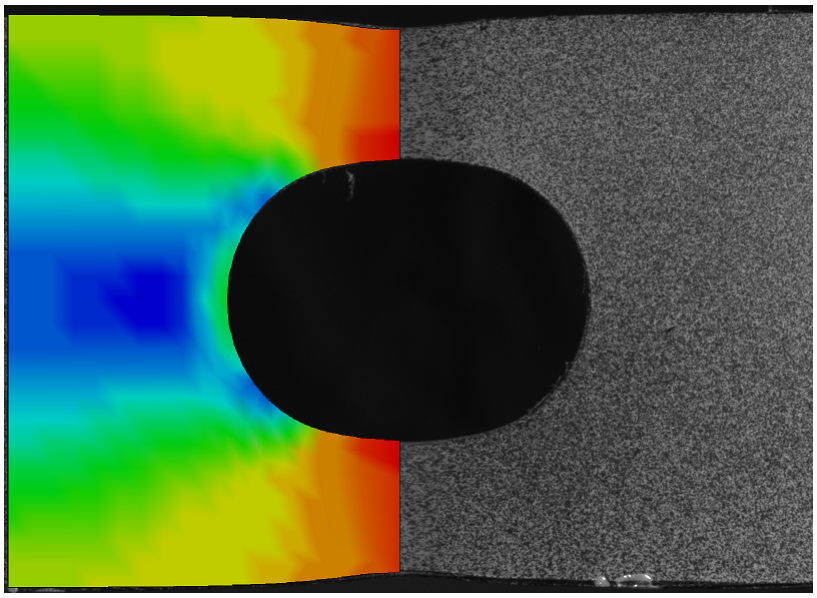

Figure 5.12: The test D1V1 and the model deformed approximately 10 mm in the longitudinal direction

Despite these inaccuracies, the finite element simulations managed to represent the problem quite well. This is exemplified in Figure 5.12, which shows the deformed specimen and model. It is seen that the shape of the specimen and the model is very similar. The load response became close to perfect after the slight adjustment of the elastic parameters. The plastic behaviour was well represented through the correct peak loads and the more or less correct plastic responses.

5.2 Impact loading on plate

This test is basically a steal spear impacting a plate of the material with a user-defined kinetic energy. The main application of the material model is, as mentioned earlier, high-strain-rate problems like impact and crashworthiness simulations [9]. The response to the high strain rates achieved in this test is thus of interest. The section will have a similar structure as the previous.

5.2.1 The material tests

The specimens used in these tests were very simple. They were quadratic plates with 10 millimetre edges and a 3 mm thickness.

The test machine was a CEAST 9350 drop tower. The basic components of the test machine are a mechanism to control the speed, weight and drop height for the steel spear and a mounting mechanism for the test specimens. The spear can be equipped with different end pieces. The one used in these tests was a half sphere with a diameter of 20 mm. Before mounting the specimen the wanted weight was placed on the spear. The plate was then mounted in the machine simply by putting it on a ramp. After a safety door was closed, a clamp was lowered to lock the plate in place. The clamp held the specimen down using a pressure of 5 bar. The next point was to configure the wanted impact energy. After this was configured the test rig was ready, and the "play" button could be pushed.

Table 5.4 on page 75 shows the specifications of tests carried out in the drop tower. They are named successively. The mass column gives the weight of the falling spear and the energy is calculated according to Equation (5.1).

$$E = \frac{1}{2}mv^2 \tag{5.1}$$

The impact energy was adjusted to the capacity of the plate. Meaning that if a test fractured, the energy was adjusted downwards, if it did not fracture, the energy level was adjusted upwards. This approach is illustrated in Table 5.4. The table also shows that the capacity of the specimens used was somewhere between 55 and 60 J. In addition the energy was varied by changing either the mass or the impact velocity.

The data used for comparison with the finite element simulations were logged by the drop tower, through a sensor in the spear. The comparison was done with the force-time and the force-displacement relations.

5.2.2 The finite element model

This finite element model has to represent a response which is quite different from the previous validation test. It is an impact problem with short response time and significant inertia forces. The objective is to test how the material model manages to represent a problem involving such high strain rates.

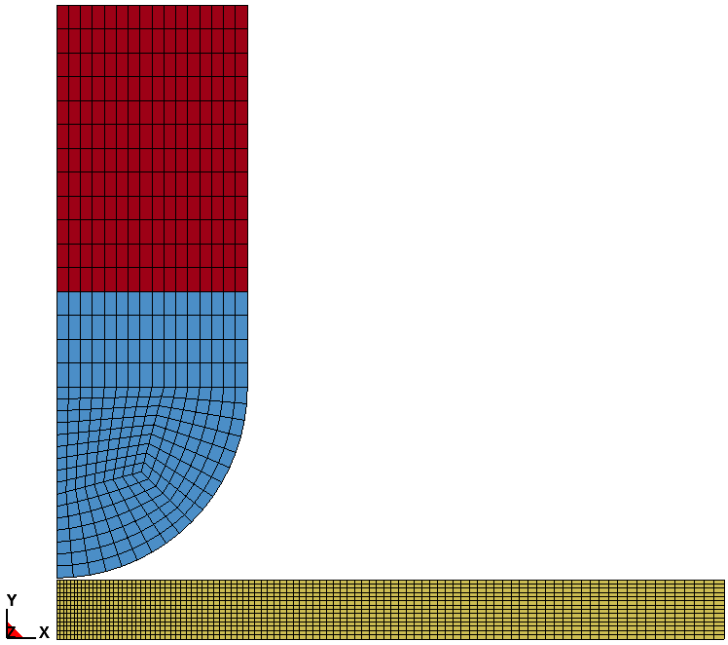

Figure 5.13: The meshed geometry

An axisymmetric approach was used to model the problem. This means that only a radian of the full geometry was modelled. Figure 5.13 shows the modelled section. The y-axis at x=0 is the symmetry axis defined by LS-DYNA. This means that the model had to be constructed with this axis as a centre. The placement of the y-axis can be seen in Figure 5.13, it corresponds to the longitudinal axis of the spear. The axisymmetric definition was given through the use of element definition 15 in LS-DYNA [6]. The optimal number of Gauss points varied with the impact energy. In the simulations of the tests where the plate eventually fractured, four Gauss-points were used, in order to eliminate the hourglass energy that would else have occurred when the material was deformed to its limits. In the tests that absorbed the fracture, a reduced integration scheme involving two Gauss-points was successfully used.

The model was split into three parts. First the plate, the yellow part in Figure 5.13, was modelled. This is only a rectangle measuring 35 mm $\times$3.1 mm. The mesh was

found by starting with a relatively coarse mesh and then refining. After some trial and error the mesh shown in Figure 5.13 was found as the most optimal. The mesh is graded so that the elements are smallest closest to where the spear impacts.

The modelling of the spear also called for some trial and error. A major difference between the previous finite element models and this, is that this is an impact problem, i.e. the inertia forces are important. To represent the correct physical problem the mass of this radian of the spear had to be exact. It was not an option to model the spear and the weight rig in full size. The solution became a two-component solution, as seen in Figure 5.13. The upper part (the red part) represents the majority of the weight of the spear. This part is not in contact with the plate and acts as a sort of point mass. The wanted mass is achieved by adjusting the mass density. To get the correct mass of 5.045 kg used in some of the tests, the mass density of this part had to be set as high as $1.064 \cdot 10^6$ kg/m^3. A problem with density values this high is that it makes the representation of the forces inaccurate. In order to fix this problem, the blue part was introduced. This is modelled as hardened steel. The steel was modelled with its real mass density of 7850 kg/m^3, which resulted in a correct representation of the forces. A cross-section in the straight area of the blue part was chosen as the reference cross-section. The spear can be considered almost rigid compared to the plate, meaning that a relatively coarse mesh could be applied in the spear without loss of accuracy.

The next thing was the contact definition. An edge-to-edge contact situation involving shell elements is not an optimal. This is mainly because shell elements in most cases are applied using edge-to-surface or surface-to-surface contact. After some more trial and error the choice fell on the contact formulation CONTACT_2D_AUTOMATIC_SINGLE_SURFACE [6]. This is an "automatic" contact definition, meaning that it defines the master and slave surface on its own. It is also especially suited for 2D problems. The friction parameters were set to $\mu_{static} = 0.25$ and $\mu_{dynamic} = 0.9 \cdot \mu_{static} = 0.225$. The penalty parameter was set to 1.5.

The boundary conditions were less complex. The right end was defined as rigid and the left edge was constrained through the axisymmetric element formulation. The spear was given an initial velocity in units mm/s according to column three of Table 5.4.

5.2.3 Results

In this section the results of the tests and simulations of the drop tower will be presented, mainly using force-time and force-displacement diagrams.

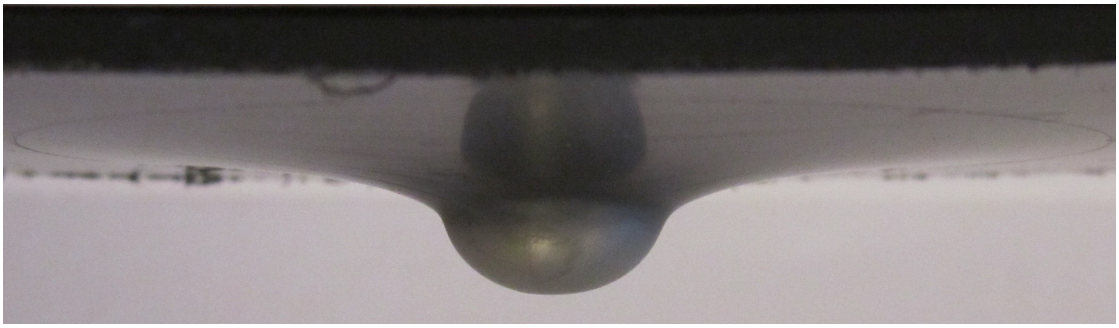

(a) The specimen used in the test DT1. The plate absorbed the impact energy of 50 J by deforming as shown.

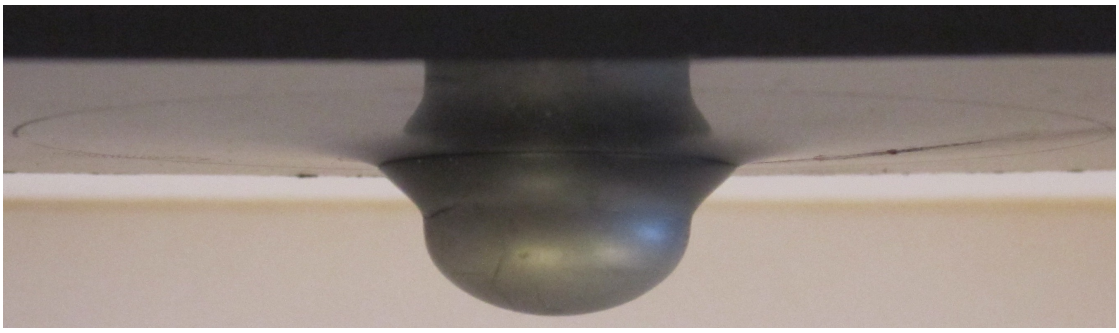

(b) The specimen used in the test DT6. The energy in this test was 55 J. The 5 J energy increase from DT1 resulted in a noticeable difference in the deformed shape

Figure 5.14: The two specimens that absorbed the impact

Fracture occurred in all the specimens where the energy was higher than 55 J. The fracture appeared to be caused by a plug-like mechanism, i.e. a shear fracture around the area of impact causing the impact area to be pushed out in one piece. The two specimens that did not fracture are shown in Figure 5.14. DT1, the test with 50 J impact energy, is shown in Figure 5.14a. It is seen that the plate has absorbed the energy by deforming. The deformation is quite smooth, and decays gradually away from the point of impact. A more local deformation is seen in Figure 5.14b. This is the deformed shape of the specimen that was used in the test DT6. In this test, the impact energy was 55 J. The deformed shape is quite different from that of DT1, even though the energy is only 5 J higher. This is probably because this energy level is close to the maximum capacity of the plate. If only 5 more joules were added, as was done in DT5, the specimen fractured.

In the previous validation tests the strain rates were in the range of 10^{-3} s^{-1} to 10^{-2} s^{-1}. In these tests the strain rates are in the range of 10^{2} s^{-1} to 10^{3} s^{-1}. Since polymers are non-newtonian, i.e. the load capacity increases with increasing strain rate, the load levels observed in this section should be significantly higher than in the previous tests.

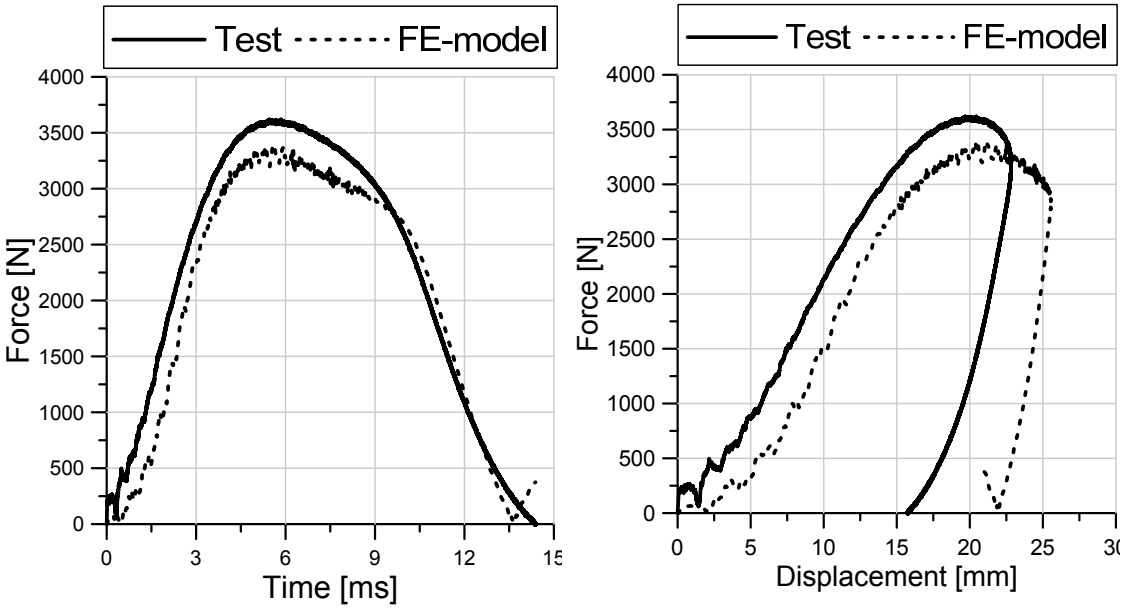

(a) The force-time diagram

(b) The force-displacement diagram

Figure 5.15: The results of test DT1

Figure 5.15 shows the results of the test DT1. Even though this is one of the "slowest" drop tower tests, the peak load is almost 1 kN higher than the highest peak load observed in the previous validation tests. The expected load increase is thus confirmed. When looking at the force-time diagram in Figure 5.15a, three phases can be observed. First load application and material absorption, then the peak load is reached and the absorption stops. The third phase is unloading. For this test, which did not fracture, are all the phases described, and the curve is smooth from start till end. If a fracture had occurred, the curve would have fallen to zero load at some point.

The result of the finite element simulation is seen as the dotted line in Figure 5.15. It is observed that both the stiffness and the peak load are a little low. The curves are relatively correct in shape, but a bit shifted to the right compared to the test results.

The deviations observed in Figure 5.15 are similar for all the tests. The deviations

can be reduced by minor alterations to the material model. An adjustment of Young's modulus reduces the deviation in the initial stiffness. The value found to give the best results is 700 MPa, which is the same value that was applied to some of the analyses of the previous validation tests. The other parameter to be altered is linked to describing the strain rate dependency. Recall the strain rate dependency of the material model (cf. Figure 4.4). The relation is modelled as a linear regression between values of the yield stress at two or more strain rates. These reference strain rates are in most cases between 10^{-3} s^{-1} and 10^{-1} s^{-1}, and the linear approximation produces good results in this strain-rate regime. The current strain rates are, as mentioned, significantly higher. And it is not unlikely that the strain-rate dependency becomes less log-linear with increasing strain rates. The above argument is stated to justify a slight increase in the parameter controlling the gradient of the strain-rate regression, namely the parameter C. This slight increase will yield a significant change in the predicted yield stress for the high strain rates seen in the drop tower tests. This naturally yields an increase in the peak load too.

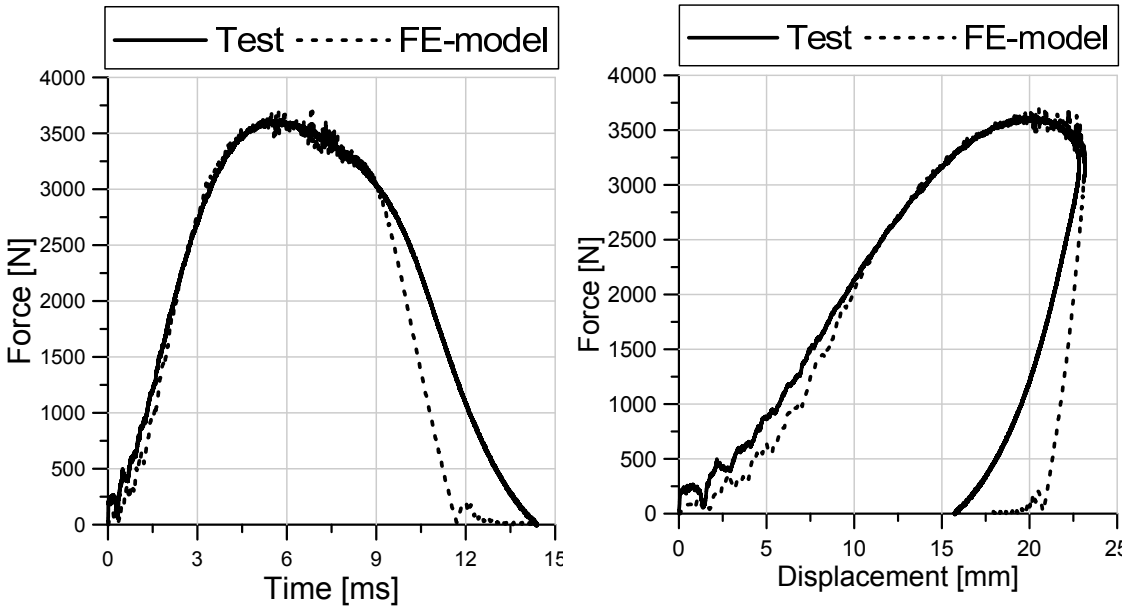

(a) The force-time diagram

(b) The force-displacement diagram

Figure 5.16: The results of the test and the analysis of DT1. Here E=700 MPa and C=0.07

Figure 5.16 shows the results of the above adjustments. E is adjusted to 700 MPa and C is set equal to 0.07. Most of the deviation in the initial phase of the response is now gone due to the increase of E. In addition the increase of the C parameter

has brought the peak load up to a near perfect match. The remaining deviation is in the unloading. This part of the response happens with another rate than the initial load response, thus yielding another modulus than the initial modulus. The representation of a different modulus in unloading than in loading can not be represented without applying viscoelastic effects, which are not included in the material model.

Figure 5.17 presents the force-time relation of the five remaining tests. The modified material model with E=700 MPa is applied in all the analyses. In addition, the parameter C is adjusted so that each analysis attain a good match with the peak load. Table 5.4 gives the specifications of each test.

Fracture points			
Test	Time [ms]	Displacement [mm]	Force [N]
DT2	4.82	25	3785
DT3	6.1	21	3762

Table 5.3: The fracture point of DT2 and DT3

Name	Mass [kg]	Velocity [m/s]	Drop [m]	Approx. energy [J]	Fracture?
DT1	5.045	4.43	1	50	No
DT2	5.045	6.26	2	100	Yes
DT3	10.045	4.43	1	100	Yes
DT4	10.045	3.864	0.761	75	Yes
DT5	5.045	4.877	1.213	60	Yes
DT6	5.045	4.67	1.112	55	No

Table 5.4: The tests carried out using the drop tower

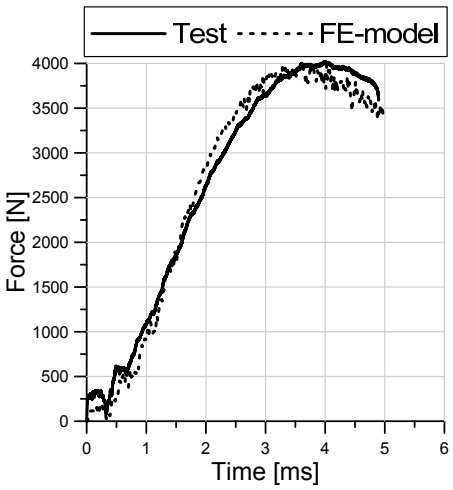

(a) DT2, C=0.08

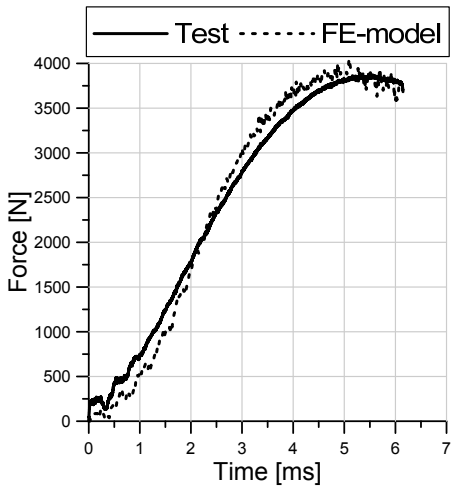

(b) DT3, C=0.08

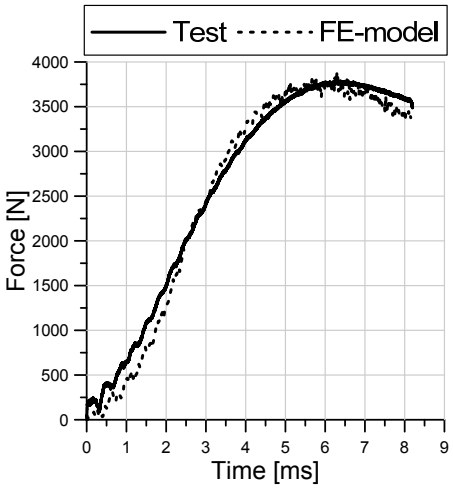

(c) DT4, C=0.075

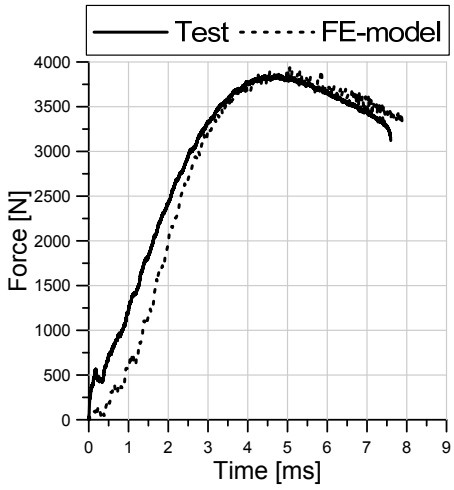

(d) DT5, C=0.08

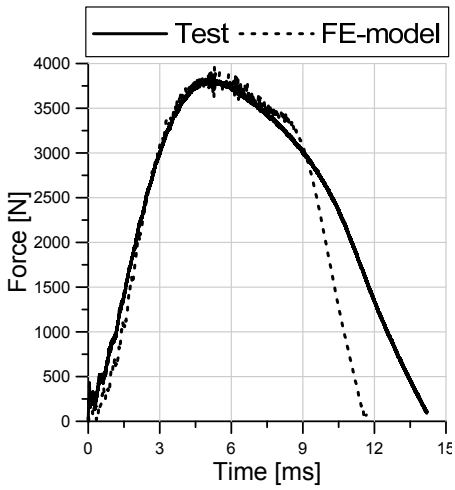

(e) DT6, C=0.08

Figure 5.17: The results of the remaining drop tower tests and simulations

5.2.4 Comparison and discussion

This test has the most complex load response of the three tests in this thesis. In spite of these complexities, the material model has managed to represent the response quite accurately.

In an impact response, the strain rate in the specimen is closely linked to the impact velocity. This is also seen in Figure 5.17. In the tests DT3 to DT5, the peak load is approximately the same (3750 N). These tests also have relatively equal impact velocities, but varying mass. DT2 confirms the theory by having the "lowest" weight, the highest impact velocity and the highest peak load.

The friction is given little attention in the previous sections. This is a quite important parameter in this problem. The friction between the spear and the specimen is significant and it involves both dynamic and static friction. No data about the actual friction coefficients between the polypropylene in question and various surfaces has been found, so the value chosen for use in the analyses is based on trial and error and general assumptions on what it usually is for polymers. A typical assumption is that $\mu_{static} = 0.2$ for polymer-metal contact and that the dynamic friction is 90% of this static friction. On this basis, values from 0.1 up to 0.5 were tried as only variable in a FE-analysis. The peak load and the numerical noise increased with increased values of μ_{static}. For smaller values the trend was opposite. The chosen value of $\mu_{static} = 0.25$ turned out be a good midpoint between load representation and numerical noise.

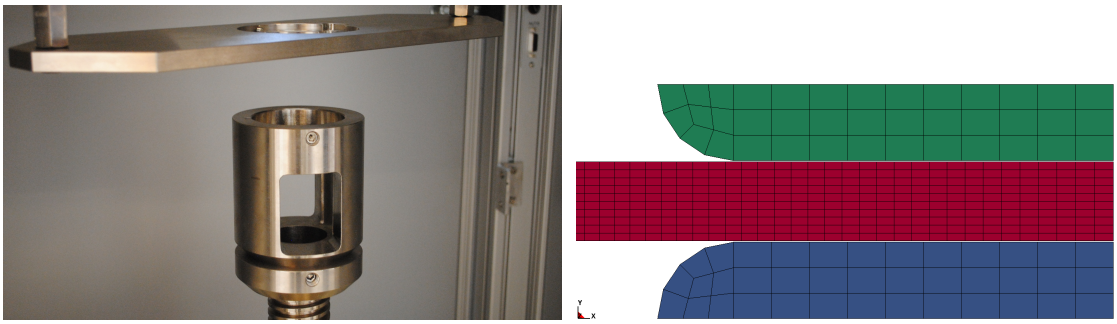

(a) The clamp mechanism of the drop tower (b) The modelled clamp mechanism

Figure 5.18: The real and the modelled boundary clamp

The boundary conditions had to resemble the clamp seen in Figure 5.18a. The upper part seen in the figure is lowered down and presses the specimen down with a chosen pressure (5 bar in these tests). Three main concepts were tried. The first was to model the clamp but not the clamping pressure, i.e. a model like in Figure 5.18b but with no extra pressure from the upper part. The plate is defined

as rigid at the nodes along the right edge of Figure 5.18b. With this model the plate has a smoothed transition from the clamped to the free state. The second method was a version of the same principle. Now the upper plate was applied a downward force corresponding to the 5 bar pressure applied in the machine. The rigid definition of the nodes in the plate was removed leaving the plate without any explicit boundary condition. The last option that was tried was simply to define the right end of the plate as rigid without modelling the clamp (see Figure 5.13). The main difference between these principles was the smoothing provided by the clamped model. And this smoothing did not affect the results to any extent. The most basic model was thus chosen.

The complexity of the problem means that there are many sources of error. The simple geometries of the specimens and the relatively foolproof mounting of the specimen in the machine make the probability of error in these phases of the process quite small. In modelling, the situation is quite different. Here the sources of error can be found in almost all elements of the model. First the question of element formulation. Could modelling the whole problem with cubic elements have given other results? It is hard to tell exactly. In principle, there should not be any difference. On the other hand could the cubic elements have made it easier to calculate the exact mass of the spear. And there might also be other effects that are not represented by the current model. One thing is for sure, a model of cubic elements would have become very computationally expensive. An advantage of the current model is that it is very effective and can be run with a lot of different parameters in a short period of time. Such operations had not been possible with the cubic model. The next uncertainty is linked to defining what parameters that are involved in the different phases of the simulation. In Section 5.2.3, good results were obtained by altering only two parameters. These two alone do most probably not represent the full response, they are only central parameters that affect the total response. When doing a parameter study the different parameters are tested one by one, making it difficult to see synergy effects. Even better results might have been achieved by further examining such synergies. The problem with this process is of course the complexity that arises.

The drop tower test involves a quite complex material response. This response is modelled using a quite simplified material model. In spite of this, the material model has proved that it is able to represent the problem in a satisfactory manner

Chapter 6

Conclusion

The previous chapters have shown the calibration and validation of the SIMlab polymer material model. The material model has been calibrated to resemble an impact modified polypropylene. This material has proved to be a bit challenging to exactly represent, but the material model has overcome most of the problems and managed the representation quite accurately.

The process started with the unaxial tension and compression tests. Through the tension tests it became clear that the material deformation was a bit unusual. It dilated significantly and if it fractured it fractured in the top of the gauge length. The fracture seemed to occur in the core and then propagate to the surface, where a more ductile external skin was stretched before the specimen finally fractured completely. The stress-strain curves showed a mixture of earlier observed behaviours for materials like PVC and HDPE [5]. The curves showed softening, but only slightly, thus being somewhere between the PVC, which softens significantly, and HDPE, which does not soften at all. Then the stress was constant for a while, through this resembling the behaviour of other versions of polypropylene, before it slightly hardened. From the tension tests it was also found that the load level was significantly lower in the specimens from the transversal direction than in those from the longitudinal direction, which means that the material was anisotropic. The compression response was found to be different from the tension response. Here the material did not soften and hardening was initiated immediately after yield.

The next step was to calibrate the material model to fit the response of the chosen baseline test. The unusual load response of the material made it a bit challenging to identify some of the material parameters and some deviations between the response curves had to be accepted. The deviations were located in the elastic

response and in the transition from the elastic to the plastic response.

The calibrated material model was now ready to be tested in finite element simulations. The first tests to be simulated were the material tests, i.e. the uniaxial tension and compression test. The representation of these tests was challenging and significant deviations were observed in the simulation of the slowest tests. The calibration was redone in order to check for errors. But the examination came up with the same result. The conclusion was that due to the significant dilatation and the irregular deformation were the material tests hard to represent exactly.

After making sure that the calibration was correct, the validation could begin. This process consisted of two different tests, which tested different properties of the material model. The first test was the plate with a centric hole. The main difference between this test and the material tests was that this specimen had a more advanced geometry and a slightly more complex load response. The other validation test was the drop tower. This test represented a dynamic problem involving high strain rates and a complex load response, it thus validated other properties of the material model than the first validation test. Through the validation tests it became clear that Young's modulus was more in the range of 700 - 750 MPa than 400 MPa. The drop tower tests showed that the strain rate dependency deviates from a log-linear behaviour for high strain rates, thus yielding a slight increase of the parameter C. By adjusting these two parameters the material model managed to represent both tests very well.

As a conclusion it can be stated that the material model has successfully managed to represent the polypropylene treated in this thesis. Even though the calibration procedure is fairly simple it has not stopped the material model from representing complex problems. A further enhancement would be to include the viscoelatic behaviour and a fracture criterion. By adding these properties can the material model represent an even wider range of problems. They should, however, be implemented in a way that does not complicate the calibration in any extent, thus conserving the simple yet complex nature of this material model.

Bibliography

[1] AH Clausen, M Polanco-Loria, MT Hovden, M Haugen, and OS Hopperstad. Experimental and numerical study of hdpe and pvc at different loading conditions. In preparation for possible journal publication, 2012.

[2] Arild Holm Clausen, Mario, Polanco-Loria, Torodd Berstad, and Odd Sture Hopperstad. A constitutive model for thermoplastics with some applications. 8th European LS-DYNA Users Conference, Strasbourg - May 2011.

[3] Hamid Daiyan. *Experimental and Numeric Investigation of the Mechanical Response of Injection Moulded Polprpoylene Materials*. PhD thesis, Faculty of Mathematics and Natural Sciences, University of Oslo, 2011. Part of the series " Series of dissertations submitted to the Faculty of Mathematics and Natural Sciences, University of Oslo".

[4] R. N. Haward and G. Thackray. The use of a mathematical model to describe isothermal stress-strain curves in glassy thermoplastics. In *Proceedings of the Royal Society of London. Series A, Mathematical and Physical Sciences*, volume 302, pages 453–472. The Royal Society, Jan. 23 1968.

[5] Martin Thuve Hovden. Tests and numerical simulations of polymer components. Master's thesis, NTNU - Norwegian University of Science and Technology, 2010.

[6] Livermore Software Technology Corporation. *LS-DYNA Keyword User's Manual*, version 971 edition, 2007.

[7] Rafael Traldi Moura, Arild H. Clausen, Egil Fagerholt, Marcìlio Alves, and Magnus Langseth. Impact on hdpe and pvc plates – experimental tests and numerical simulations. *International Journal of Impact Engineering*, 37:580 – 598, 2010.

[8] M. Polanco-Loria, H. Daiyan, and F. Grytten. Material parameters identification: An inverse modeling methodology applicable for thermoplastic materials. *Polymer Engineering And Science*, pages 438 – 448, 2012.

[9] Mario Polanco-Loria, Arild H. Clausen, Torodd Berstad, and Odd Sture Hopperstad and. Constitutive model for thermoplastics with structural applications. *International Journal of Impact Engineering*, 37:1207–1219, 2010.

[10] Ram Raghave, Robert M. Caddell, and Gregory S. Y. Yeh. The macroscopic yield behaviour of polymers. *Journal Of Materials Science*, 8:225 – 232, 1973).

[11] Arie Ram. *Fundamentals of polymer engineering*. New York: Plenum Press, 1997.

[12] Joachim Rösler, Martin Bäker, and Harald Harders. *Mechanical Behaviour of Engineering Materials : Metals, Ceramics, Polymers, and Composites*. Berlin, Heidelberg : Springer Berlin Heidelberg, 2007.

Appendices

June 7, 2012

Appendix A

Material tests

This part contains a sheet for every material test that was carried out. It starts with the calibration tests, then the plate-with-centric-hole(PWCH) tests are presented and at the end the drop tower tests are presented.

The calibration tests are presented with pictures of the tested specimen, three diagrams, a table containing key information and a short description. The diagrams are a force-displacement diagram, a stress-strain diagram and a strain diagram. The strain diagram contains the contraction parameter ρ and the transversal strain plotted against the longitudinal strain. The transversal strain curve is cut before its final value to better show the part of the curve that is of interest($\varepsilon_l \leq 0.1$). The compression tests are also shown. The post-test measures of the compression tests are a bit too high compared to the final strain value shown in the stress-strain diagram. This is because the specimens swelled after the load was removed.

The PWCH and drop tower tests are presented in a similar manner as the calibration tests. The plots presented for the PWCH tests are the force-displacement diagram and plots showing the deformation at the different points on the specimen. For the drop tower tests the force-time, velocity-time and displacement-time relation are shown.

A.1 Calibration

A.1.1 T1-L1, $\dot{\varepsilon} = 10^{-3}$ $\mathbf{s}^{-1}$

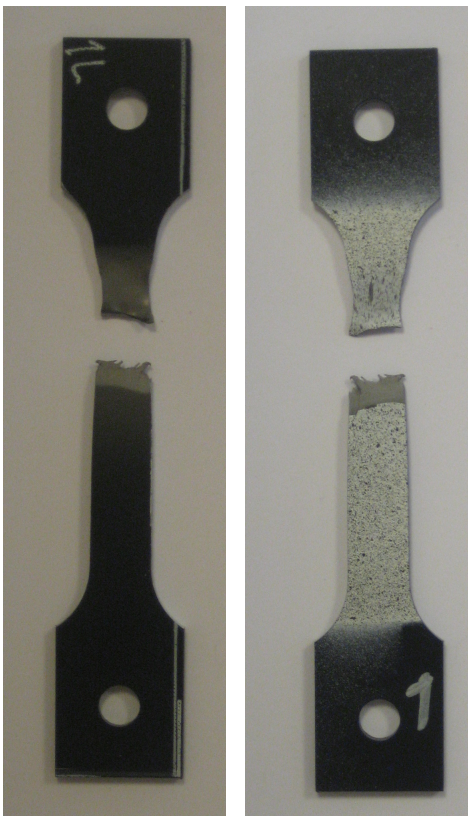

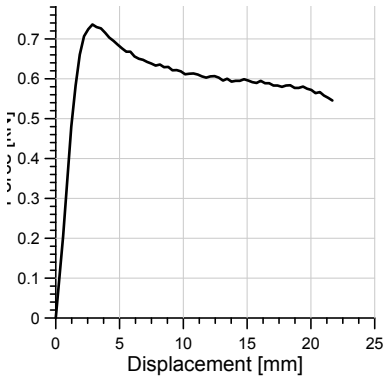

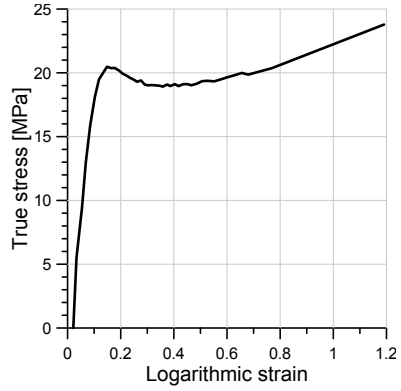

Material data			
Young's modulus			240 MPa
Yield stress			20 MPa
	b [mm]	t [mm]	A [mm^2]
Initial dimensions	12.0	3.1	37.2
After test	11.6	2.9	33.6

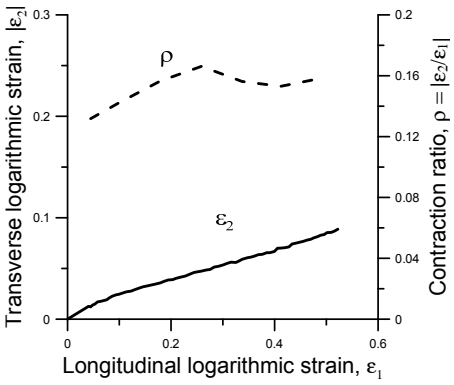

The test was not valid and is therefore not included in any further processes of this thesis. The purpose of including it here is to show what level of scatter that was accepted.

A.1.2 T2-L1, $\dot{\varepsilon} = 10^{-3}$ $\mathbf{s}^{-1}$

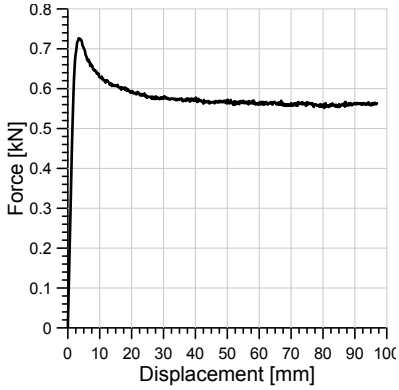

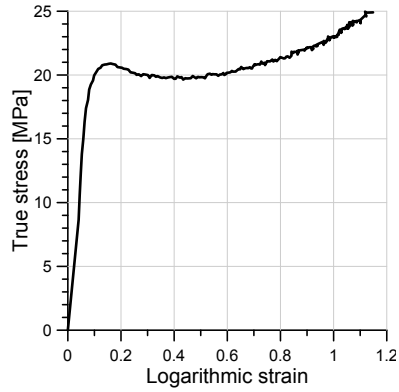

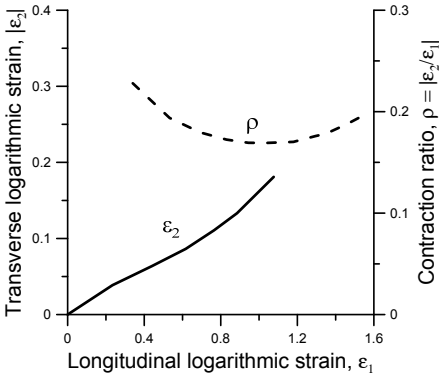

Material data			
Young's modulus			250 MPa
Yield stress			20 MPa
	b [mm]	t [mm]	A $[mm^2]$
Initial dimensions	12.0	3.1	37.2
After test	9.0	1.9	17.1

The test deformed without developing a distinct neck and did not fracture. The material has a distinct yield point and hardens approximately 5 MPa.

A.1.3 T3-L1, $\dot{\varepsilon} = 10^{-3}$ $\mathbf{s}^{-1}$

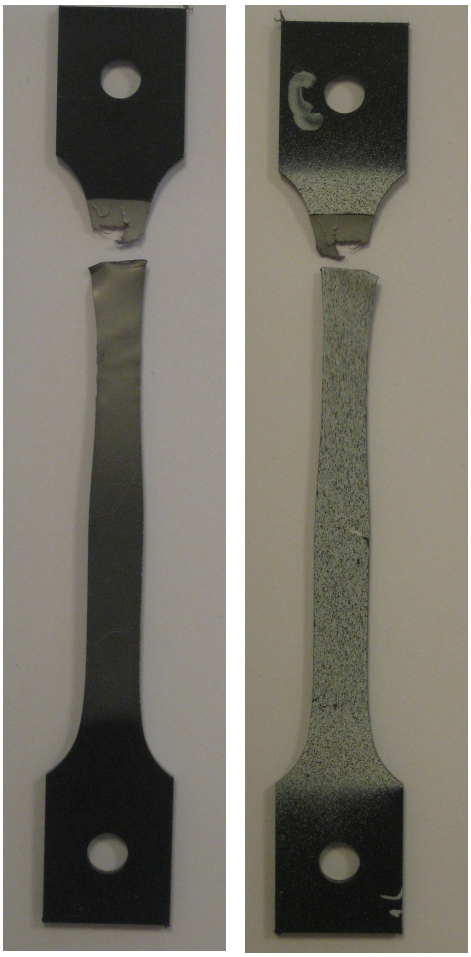

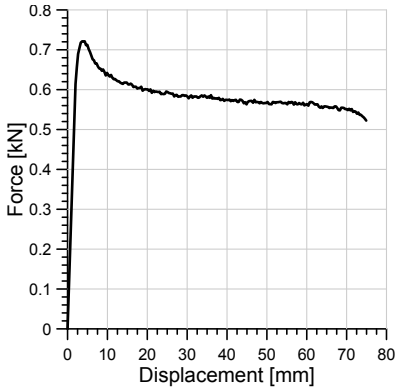

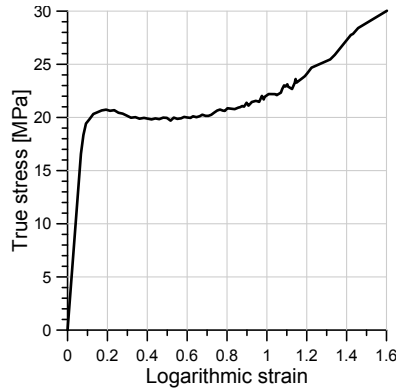

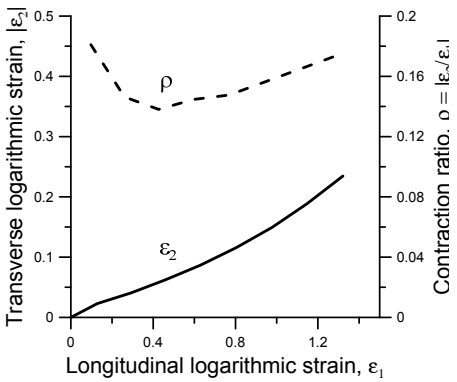

Material data			
Young's modulus			250 MPa
Yield stress			20 MPa
	b [mm]	t [mm]	A [mm^2]
Initial dimensions	11.9	3.1	36.9
After test	9.5	1.8	17.1

The test developed a neck and fractured. This test was chosen as the baseline test for use in the calibration. The external layer is clearly visible in the pictures.

A.1.4 T4-L1, $\dot{\varepsilon} = 10^{-2}$ s^{-1}

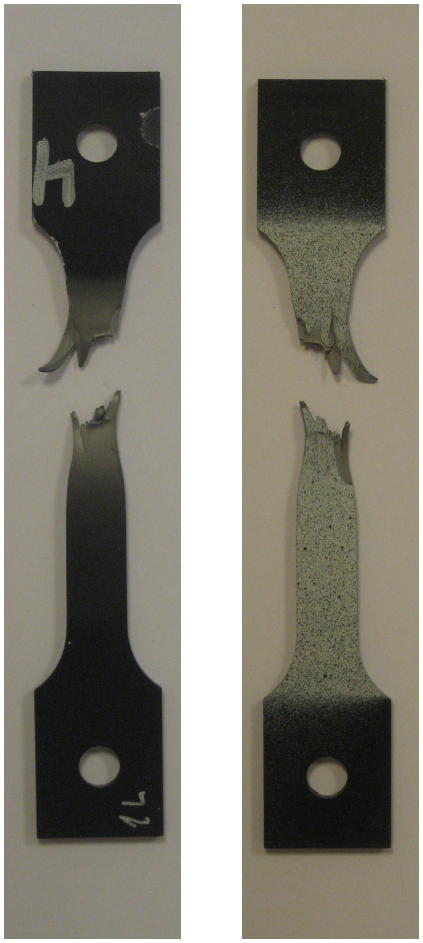

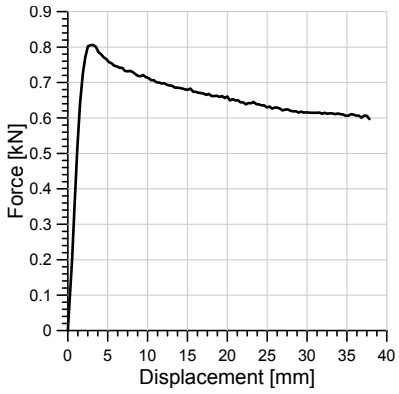

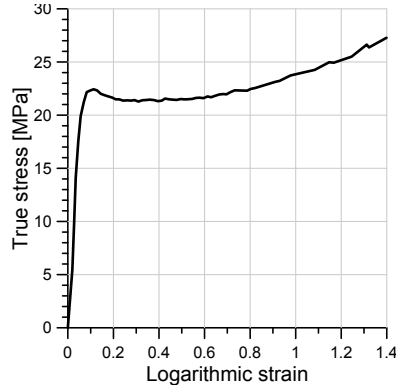

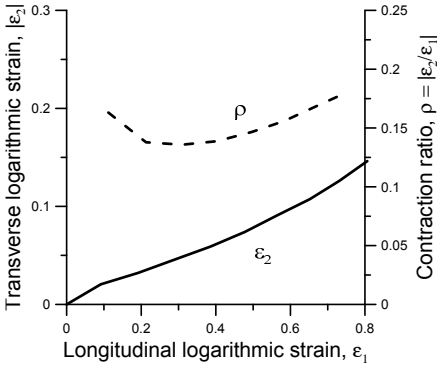

Material data			
Young's modulus			380 MPa
Yield stress			22 MPa
	b [mm]	t [mm]	A [mm^2]
Initial dimensions	12.0	3.1	37.2
After test	11.4	3.0	34.2

The first test at a higher strain rate. The test developed a neck and fractured as show. The yield point is more distinct than at the previous strain rate. The yield stress and Young's modulus have also increased.

A.1.5 T5-L1, $\dot{\varepsilon} = 10^{-2}$ $\mathbf{s}^{-1}$

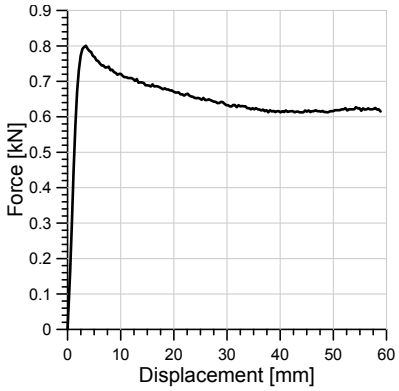

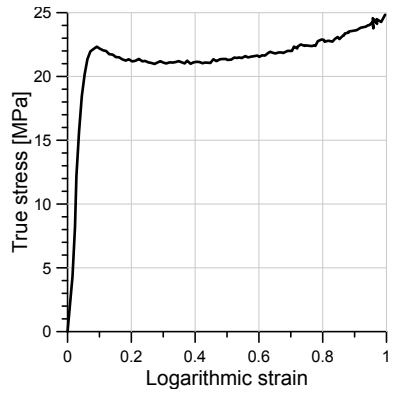

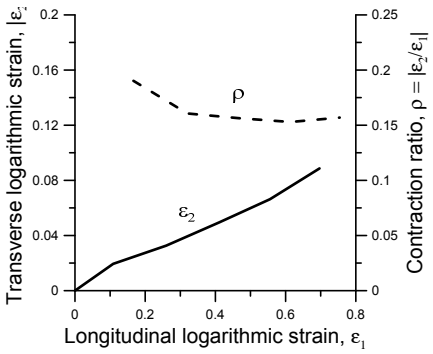

Material data			
Young's modulus			410 MPa
Yield stress			22 MPa
	b [mm]	t [mm]	A [mm^2]
Initial dimensions	11.9	3.1	36.9
After test	10.1	2.0	20.2

A neck occurs and propagates. The fracture is gradual, with the core fracturing first and then outer skin. The fractured core material is seen as the tip of the shortest part in the pictures.

A.1.6 T6-L2, $\dot{\varepsilon} = 10^{-2}$ $\mathbf{s}^{-1}$

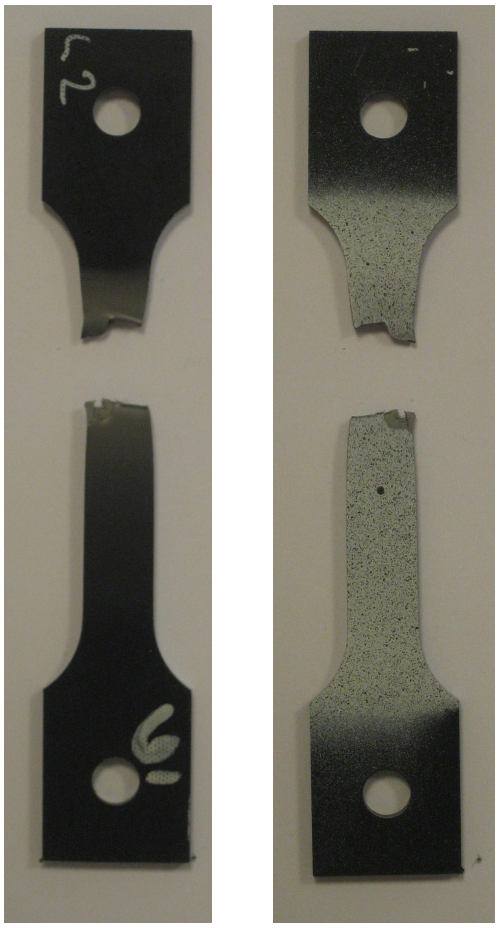

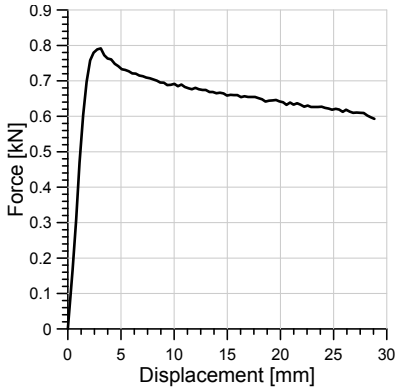

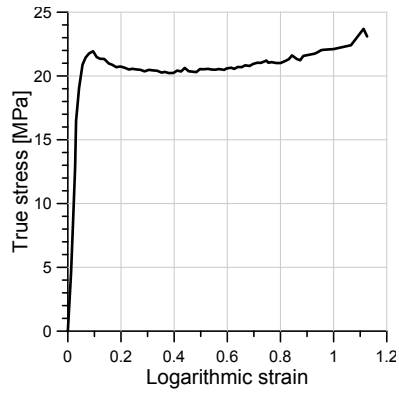

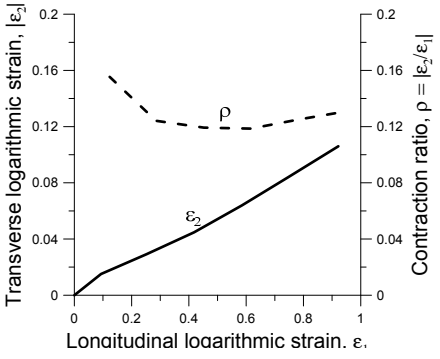

Material data			
Young's modulus			410 MPa
Yield stress			22 MPa
	b [mm]	t [mm]	A [mm^2]
Initial dimensions	11.9	3.1	36.9
After test	11.4	2.8	31.9

A specimen from the second plate from which specimens were machined. Almost no necking and a very local fracture. It hardens less than the specimens from plate 1.

A.1.7 T7-L2, $\dot{\varepsilon} = 10^{-2}$ $\mathbf{s}^{-1}$

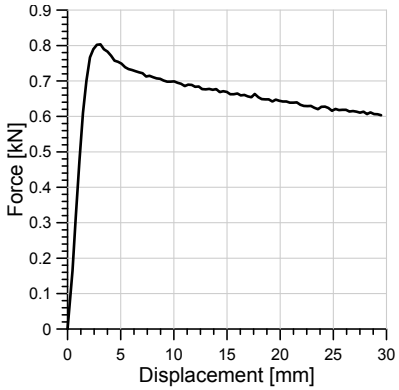

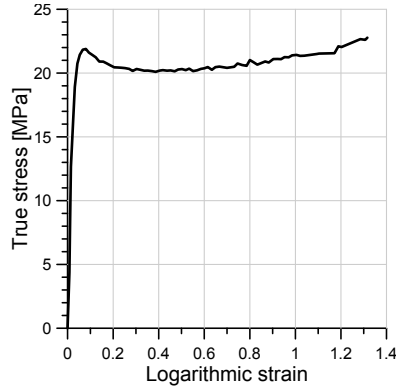

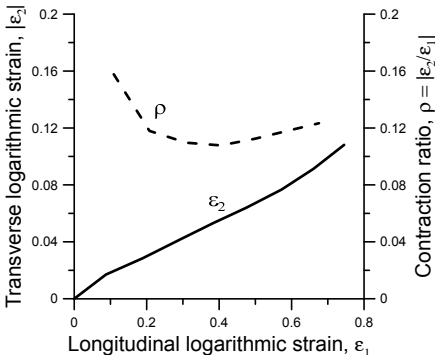

Material data			
Young's modulus			400 MPa
Yield stress			22 MPa
	b [mm]	t [mm]	A [mm^2]
Initial dimensions	12.0	3.2	38.4
After test	11.1	2.5	27.8

A slight necking is observed, and then a similar fracture as in T6-L2. The stress-strain curve has a distinct yield point and a slight hardening.

A.1.8 T8-L1, $\dot{\varepsilon} = 10^{-2}$ $\mathbf{s}^{-1}$

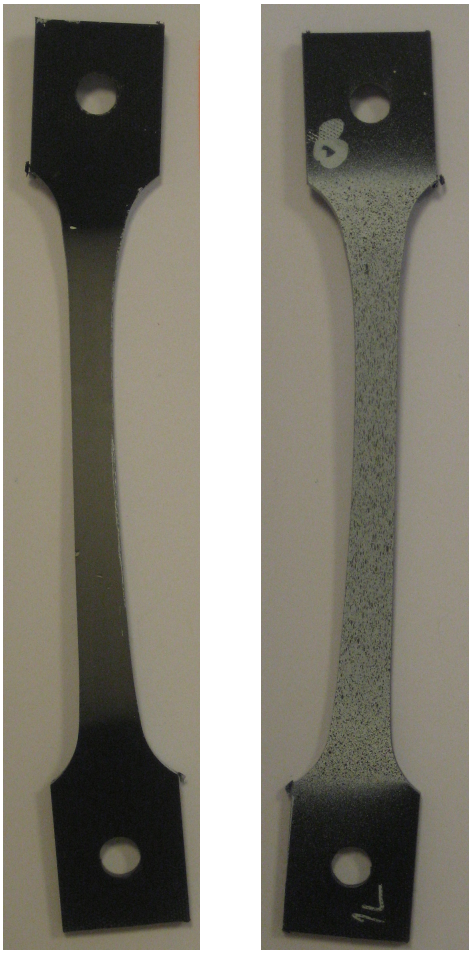

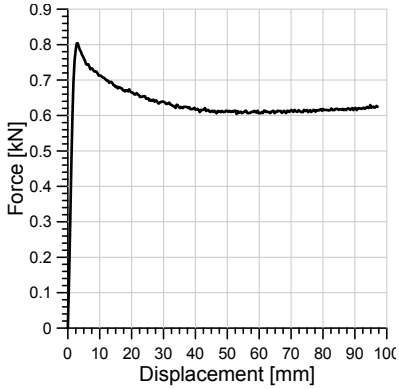

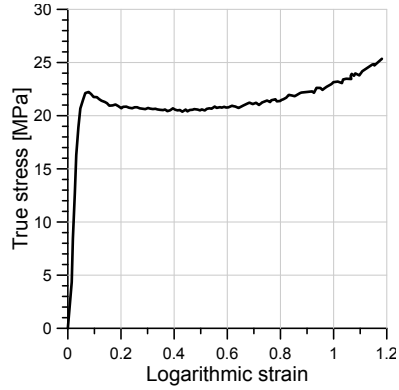

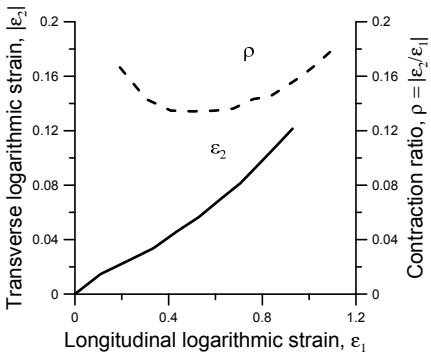

Material data			
Young's modulus			420 MPa
Yield stress			22 MPa
	b [mm]	t [mm]	A $[mm^2]$
Initial dimensions	12.0	3.1	37.2
After test	8.7	2.3	20.0

A last specimen from the first plate at this strain rate. Has a similar response as T2-L1. Withstands large strains and does not fracture

A.1.9 T9-T2, $\dot{\varepsilon} = 10^{-2}$ s^{-1}

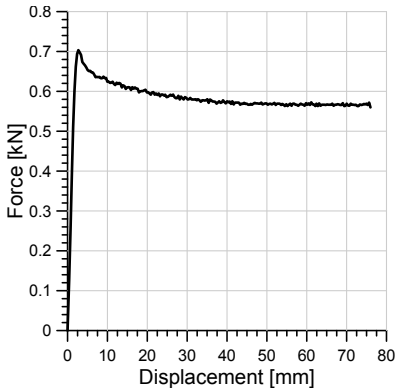

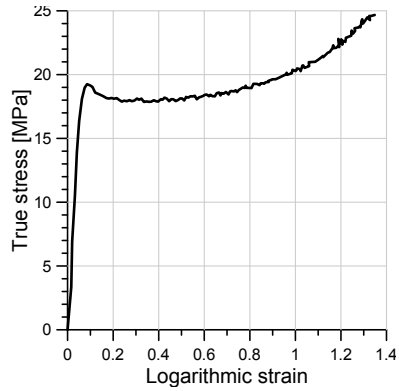

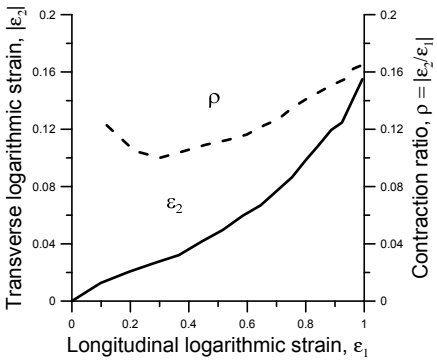

Material data			
Young's modulus			340 MPa
Yield stress			19 MPa
	b [mm]	t [mm]	A [mm^2]
Initial dimensions	12.0	3.1	37.2
After test	9.7	2.4	23.3

A specimen from the transversal direction of the second plate. Uniform deformation. Distinct yield point and more hardening than the longitudinal specimens.

A.1.10 T10-T2, $\dot{\varepsilon} = 10^{-2}$ $\mathbf{s}^{-1}$

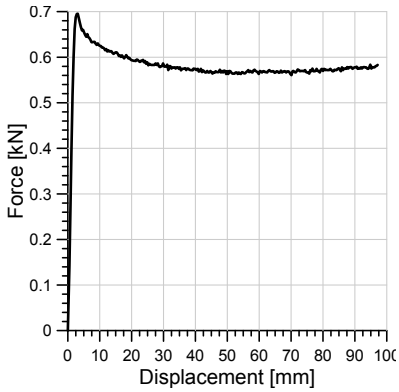

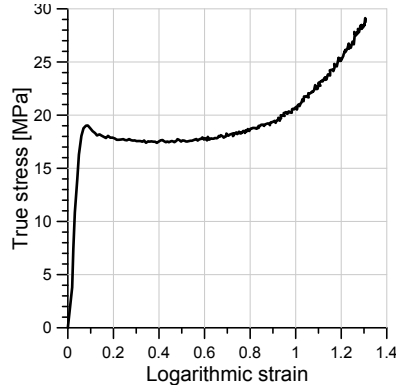

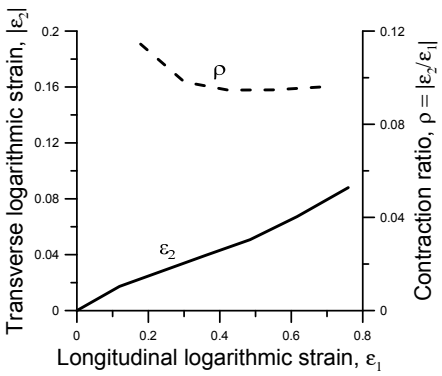

Material data			
Young's modulus			330 MPa
Yield stress			19 MPa
	b [mm]	t [mm]	A [mm^2]
Initial dimensions	12.0	3.1	37.2
After test	9.0	2.3	20.7

A specimen from the transversal direction of the second plate. Uniform deformation. Distinct yield point and more hardening than the longitudinal specimens and the previous transversal specimen T9-T2

A.1.11 T11-L1, $\dot{\varepsilon} = 10^{-1}$ s^{-1}

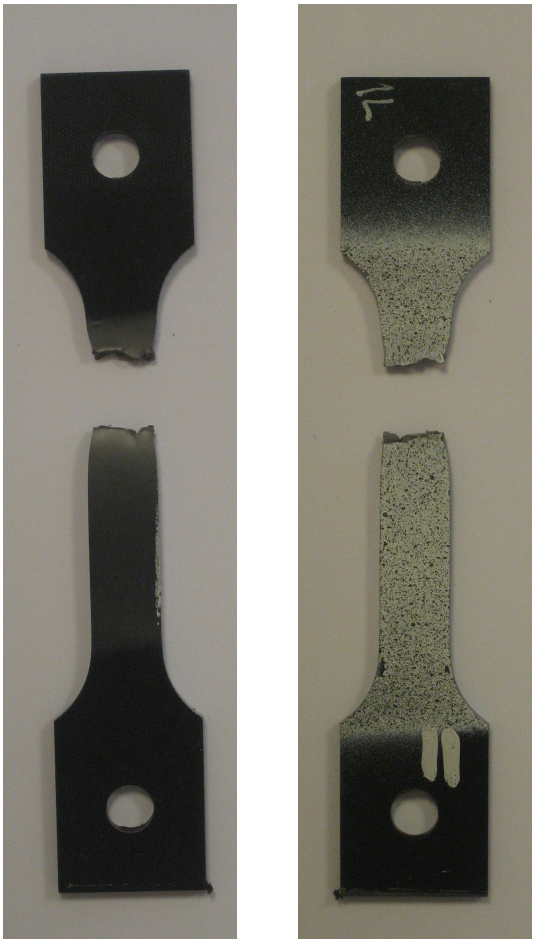

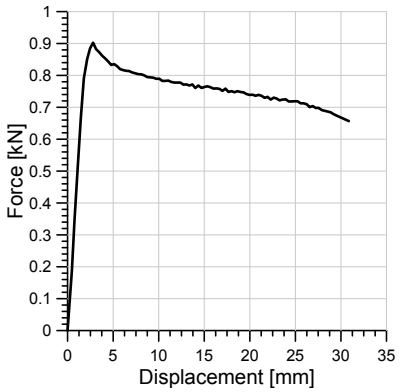

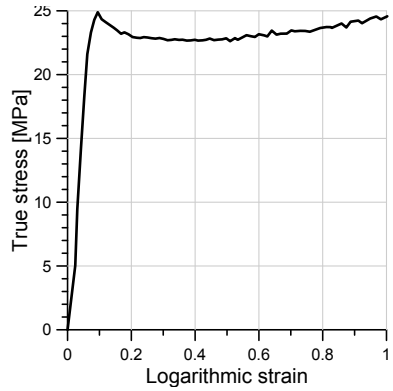

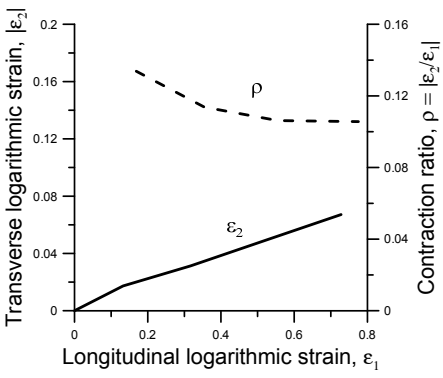

Material data			
Young's modulus			360 MPa
Yield stress			25 MPa
	b [mm]	t [mm]	A [mm^2]
Initial dimensions	12.0	3.1	37.2
After test	11.6	3.0	34.8

The first specimen from the highest strain rate. The fracture occurred after 16 seconds. Necking tendency near the fracture. The stress-strain diagram shows a distinct yield point and almost no hardening. Low ρ value

A.1.12 T12-L1, $\dot{\varepsilon} = 10^{-1}$ s^{-1}

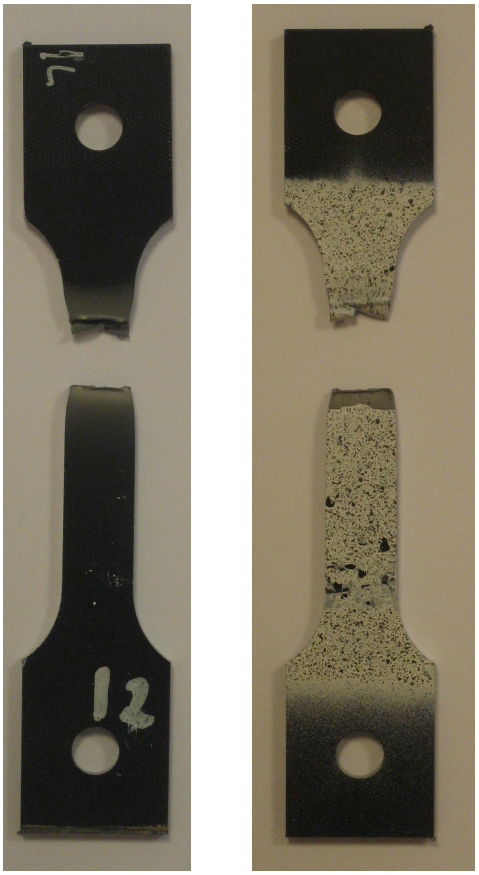

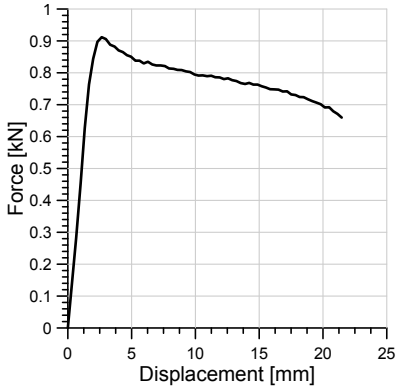

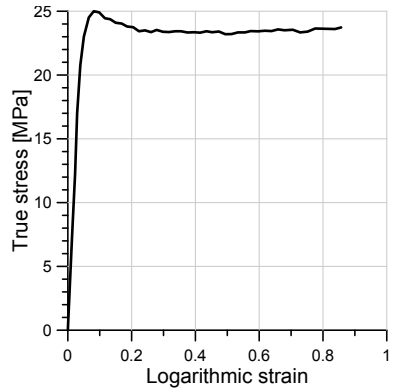

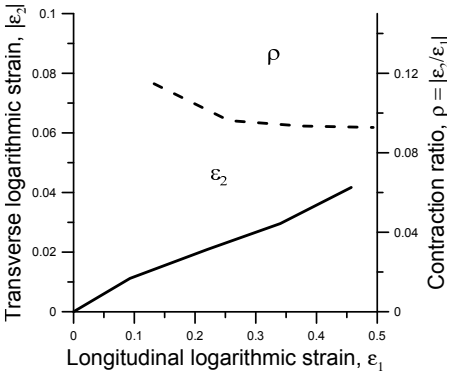

Material data			
Young's modulus			480 MPa
Yield stress			25 MPa
	b [mm]	t [mm]	A [mm^2]
Initial dimensions	12.0	3.1	37.2
After test	11.7	3.0	35.1

Necking tendency near the fracture. The stress-strain diagram shows a distinct yield point and no hardening.

A.1.13 T13-T2, $\dot{\varepsilon} = 10^{-1}$ s^{-1}

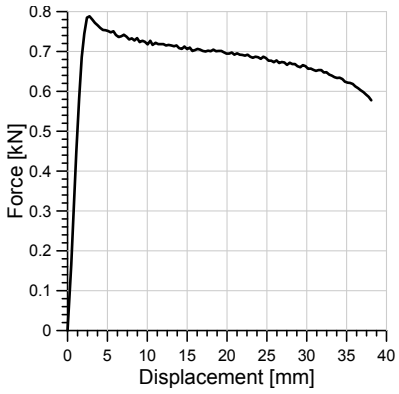

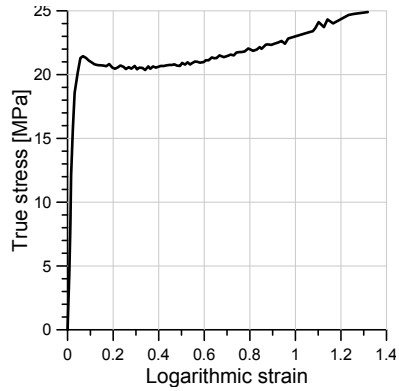

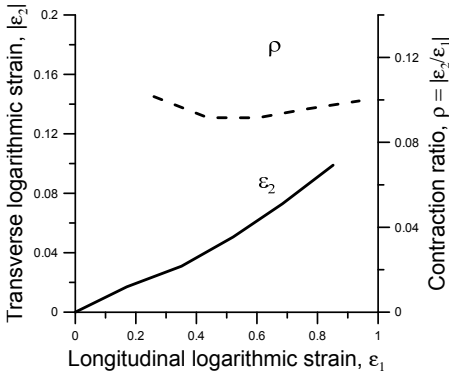

Material data			
Young's modulus			380 MPa
Yield stress			21 MPa
	b [mm]	t [mm]	A [mm^2]
Initial dimensions	12.0	3.1	37.2
After test	11.5	3.0	34.5

The specimen is from the transversal direction of plate two. Local necking occurs close to the fracture. The tip in the gauge area of the lower part indicates that the core has fractured a bit earlier than the outer layer. The stress-strain diagram shows a distinct yield point and hardening. More hardening in this than in the two from the longitudinal direction.

A.1.14 T14-T2, $\dot{\varepsilon} = 10^{-1}$ $\mathbf{s}^{-1}$

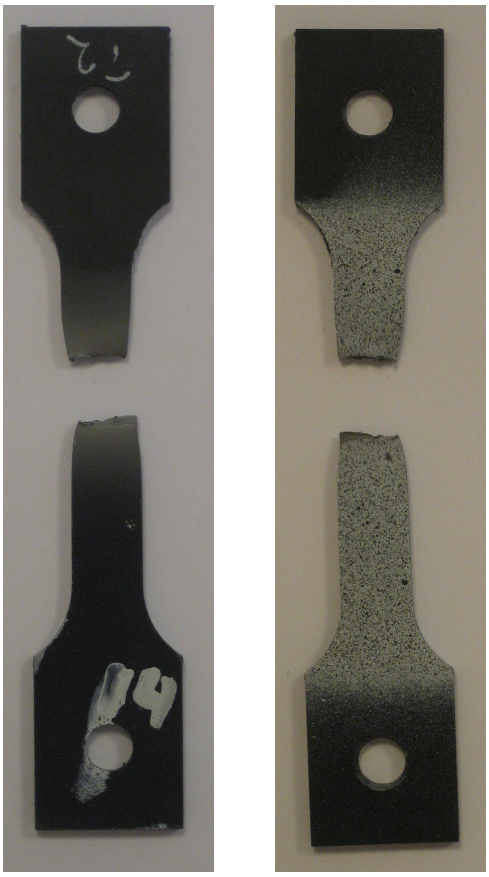

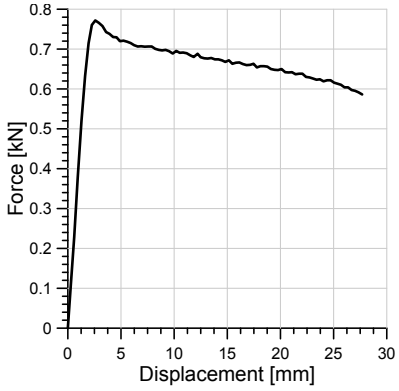

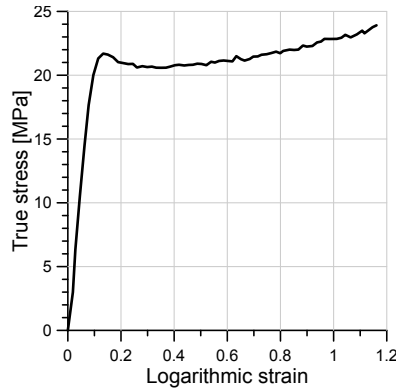

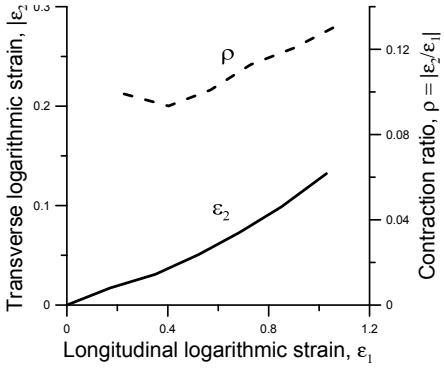

Material data			
Young's modulus			240 MPa
Yield stress			21 MPa
	b [mm]	t [mm]	A [mm^2]
Initial dimensions	12.0	3.1	37.2
After test	11.2	2.8	31.4

The specimen is from the transversal direction of plate two. Almost no necking. The stress-strain diagram shows a distinct yield point and a slight hardening. More hardening in this than in the two from the longitudinal direction.

A.1.15 C1, $\dot{\varepsilon} = 10^{-3}$ s^{-1}

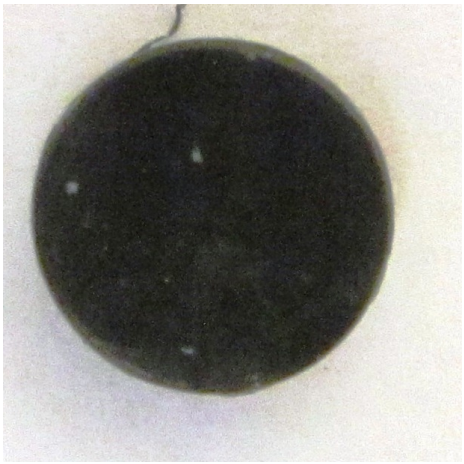

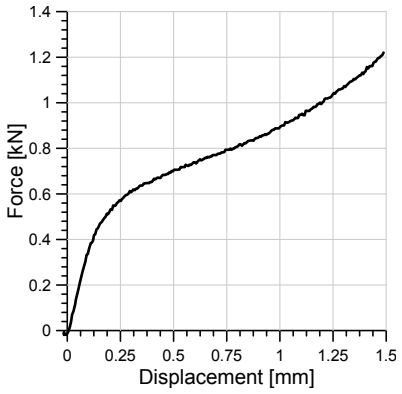

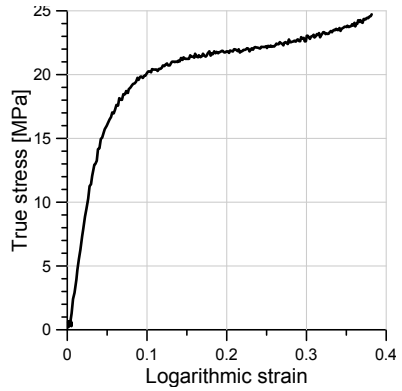

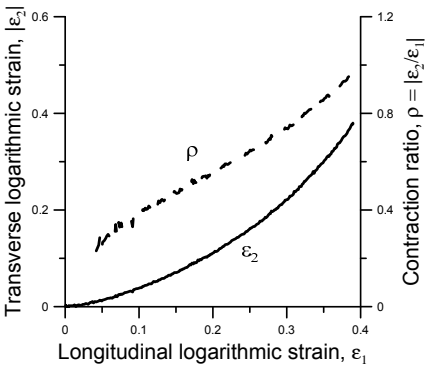

Material data			
Young's modulus			380 MPa
Yield stress			21 MPa
	D [mm]	t [mm]	A=πr^2 [mm^2]
Initial dimensions	6.1	3.2	29.2
After test	7.3	2.2	41.9

The compression tests were stopped at approximately $\varepsilon = 0.5$. The specimen deforms without barreling. There is no distinct yield point and only a slight hardening.

A.1.16 C2, $\dot{\varepsilon} = 10^{-3}$ s^{-1}

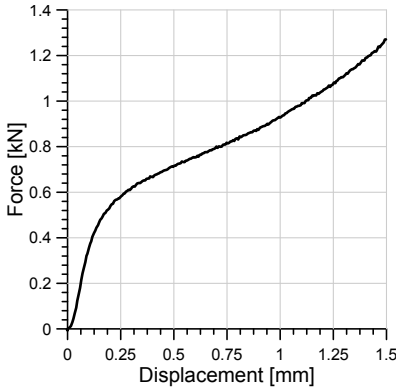

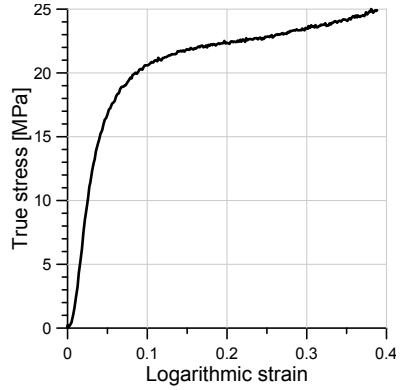

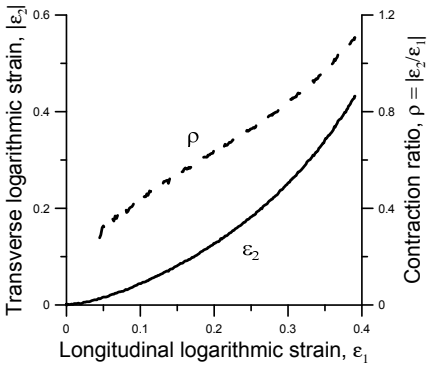

Material data			
Young's modulus			380 MPa
Yield stress			21 MPa
	D [mm]	t [mm]	A=πr^2 [mm^2]
Initial dimensions	6.0	3.2	28.3
After test	7.3	2.1	41.9

The compression tests were stopped at approximately $\varepsilon = 0.5$. The specimen deforms without barreling. There is no distinct yield point and only a slight hardening.

A.1.17 C3, $\dot{\varepsilon} = 10^{-2}$ s^{-1}

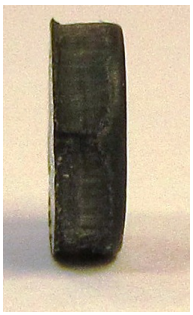

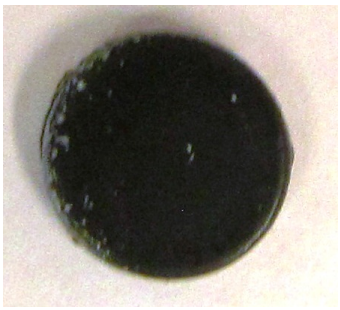

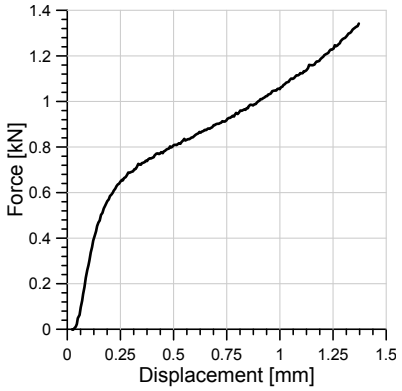

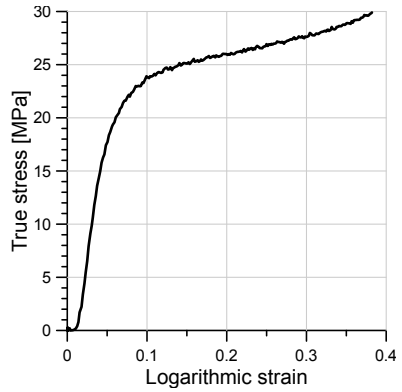

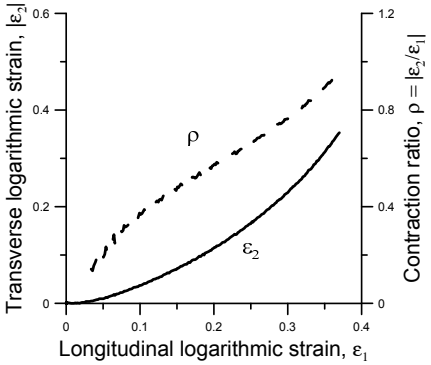

Material data			
Young's modulus			470 MPa
Yield stress			25 MPa
	D [mm]	t [mm]	A=πr^2 [mm^2]
Initial dimensions	6.0	3.2	28.3
After test	7.3	2.1	41.9

This test has significantly higher yield stress than the two previous test. The difference in yield stress is larger than the expected difference due to the increased strain rate. The stress-strain curve shows no softening and a 2-4 MPa hardening.

A.2 Plate with centric hole

A.2.1 D1V1, v=0.05 mm/s

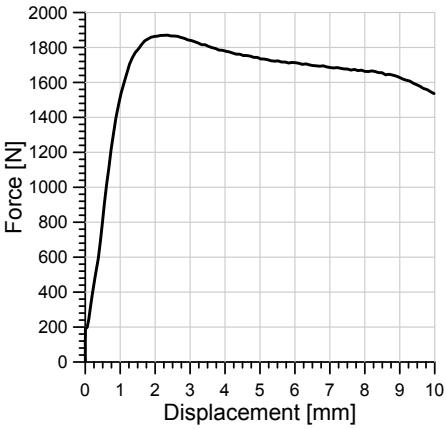

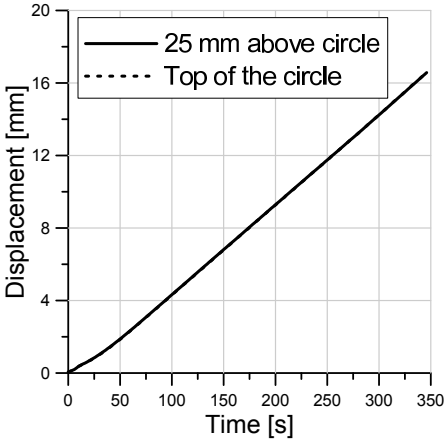

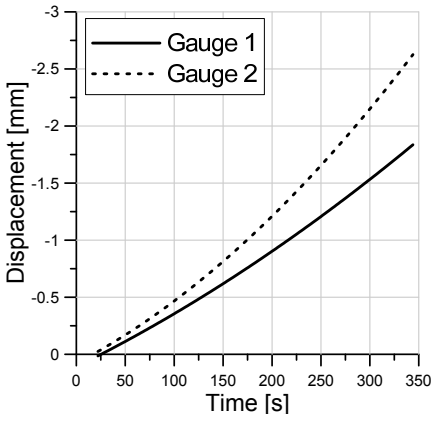

Test specifications			
Approx. $\dot{\varepsilon}_{gauge}[\mathrm{s}^{-1}]$		0.0025	
	$b_{t,1}$ [mm]	$b_{t,2}$ [mm]	D [mm]
Initial dimensions	15.4	15.2	28.9

The majority of the deformation took place in the gauges. The deformation in each gauge is a bit different, indicating some effect of the asymmetric placement of the hole. The specimen did not fully fracture and the outer skin was still intact some places when the specimen was removed from the test machine.

A.2.2 D2V1, v=0.05 mm/s

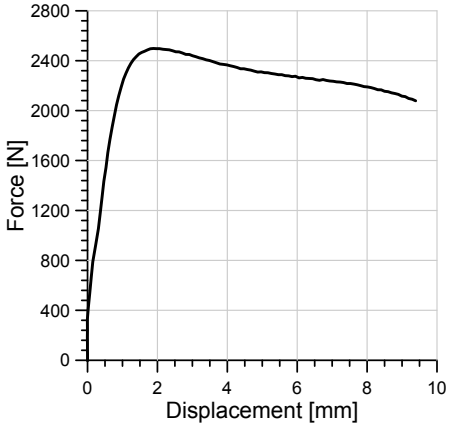

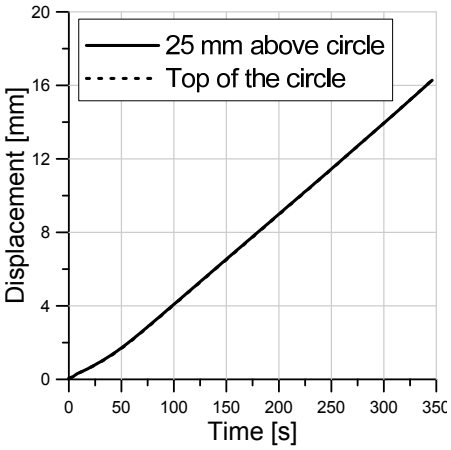

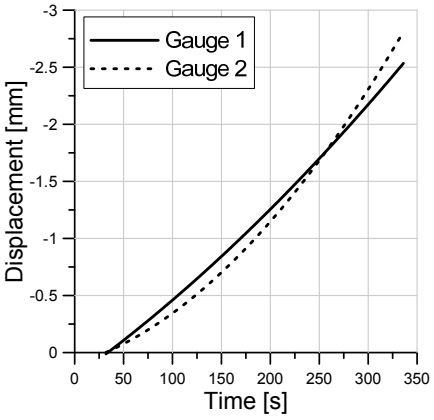

Test specifications			
Approx. $\dot{\varepsilon}_{gauge}[\mathrm{s}^{-1}]$		0.0025	
	$b_{t,1}$ [mm]	$b_{t,2}$ [mm]	D [mm]
Initial dimensions	20.1	20.4	19.8

The majority of the deformation took place in the gauges. The deformation in each gauge is a bit different, indicating some effect of the asymmetric placement of the hole. The specimen did not fully fracture and the outer skin was still intact some places when the specimen was removed from the test machine. It the tips on the gauges of the top piece indicates that the core has fractured before the outer skin.

A.2.3 D1V2, v=0.5 mm/s

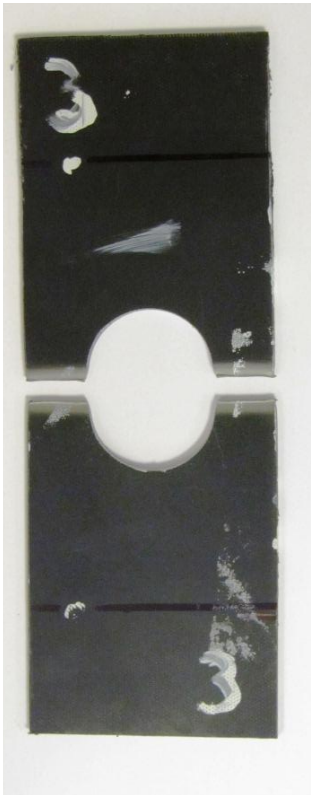

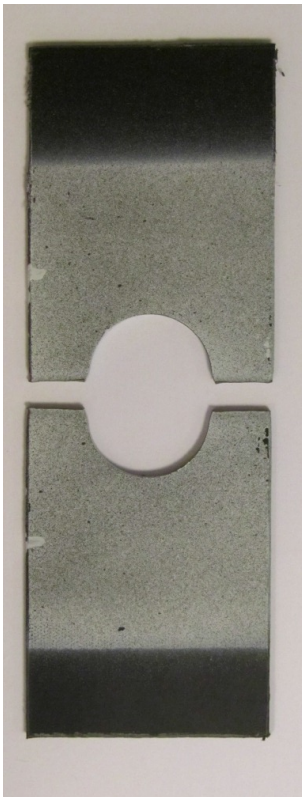

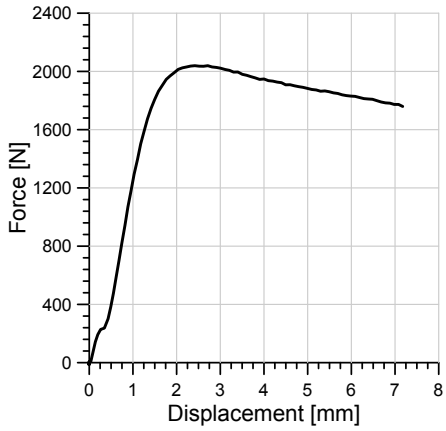

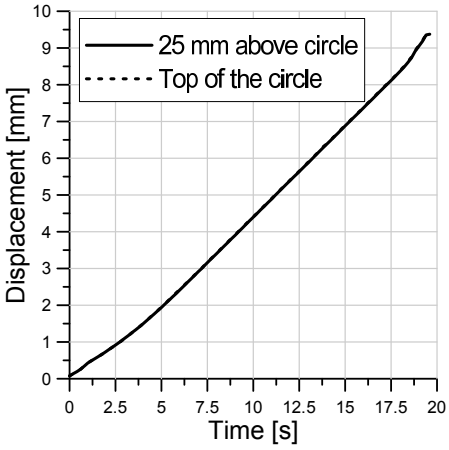

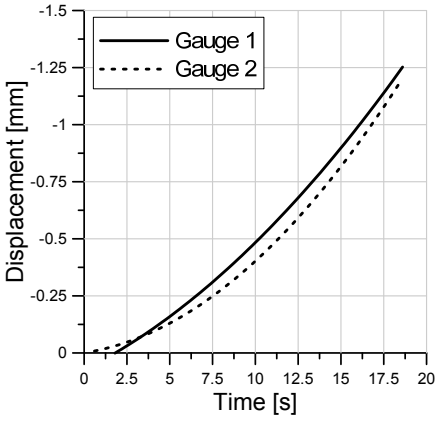

Test specifications			
Approx. $\dot{\varepsilon}_{gauge}[\mathrm{s}^{-1}]$		0.025	
	$b_{t,1}$ [mm]	$b_{t,2}$ [mm]	D [mm]
Initial dimensions	15.1	15.3	30.0

Very local deformation and fracture. The gauges deform only 1.25 mm. Except for the fracture in the gauge area, is the hole more or less unaffected. The core and the outer skin have fractured simultaneously. The transversal deformation in the gauges is quite equal.

A.2.4 D2V2, v=0.5 mm/s

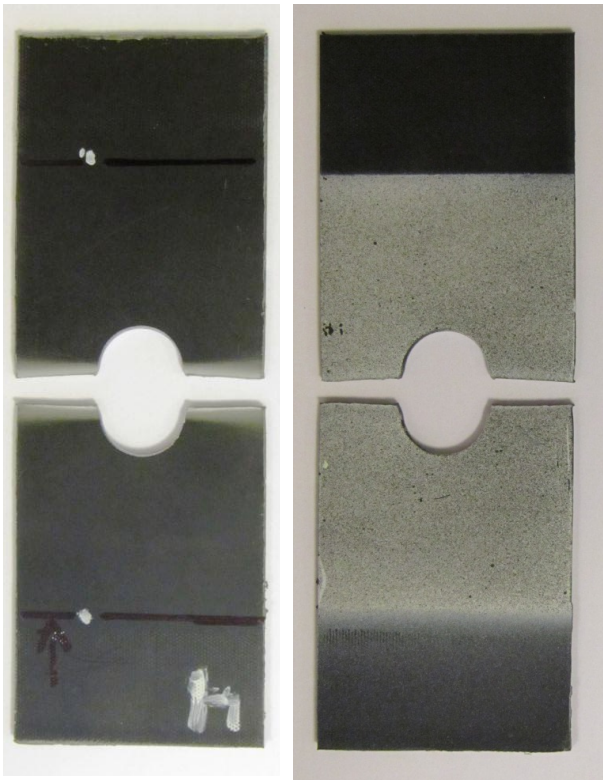

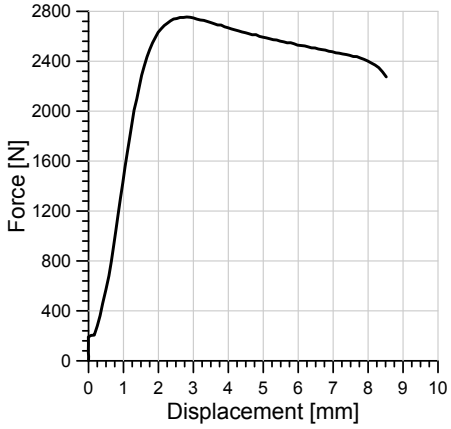

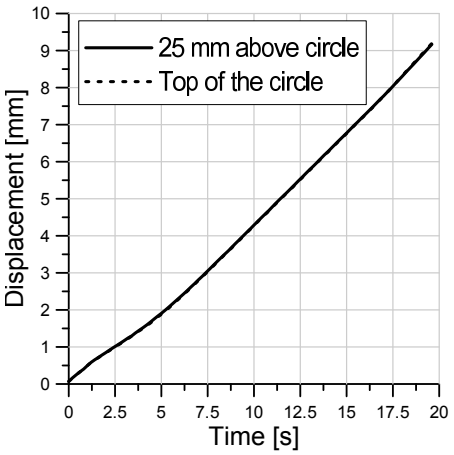

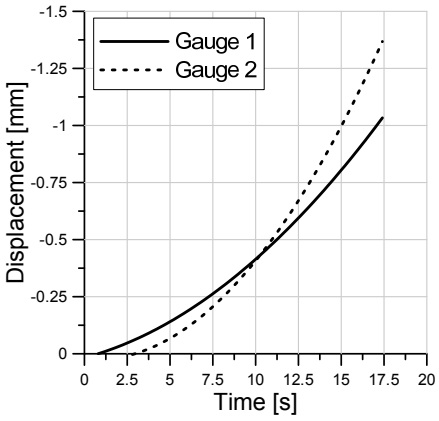

Test specifications			
Approx. $\dot{\varepsilon}_{gauge}[\mathrm{s}^{-1}]$		0.025	
	$b_{t,1}$ [mm]	$b_{t,2}$ [mm]	D [mm]
Initial dimensions	20.5	19.8	19.8

Highest peak load. A local fracture occurs. The core and the outer skin have fractured simultaneously. The transversal deformation in the gauges is different confirming the asymmetrical placement of the hole(cf. the table).

A.3 Drop tower

A.3.1 DT1, E∼50 J

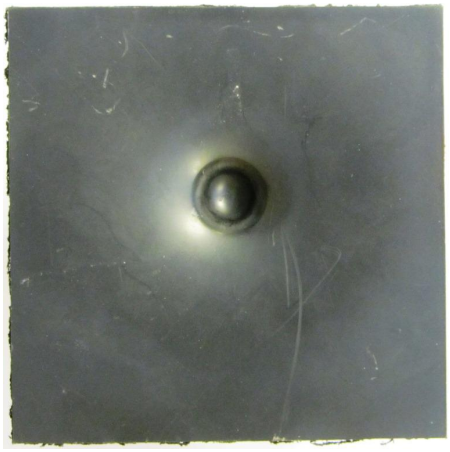

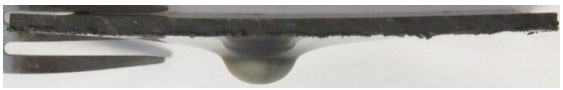

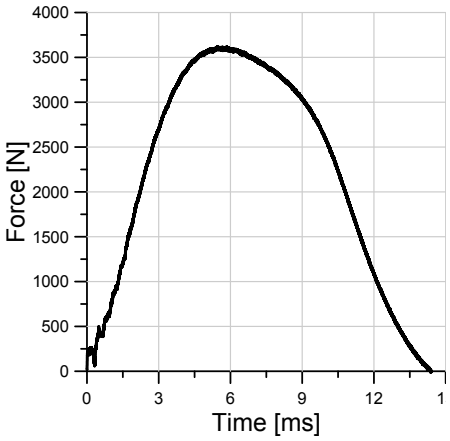

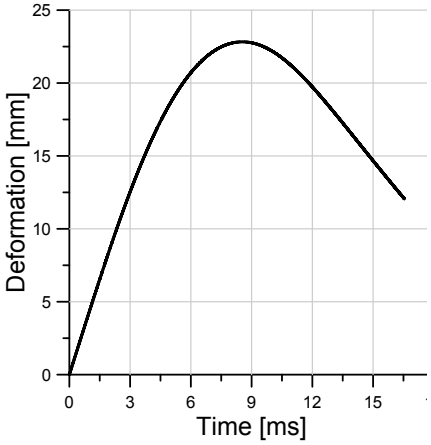

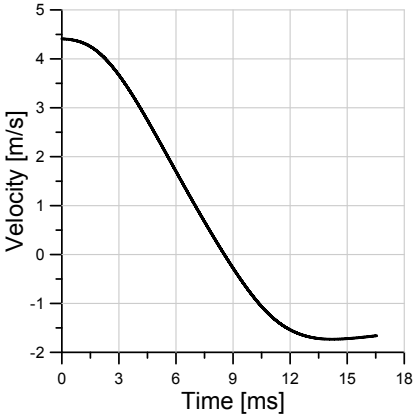

Test specifications	
Spear mass [kg]	5.045
Impact velocity [m/s]	4.43
Drop height [m]	1

The specimen absorbed the impact and deformed as shown in the pictures. The ring where the plate was clamped is shown in the middle picture. The spear bounced back a bit after the impact thus the negative speed at the end of the velocity-time plot.

A.3.2 DT2, E∼100 J

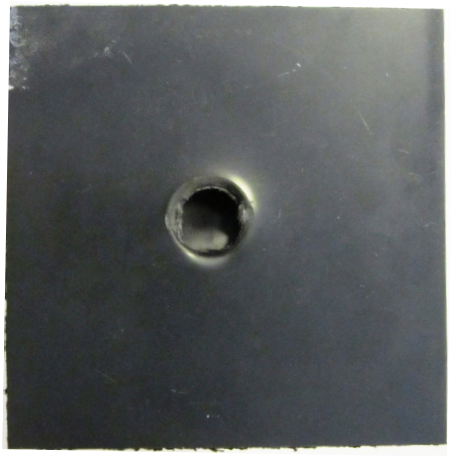

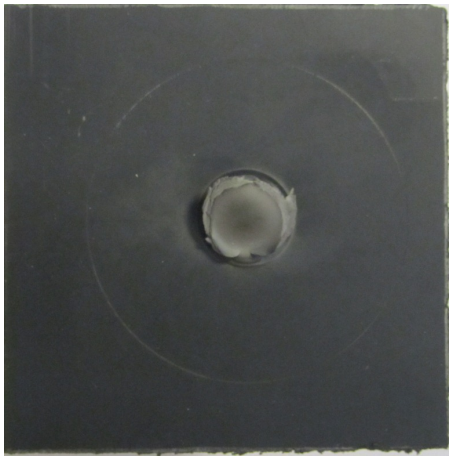

Test specifications	
Spear mass [kg]	5.045
Impact velocity [m/s]	6.26
Drop height [m]	2

The specimen fractured and the impact area was nearly parted from the rest of the specimen by a plug-like fracture mechanism.

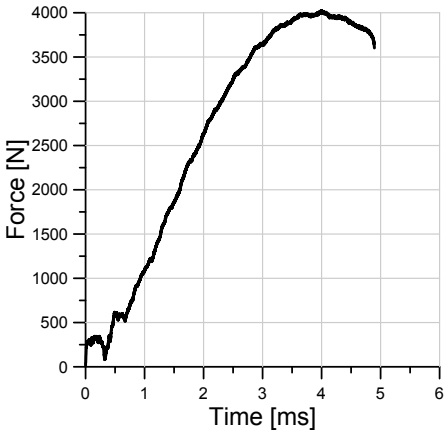

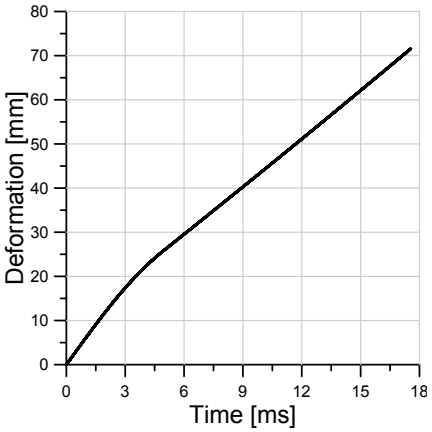

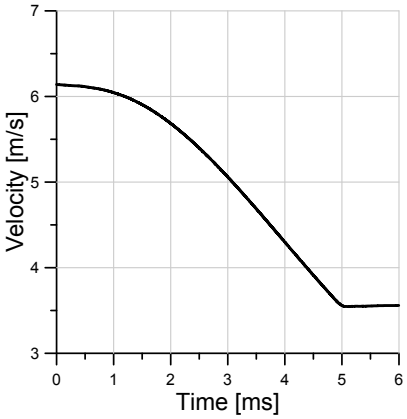

A.3.3 DT3, E∼100 J

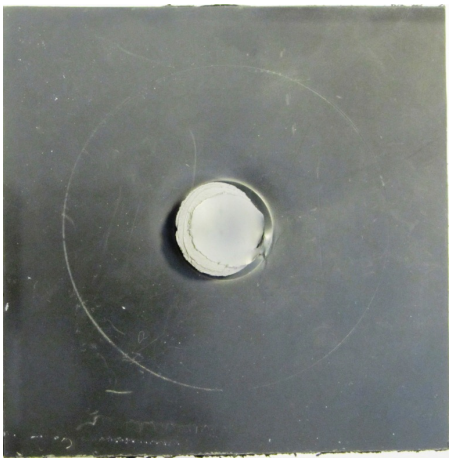

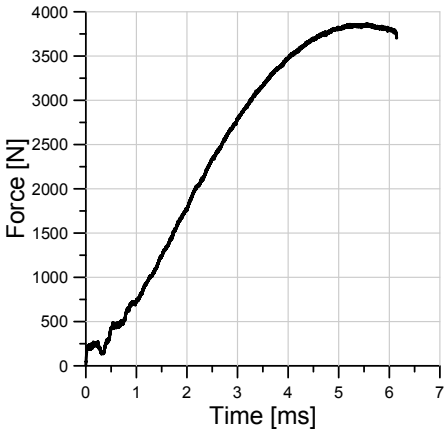

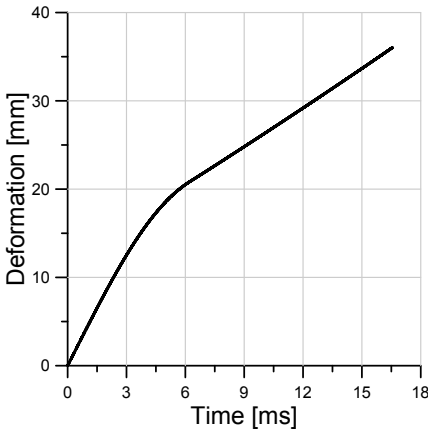

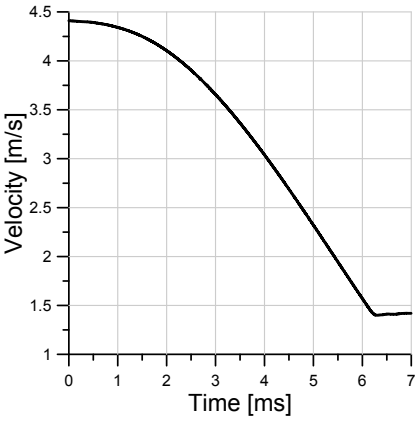

Test specifications	
Spear mass [kg]	10.045
Impact velocity [m/s]	4.43
Drop height [m]	1

The specimen fractured and the impact area was nearly parted from the rest of the specimen by a plug-like fracture mechanism.

A.3.4 DT4, E∼75 J

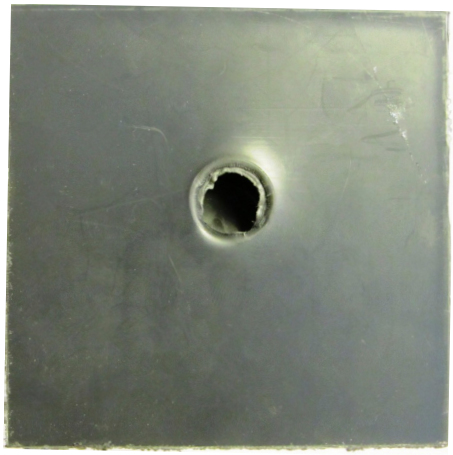

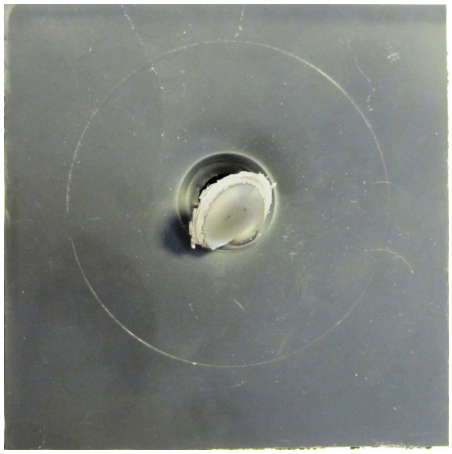

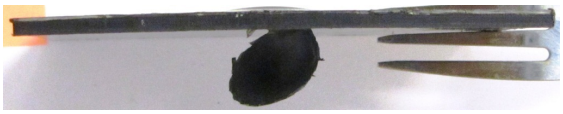

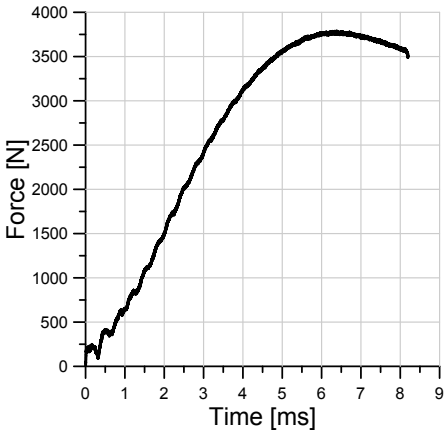

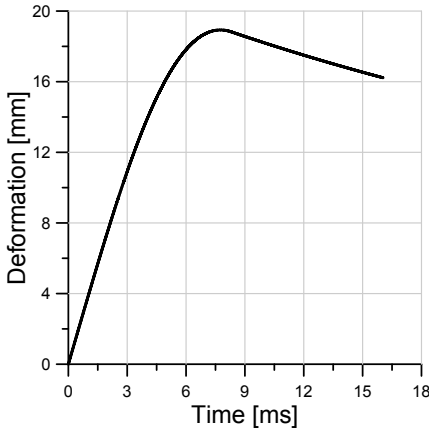

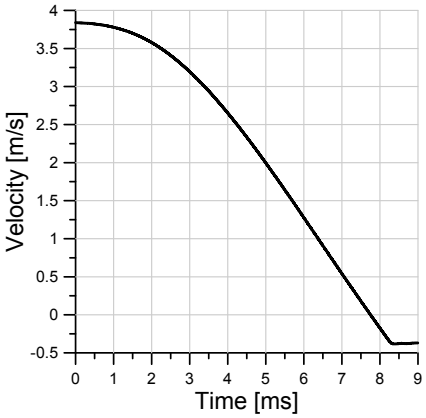

Test specifications	
Spear mass [kg]	10.045
Impact velocity [m/s]	3.86
Drop height [m]	0.76

The specimen fractured and the impact area was nearly parted from the rest of the specimen by a plug-like fracture mechanism. It should be noted that the velocity ends up with at negative value at the end. This is a little strange since the specimen fractures. The reason is not known.

A.3.5 DT5, E∼60 J

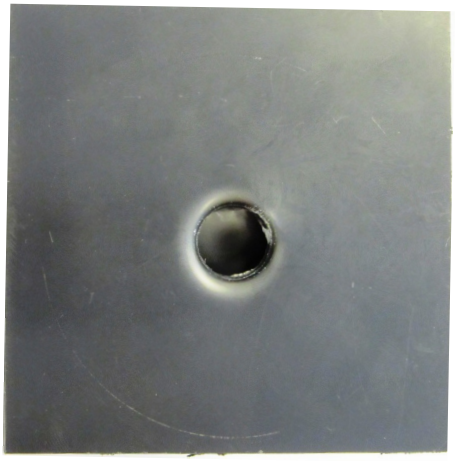

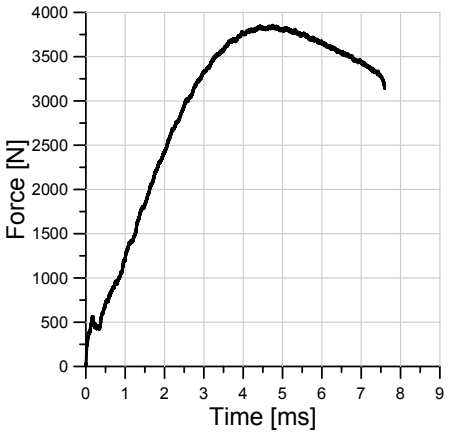

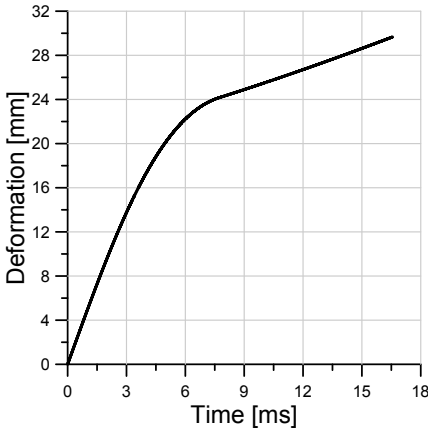

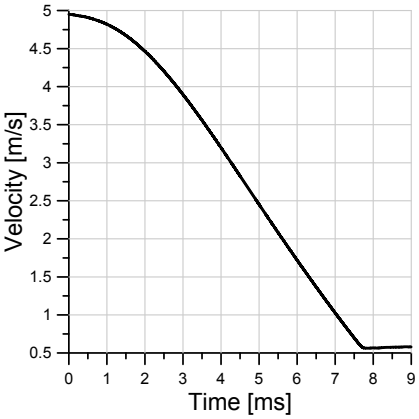

Test specifications	
Spear mass [kg]	5.045
Impact velocity [m/s]	4.88
Drop height [m]	1.21

The specimen fractured and the impact area was nearly parted from the rest of the specimen by a plug-like fracture mechanism.

A.3.6 DT6, E∼55 J

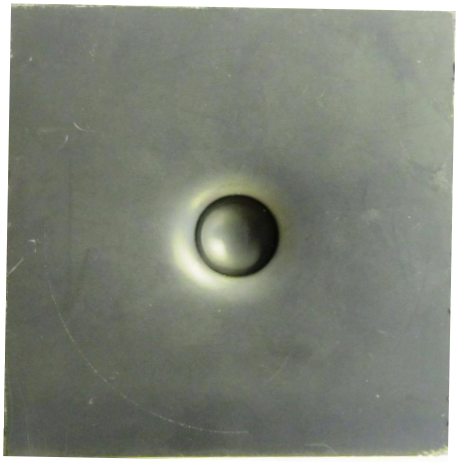

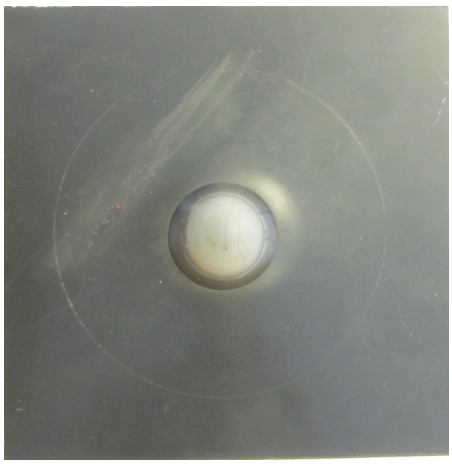

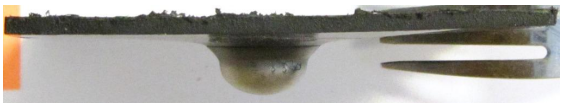

Test specifications	
Spear mass [kg]	5.045
Impact velocity [m/s]	4.67
Drop height [m]	1.11

The specimen absorbs the impact and recoils the spear

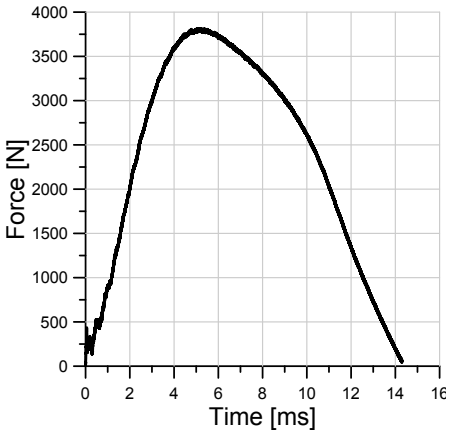

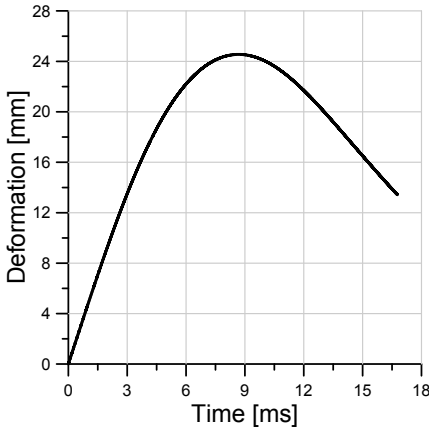

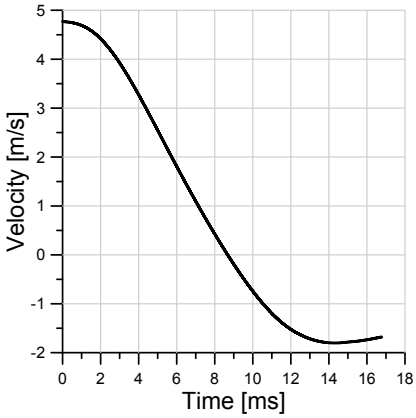

Appendix B

Matlab scripts

The Matlab scripts are added in the appendix in order to show the derivation of some of the results mentioned in the thesis. The scripts are described so that it should be possible to follow them without knowing the code beforehand. Some basic knowledge is, however, needed in order to understand them.

The scripts are arranged by the appearance in the thesis.

B.1 Finding the critical cross-section of the material tests

This script finds the cross-section with the highest strain values along the specimen length. It uses the strain matrices from 7D as input and returns the longitudinal and transversal strain in separate vectors.

```
clear all                % Clearing the memory
clc                      % and the command window

file = 'T2';             % Defines the test that is to be analyzed
testnumber = 2;          % Defines which Excel-sheet the data should be
                         % written to.

load('-mat',file)            % Loads the ".mat" file with name "file".

names = load('-mat',file);  % Lists the names and the dimension
                            % of all the matrices in file.mat into the
                            % vector "names"

MatNum = fieldnames(names, '-full');    % Gets the names of the matrices
                                        % from "names"

NumFrame = (length(MatNum))/2;          % Finds the number of matrice-names
                                        % in MatNum and divides it by 2.
                                        % This is because half the matrices
                                        % are the longitudinal strain the
                                        % other half the transversal strain

dim = size(elnmaxi001);                 % Finds the dimension of the
                                        % matrices.

% The following for loops read an "elnmaxiXXX/elnminiXXX" matrix and
% register it as the matrix Ml/Mt. The next line then finds the mean of
% each row of Ml and puts it into the matrix meanRVl. meanRVl has the same
% amount of columns as there are elnmaxi matrices. The next line
% then constructs a vector containing the mean of each row of meanRVl and
% thus a second mean over all the rows of Ml.

for i = 1:NumFrame
    for j = 1:dim(1,1)
        Ml = eval([sprintf('elnmaxi%.3d',i)]);
        meanRVl(j,i) = mean(Ml(j,:));
        maxMeanl(j,1) = nanmean(meanRVl(j,:));
    end
end

for m = 1:NumFrame
    for n = 1:dim(1,1)
        Mt = eval([sprintf('elnmini%.3d',m)]);
        meanRVt(n,m) = abs(mean(Mt(n,:)));
        maxMeant(n,1) = abs(nanmean(meanRVt(n,:)));
        counter(n) = n;
    end
    loops(m) = m;
end

[row col] = find(meanRVl==max(max(meanRVl)));   % Finds the row and column
                                                % containing the maximum
                                                % mean strain value of
                                                % all the means in meanRVl
```

```
[r] = find(maxMeanl==max(max(maxMeanl)));    % Finds the cell containing the
                                             % maximum mean strain value

[rowt colt] = find(meanRVt==max(max(meanRVt))); % The same as above but for
[rt] = find(maxMeant==max(max(maxMeant)));      % the transversal direcion.

dimmRV = size(meanRVl);      % Finds the dimension of meanRVl

for k = 1:dimmRV(1,2)
    epsmax(k) = meanRVl(r,k);    % Reads the mean longitudinal strain along
    epsmin(k) = meanRVt(rt,k);   % the row r/rt, which is the row with the
end                              % highest mean strain.

h1 = figure;                 % Plots the curves shown in the figure below
subplot(2,1,1)
title('strains')
plot(loops,epsmax,'b-')
hold on
plot(loops,epsmin,'r-')
axis([0 300 0 1.3])
xlabel('Loops')
ylabel('Strain')
subplot(2,1,2)
title('Critical Cross-Section')
plot(maxMeanl,-counter,'b-')
hold on
plot(maxMeant,j-counter,'r-')
axis([0 1.1*max(maxMeanl) -dimmRV(1,1) 0])
xlabel('Mean strains')
ylabel('(-)Critical row')

% The following lines write the vectors epsmax and epsmin to the
% Excel sheet "DIC strain.xlsx"

filename = 'DIC Strain.xlsx';
xlswrite(filename,epsmax',testnumber,'A2')
xlswrite(filename,epsmin',testnumber,'C2')
```

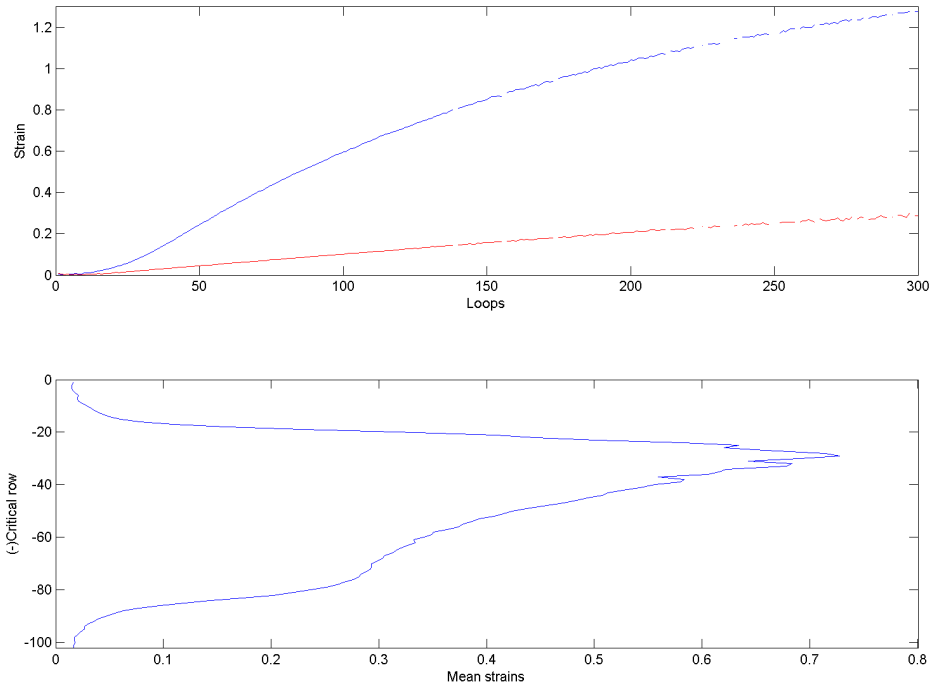

Figure B.1: The plot produced by the script above. The critical row is row 29 for the test analysed in the code.

B.2 The true stress-strain curve for the compression tests

The following script was applied to calculate the logarithmic strains and the true stress in the compression tests. The code uses the pictures taken by the rig camera to define the geometry of the specimen throughout the test. At the end is the result written to a Excel file so that it can be easily applied in other analyses. The script has to be located in the same folder as the pictures in order to work.

```
clear all                % Clearing the memory
clc                      % and the command window

% Reading all the picture names into the matrix NumBmp
NumBmp = dir('PP-1C-T15_2012_02_28_15h35m01s_Cam1_Frame_*.bmp');
% delFrame defines the frame in which the deformation starts
delFrame = 0;
% A difference needed for the for loops
NetNumFrame = length(NumBmp)-delFrame;
% The next two lines defines which sheet of the Excel file with the name
% filename the data should be written to. This allows for efficient
% processing of multiple tests.
SheetNumber = 1;
filename = 'CompData.xlsx';

% Predefining the matrices
fWProw = zeros(1,NetNumFrame);
lWProw = zeros(1,NetNumFrame);
mWProw = zeros(1,NetNumFrame);
fWPcol = zeros(1,NetNumFrame);
lWPcol = zeros(1,NetNumFrame);
Hdef = zeros(1,NetNumFrame);
Ddef = zeros(1,NetNumFrame);
t = zeros(1,NetNumFrame);

% The following for loop loads one of the pictures taken by the camera in
% the test rig. It then turns it into a picture containing only black and
% white based on a level defining which colors that are to be white and
% which that are to be black. A picture in black and white is the same as a
% matrix containing only ones(white) and zeroes(black). The transitions
% from black to white are used to define the geometry of the specimen
% at any point in time.

for i = 1:NetNumFrame
    level = graythresh(imread(NumBmp(i).name)); % Defining the point on the
                                                % greyscale where black and
                                                % white should be parted

    bw = im2bw(imread(NumBmp(i).name),level);   % Making picture NumBmp(i)
                                                % into a picture containing
                                                % only black and white

    wb = 1-bw;  % Defines an version of the picture where black and white
                % are switched

    % The next two lines find the rows that define the top and bottom of
    % the specimen
    fWProw(i) = find(bw(:,2448),1,'first');
    lWProw(i) = find(bw(:,2448),1,'last');
    mWProw(i) = round((fWProw(i)+lWProw(i))/2); % Defines the midpoint of
                                                % the specimen

    % These lines find the vertical sides of the specimen
    fWPcol(i) = find(wb(mWProw(i),:),1,'first');
    lWPcol(i) = find(wb(mWProw(i),:),1,'last');
```

```
    % These lines define the difference between the rows and columns
    % marking the transitions from black to white. This difference give the
    % height and diameter of the specimen throughout the course of the test
    Hdef(i) = lWProw(i) - fWProw(i);
    Ddef(i) = lWPcol(i) - fWPcol(i);
end

d0 = 6.09;              % Uses the diameter of specimen to define the ratio
mmPRpix = d0/Ddef(1);   % of millimetres/pixel.

Hdefmm = Hdef*mmPRpix;  % Defining the height and diameter in millimetres
Ddefmm = Ddef*mmPRpix;  % instead of pixels.

% Defning the Excel file that the force and displacement
% data are to be read from
file = '...\BMP\Comp.xls';
SheetNumber = 1;

% Ddefining the area and height at t=0
A0 = (pi()*d0^2)/4;
L0 = 3.2;

% Defining the displacement and force vectors
U = xlsread(file,SheetNumber,'B2:B3000');
Ut = Ddefmm-Ddefmm(1);
F = 1000*xlsread(file,SheetNumber,'C2:C3000');

% Predefining vectors for increased performance
A = zeros(NetNumFrame,1);
stress = zeros(NetNumFrame,1);
epsPIC = zeros(NetNumFrame,1);

% Calculating the longitudinal and transversal logarithmic strains and the
% true stress

for j = 1:NetNumFrame
    epsLOG(j) = abs(log(1-(U(j)/L0)));
    epsTRAN(j) = abs(log(1-(Ut(j)/d0)));
    A(j) = (pi()*Ddefmm(j)^2)/4;
    stress(j) = abs(F(j)/A(j));
end

% Writing the vectors to the Excel file named "filename"(defined earlier)
xlswrite(filename,epsLOG',SheetNumber,'A2')
xlswrite(filename,eps,1,'C2')
xlswrite(filename,stress,SheetNumber,'E2')
```

B.3 Calculation of the yields stresses

The yield stresses were calculated using Considère's criterion. This is stated as:

$$\frac{d\sigma_{true}}{d\varepsilon_{log}} = \sigma_{true} \tag{B.1}$$

A graphical representation is shown in Figure B.2a.

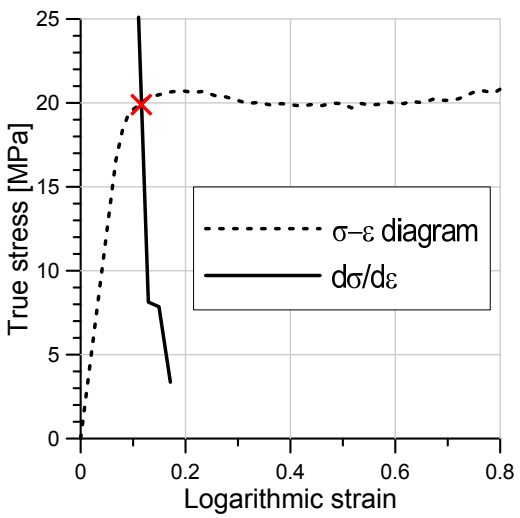

(a) The yield stress calculation of test T3-L1

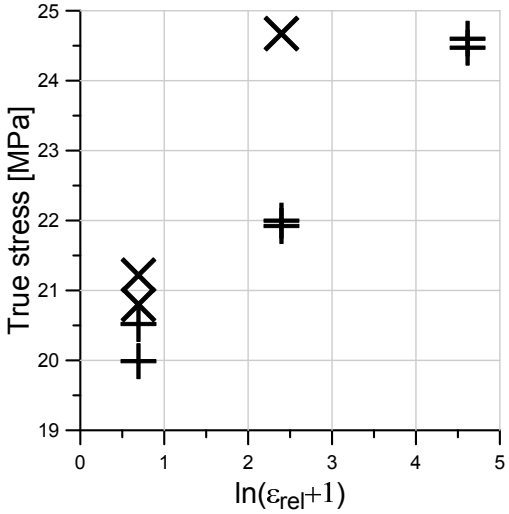

(b) The relation between the yield stresses and the strain rate. (+) are tension tests and (×) are compression tests

Figure B.2: The method used to identify the yield stresses and the yield stresses in relation to the strain rate

The Matlab script calculates the yield stresses for a single test. The needed inputs are the tension test number and how much of the stress-strain curve that is to be used in the calculation. The latter argument is defined by defining the last cell of the strain and stress vector that are to be used in the calculations. To find the coordinates of the crossing curves, a function made by the German Matlab user Sebastian Hölz is applied. This function is named "Curve Intersect 2" and is applied as a user defined function in Matlab. The function is shown at the end of this section.

The code was modified to work with the compression tests and with series of tests. These codes are not shown here.

```
clear all           % Clearing the memory
clc                 % and the command window

s=1; c=20;          % s equals the testnumber and c is the endcell of the
                    % strain vector and the stress vector.

% The two next lines reads the longitudinal logarithmic strain and the true
% stress from an Excel-file
epsRead = epsL(s);
stressRead = StressCalc(s);

% These lines adjust the length of the stress and strain vector
eps = epsRead(1:min(length(stressRead),length(epsRead)));
stress = stressRead(1:min(length(stressRead),length(epsRead)));

rows = find(eps<0.75,1,'last'); % Defines an upper limit for the strain
                                % values that are to be used.

% Predefining the vectors for the for loop
consid = zeros(rows,1);
deps = zeros(rows,1);
dstress = zeros(rows,1);

% The following loop calculates the vector representing d(epsilon)/d(sigma)
for i = 2:min(length(consid))
    deps(i-1) = mean(eps(i))-mean(eps(i-1));
    dstress(i-1) = mean(stress(i))-mean(stress(i-1));
    consid(i-1) = dstress(i-1)/deps(i-1);
end

endcell = c;    % Defining c to be the endcell

% The following line applies the function Curve Intersect 2
[x y] = curveintersect(eps,stress,eps(1:endcell),consid(1:endcell));

% Puts the result of the function curveintersect into the vector coord
coord = [x y];

% Sets sigmaY equal to the y-coordinate found from curveintersect
sigmaY = coord(1,2);
```

```
Copyright (c) 2009, Sebastian Hölz
All rights reserved.

Redistribution and use in source and binary forms, with or without
modification, are permitted provided that the following conditions are
met:

    * Redistributions of source code must retain the above copyright
      notice, this list of conditions and the following disclaimer.
    * Redistributions in binary form must reproduce the above copyright
      notice, this list of conditions and the following disclaimer in
      the documentation and/or other materials provided with the distribution

THIS SOFTWARE IS PROVIDED BY THE COPYRIGHT HOLDERS AND CONTRIBUTORS "AS IS"
AND ANY EXPRESS OR IMPLIED WARRANTIES, INCLUDING, BUT NOT LIMITED TO, THE
IMPLIED WARRANTIES OF MERCHANTABILITY AND FITNESS FOR A PARTICULAR PURPOSE
ARE DISCLAIMED. IN NO EVENT SHALL THE COPYRIGHT OWNER OR CONTRIBUTORS BE
LIABLE FOR ANY DIRECT, INDIRECT, INCIDENTAL, SPECIAL, EXEMPLARY, OR
CONSEQUENTIAL DAMAGES (INCLUDING, BUT NOT LIMITED TO, PROCUREMENT OF
SUBSTITUTE GOODS OR SERVICES; LOSS OF USE, DATA, OR PROFITS; OR BUSINESS
INTERRUPTION) HOWEVER CAUSED AND ON ANY THEORY OF LIABILITY, WHETHER IN
CONTRACT, STRICT LIABILITY, OR TORT (INCLUDING NEGLIGENCE OR OTHERWISE)
ARISING IN ANY WAY OUT OF THE USE OF THIS SOFTWARE, EVEN IF ADVISED OF THE
POSSIBILITY OF SUCH DAMAGE.


function [x,y]=curveintersect(varargin)
% Curve Intersections.
% [X,Y]=CURVEINTERSECT(H1,H2) or [X,Y]=CURVEINTERSECT([H1 H2]) finds the
% intersection points of the two curves on the X-Y plane identified
% by the line or lineseries object handles H1 and H2.
%
% [X,Y]=CURVEINTERSECT(X1,Y1,X2,Y2) finds the intersection points of the
% two curves described by the vector data pairs (X1,Y1) and (X2,Y2).
%
% X and Y are empty if no intersection exists.
%
% Example
% -------
% x1=rand(10,1); y1=rand(10,1); x2=rand(10,1); y2=rand(10,1);
% [x,y]=curveintersect(x1,y1,x2,y2);
% plot(x1,y1,'k',x2,y2,'b',x,y,'ro')
%
% Original Version (-> curveintersect_local)
% ------------------------------------------
% D.C. Hanselman, University of Maine, Orono, ME 04469
% Mastering MATLAB 7
% 2005-01-06
%
% Improved Version (-> this function)
% -----------------------------------
% S. Hlz, TU Berlin, Germany
% v 1.0: October 2005
% v 1.1: April   2006     Fixed some minor bugs in function 'mminvinterp'

x=[]; y=[];
```

```
[x1,y1,x2,y2]=local_parseinputs(varargin{:});
ind_x1=sign(diff(x1)); ind_x2=sign(diff(x2));

ind1=1;
while ind1<length(x1)
    ind_max = ind1+min(find(ind_x1(ind1:end)~=ind_x1(ind1)))-1;
    if isempty(ind_max) | ind_max==ind1; ind_max=length(x1); end
    ind1=ind1:ind_max;

    ind2=1;
    while ind2<length(x2)
        ind_max = ind2+min(find(ind_x2(ind2:end)~=ind_x2(ind2)))-1;
        if isempty(ind_max) | ind_max==ind2; ind_max=length(x2); end
        ind2=ind2:ind_max;

        % Fallunterscheidung
        if ind_x1(ind1(1))==0 & ind_x2(ind2(1))~=0
            x_loc=x1(ind1(1));
            y_loc=interp1(x2(ind2),y2(ind2),x_loc);
            if ~(y_loc>=min(y1(ind1)) && y_loc<=max(y1(ind1))); y_loc=[];
x_loc=[]; end

        elseif ind_x2(ind2(1))==0 & ind_x1(ind1(1))~=0
            x_loc=x2(ind2(1));
            y_loc=interp1(x1(ind1),y1(ind1),x_loc);
            if ~(y_loc>=min(y2(ind2)) && y_loc<=max(y2(ind2))); y_loc=[];
x_loc=[]; end

        elseif ind_x2(ind2(1))~=0 & ind_x1(ind1(1))~=0

[x_loc,y_loc]=curveintersect_local(x1(ind1),y1(ind1),x2(ind2),y2(ind2));

        elseif ind_x2(ind2(1))==0 & ind_x1(ind1(1))==0
            [x_loc,y_loc]=deal([]);

        end
        x=[x; x_loc(:)];
        y=[y; y_loc(:)];
        ind2=ind2(end);
    end
    ind1=ind1(end);
end



% ------------------------------------------------
function [x,y]=curveintersect_local(x1,y1,x2,y2)

if ~isequal(x1,x2)
   xx=unique([x1 x2]); % get unique data points
   xx=xx(xx>=max(min(x1),min(x2)) & xx<=min(max(x1),max(x2)));
   if numel(xx)<2
      x=[];
      y=[];
      return
```

```
   end
   yy=interp1(x1,y1,xx)-interp1(x2,y2,xx);
else
   xx=x1;
   yy=y1-y2;
end
x=mminvinterp(xx,yy,0); % find zero crossings of difference
if ~isempty(x)
   y=interp1(x1,y1,x);
else
   x=[];
   y=[];
end

%-------------------------------------------------------------------------
%-------------------------------------------------------------------------
function [xo,yo]=mminvinterp(x,y,yo)
%MMINVINTERP 1-D Inverse Interpolation. From the text "Mastering MATLAB 7"
% [Xo, Yo]=MMINVINTERP(X,Y,Yo) linearly interpolates the vector Y to find
% the scalar value Yo and returns all corresponding values Xo interpolated
% from the X vector. Xo is empty if no crossings are found. For
% convenience, the output Yo is simply the scalar input Yo replicated so
% that size(Xo)=size(Yo).
% If Y maps uniquely into X, use INTERP1(Y,X,Yo) instead.
%
% See also INTERP1.

if nargin~=3
   error('Three Input Arguments Required.')
end
n = numel(y);
if ~isequal(n,numel(x))
   error('X and Y Must have the Same Number of Elements.')
end
if ~isscalar(yo)
   error('Yo Must be a Scalar.')
end

x=x(:); % stretch input vectors into column vectors
y=y(:);

if yo<min(y) || yo>max(y) % quick exit if no values exist
   xo = [];
   yo = [];
else                      % find the desired points

   below = y<yo;          % True where below yo
   above = y>yo;          % True where above yo
   on    = y==yo;         % True where on yo

   kth = (below(1:n-1)&above(2:n)) | (above(1:n-1)&below(2:n));     % point k
   kp1 = [false; kth];                                             % point
k+1

   xo = [];                                                        % distance
between x(k+1) and x(k)
```

```
   if any(kth);
       alpha = (yo - y(kth))./(y(kp1)-y(kth));
       xo = alpha.*(x(kp1)-x(kth)) + x(kth);
   end
   xo = sort([xo; x(on)]);                                          % add
points, which are directly on line

   yo = repmat(yo,size(xo));                                        %
duplicate yo to match xo points found
end
%-------------------------------------------------------------------------
function [x1,y1,x2,y2]=local_parseinputs(varargin)

if nargin==1 % [X,Y]=CURVEINTERSECT([H1 H2])
   arg=varargin{1};
   if numel(arg)==2 && ...
      all(ishandle(arg)) && all(strcmp(get(arg,'type'),'line'))
      data=get(arg,{'XData','YData'});
      [x1,x2,y1,y2]=deal(data{:});
   else
      error('Input Must Contain Two Handles to Line Objects.')
   end
elseif nargin==2 % [X,Y]=CURVEINTERSECT(H1,H2)
   arg1=varargin{1};
   arg2=varargin{2};
   if numel(arg1)==1 && ishandle(arg1) && strcmp(get(arg1,'type'),'line')...
   && numel(arg2)==1 && ishandle(arg2) && strcmp(get(arg2,'type'),'line')

      data=get([arg1;arg2],{'XData','YData'});
      [x1,x2,y1,y2]=deal(data{:});
   else
      error('Input Must Contain Two Handles to Line Objects.')
   end
elseif nargin==4
   [x1,y1,x2,y2]=deal(varargin{:});
   if ~isequal(numel(x1),numel(y1))
      error('X1 and Y1 Must Contain the Same Number of Elements.')
   elseif ~isequal(numel(x2),numel(y2))
      error('X2 and Y2 Must Contain the Same Number of Elements.')
   end
   x1=reshape(x1,1,[]); % make data into rows
   x2=reshape(x2,1,[]);
   y1=reshape(y1,1,[]);
   y2=reshape(y2,1,[]);

else
   error('Incorrect Number of Input Arguments.')
end
if min(x1)>max(x2) | min(x2)>max(x1) | min(y2)>max(y1) | min(y1)>max(y2) %
Polygons can not have intersections
    x1=[]; y1=[]; x2=[]; y2=[]; return
end
if numel(x1)<2 || numel(x2)<2 || numel(y1)<2 || numel(y2)<2
   error('At Least Two Data Points are Required for Each Curve.')
end
```

B.4 Plate with centric hole

B.4.1 The transversal displacement in the gauges

This script calculates the transversal deformation of the gauges by using a similar approach as for the compression tests. The script reads the pictures from the test-rig camera and turns them into ones and zeroes(black and white). The transitions between black and white will change from picture to picture. By storing the position of this transition from each picture the displacements can be represented.

Due to noise in the pictures taken during the tests are the deformations represented by exponential regression functions. This introduces a small deviation in the displacements but it also makes them much easier to compare.

The script has to be located in the same folder as the pictures in order to work.

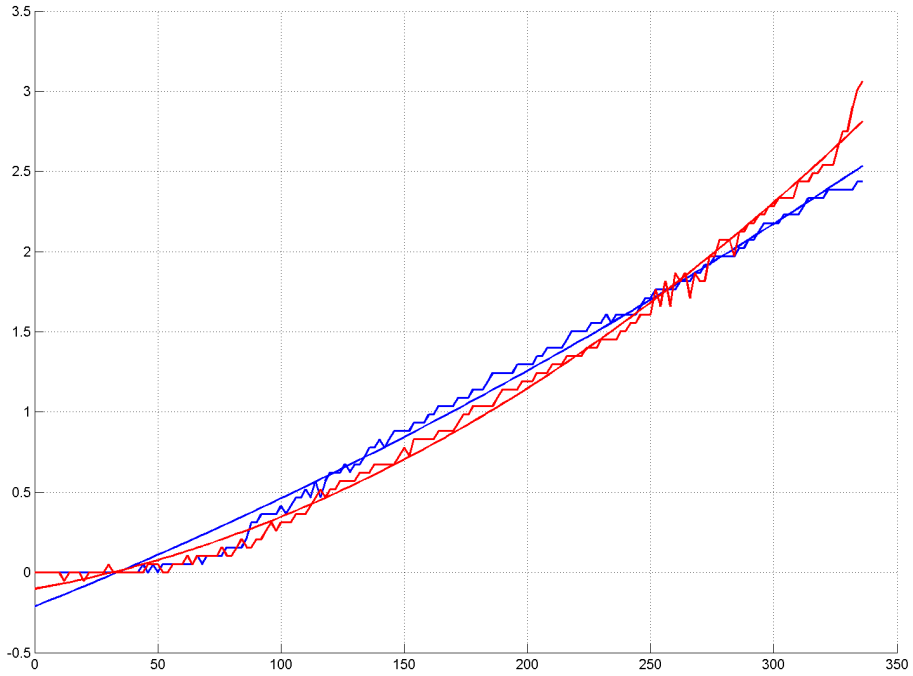

Figure B.3: The plot produced by the script. The plot shows the transversal deformation of the test D2V1(the uneven curve) and the curve fitted to the data(the smooth curve)

```
clear all % Clear the memory
clc       % Clear the command window

% These five lines define the input and output files used in the script.
% It starts with defining the sheet of the Excel file "filename.xlsx" that
% the data should be written to. Then is the name of the pictures defined
% in the vector NumBmp. The last two lines define the applied time vector.
SheetNumber = 2;
filename = 'dx.xlsx';
NumBmp = dir('PPV-02_2012_03_19_13h07m37s_Cam1_Frame_*.bmp');
timeread = dlmread('PPV-02.txt','\t',1,0);
time=timeread(:,1);

delFrame = 100; % Defines how many pictures that are to removed at the end
                % of the picture series

StartFrame = 1; % Defines the starting picture
EndFrame = length(NumBmp)-delFrame; % Defines the difference between start
                                    % and end

mmPp = 19.76/(1481-1100);% The mm to pixel ratio. It is calculated with
                         % respect to the diameter of the hole.
                  % -> diameter in mm/number of pixels across the diameter

% The if loop adjusts the number of pictures to be processed based on how
% many pictures that are removed in the beginning and the end.
if StartFrame > 1
    FrameDiff = EndFrame - StartFrame;
else
    FrameDiff = EndFrame;
end

level = 0.25; % Defines the greyscale limit

% The next two lines define the size of the pictures by converting a
% picture into a matrix and finding the dimension of the matrix
dimBW = im2bw(imread(NumBmp(50+(StartFrame-1)).name),level);
dim = size(dimBW);

% StartRow and EndRow define the rows that are located more or less at the
% top and at the bottom of the gauges in the picture, i.e. they give the
% location of the gauges in the picture.
StartRow = 630;
EndRow = 1500;

RowDiff = EndRow-StartRow; % Difference used in the for loop

for i = StartFrame:FrameDiff
    % Reads the picture
    bw = im2bw(imread(NumBmp(i+(StartFrame-1)).name),level);
    for j = 1:1:RowDiff
        % The next four lines of code define the transitions from black to
        % white in the gauge areas. The two upper lines define one
        % gauge, the two below define the other.
        fWPcolII = find(bw(StartRow+j,670:(dim(2)/2)),1,'first');
```

```
        lWPcolII = find(bw(StartRow+j,670:(dim(2)/2)),1,'last');

        fWPcolVI = find(bw(StartRow+j,(dim(2)/2):1840),1,'first');
        lWPcolVI = find(bw(StartRow+j,(dim(2)/2):1840),1,'last');

        %The difference between the transition points is found
        coldiffII(j) = lWPcolII - fWPcolII;
        coldiffII(~coldiffII) = inf;

        coldiffVI(j) = lWPcolVI - fWPcolVI;
        coldiffVI(~coldiffVI) = inf;
    end
    % The deformation is stored as the minimum distance between transitions
    % for every picture.
    dxIIpix(i-(StartFrame-1))= min(coldiffII);
    dxVIpix(i-(StartFrame-1))= min(coldiffVI);
end

t = time(1:length(dxIIpix)); % Defines the length of the time vector.

dxII = mmPp*(dxIIpix(1)-dxIIpix); % Converts the deformations from pixels
dxVI = mmPp*(dxVIpix(1)-dxVIpix); % to millimetres

tdcII = polyfit(t,dxII',2); %
dxIIfit = polyval(tdcII,t); % These four lines find an exponential function
                            % that fits the deformation curves
tdcVI = polyfit(t,dxVI',2); %
dxVIfit = polyval(tdcVI,t); %

% Plots a figure of the deformations and the fitted curve
h1 = figure;
hold on
grid on
plot(t,dxII)
plot(t,dxIIfit)
plot(t,dxVI,'r-')
plot(t,dxVIfit,'r-')

% These last three lines write the resulting vectors to the defined Excel file
xlswrite(filename,t,SheetNumber,'A3')
xlswrite(filename,dxIIfit,SheetNumber,'C3')
xlswrite(filename,dxVIfit,SheetNumber,'E3')
```

B.4.2 Identifying the correct deformation rate

This script finds the correct deformation rate based on strain data from the DIC software. The input is longitudinal strain matrices and the output is an approximated strain and deformation rate for the gauge of the analysed test.

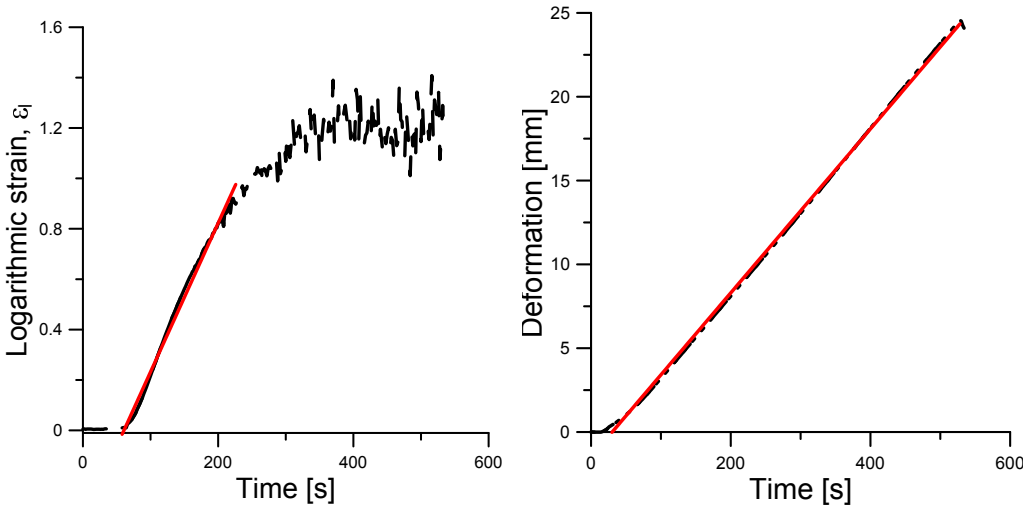

(a) Regression of the longitudinal strain. The gradient of the red line corresponds to the strain rate measured in the gauge of the material test

(b) Regression of the longitudinal deformation. The gradient of the red line corresponds to the deformation speed experienced in the gauge of the material test

Figure B.4: Calculation of the strain and deformation rate of test D2V1

Figure B.4 shows the curves produced by the script. The strain-time plot is used to define the range where the linear regression should be made. This means that a range including the strains from t=0 till t=end will yield a near straight line from the origin to approximately $\varepsilon = 1.2$, t=450 s. Such a curve will not represent the correct strain rate. The curve shown in Figure B.4a is adjusted so that the strain rate is more or less correct.

```
clear all % Clear the memory
clc       % Clear the command window

file = 'PPV 1';
testnumber = 1;

mmPp = 29.85/(1507-935); % The mm to pixel ratio. It is calculated with
                         % respect to the diameter of the hole.
                  % -> diameter in mm/number of pixels across the diameter

load('-mat',file) % Loads the ".mat" file with name "file"
names = load('-mat',file); % Lists the names and the dimension
                           % of all the matrices in file.mat into the
                           % vector "names"

MatNum = fieldnames(names, '-full');  % Gets the names of the matrices
                                      % from "names"

NumFrame = (length(MatNum))/4;        % Finds the number of matrice-names
                                      % in MatNum and divides it by 2.
                                      % This is because half the matrices
                                      % are the longitudinal strain the
                                      % other half the transversal strain

dim = size(dy001);                    % Finds the dimension of the
                                      % matrices.

% The for loop below finds the longitudinal strain in the cross-section
% with the highest strains. This cross-section is identified by finding the
% mean of each row of elnmaxiXXX matrix and putting this into the matrix
% meanRVl. The next step is to find the means of all the rows in meanRVl
% and putting them into the vector maxMeanl. The cell having the highest
% value corresponds to the row located at the same place as the critical
% cross-section.
for i = 1:NumFrame
    for j = 1:dim(1,1)
        Ml = eval([sprintf('elnmaxi%.3d',i)]); % Reads the matrix
        meanRVl(j,i) = nanmean(Ml(j,:));       % Finds the mean of each row
        maxMeanl(j,1) = nanmean(meanRVl(j,:)); % Finds the mean of each
    end                                        % row in meanRVl

    [r c] = find(maxMeanl==max(max(maxMeanl))); % Finds the cell containing
                                                % the highest strain value
    epsL(i) = nanmean(Ml(r,:));    % Defines the longitudinal strain vector
end

% Does a similar operation as the script above but for the longitudinal
% displacements.
for m = 1:NumFrame
    for n = 1:dim(1,1)
        My = eval([sprintf('dy%.3d',m)]);
        meanRVy(n,m) = mean(My(n,:));
        maxMeany(n,1) = nanmean(meanRVy(n,:));
    end
```

```
    dyI(m) = mmPp*mean(My(1,:)); % Defines the longitudinal displacement
vector
end

% These two lines define a time vector based on "DIC FvsU.xlsx"
tread = xlsread('DIC FvsU.xlsx',testnumber,'A3:A600');
t = tread(1:length(epsL));

% The next six lines find the linear part of the
% strain-time/displacement-time curve. The last line in each set of three
% defines the strain/displacement vector in the relevant range.
fcell = find(epsL>0.01,1);
lcell = find(t>245,1);
intereps = epsL(fcell:lcell);

fcelly = find(dyI>0,1);
lcelly = find(dyI==max(dyI),1);
interdyI = dyI(fcelly:lcelly);

% These four lines find a linear fit(y=ax+b) to the
% strain-time/displacement-time curve
fitter = fit(t(fcell:lcell),intereps','poly1'); % Strains
fittery = fit(t(fcelly:lcelly),interdyI','poly1'); % Displacements

epscoeff = coeffvalues(fitter); % Puts the coefficients of the linear
dycoeff = coeffvalues(fittery); % regression curve into a vector.
                                % y=ax+b -> [a b]

% These lines get the gradient of the interpolated curve
veps = epscoeff(1); % [a]
v = dycoeff(1);     % [a]

% Since half the gauge is modelled the gradients are scaled to fit the
% model
scaled_veps100 = veps*0.5
scaled_v100 = 0.5*v

% Plots the strain-time and the displacement-time curves. The linear range
% is found by interpolation using these plots.

h1 = figure;
hold on
grid on
plot(t,epsL,'m:')
plot(t(fcell:lcell),intereps,'r-')
plot(t(fcell:lcell),fitter(t(fcell:lcell)))

h2 = figure;
hold on
grid on
plot(t,dyI,'m:')
plot(t(fcelly:lcelly),interdyI,'r-')
plot(t(fcelly:lcelly),fittery(t(fcelly:lcelly)))
```

B.4.3 The longitudinal displacements

The script input is the longitudinal displacement matrix. The user then have to define two points in the matrix from where the deformation should be stored. The two points chosen in this analysis are:

- 25 millimetre above the circle
- At the "top" of the circle

The points are defined by finding the corresponding coordinates in the matrix "dy001" using the "data cursor" tool.

```
clear all % Clear the memory
clc       % Clear the command window

file = 'PPV 1'; % Defines the test that is to be analyzed
testnumber = 1; % Defines which Excel-sheet the data should be
                % written to. This makes it easy process mutiple tests with
                % the same script

mmPp = 29.85/(1507-935); % The mm to pixel ratio. It is calculated with
                         % respect to the diameter of the hole.
                 % -> diameter in mm/number of pixels across the diameter

load('-mat',file)           % Loads the ".mat" file with name "file".

names = load('-mat',file);  % Lists the names and the dimension
                            % of all the matrices in file.mat into the
                            % vector "names"

MatNum = fieldnames(names, '-full');    % Gets the names of the matrices
                                        % from "names"

NumFrame = (length(MatNum))/4;          % Finds the number of matrice-names
                                        % in MatNum and divides it by 4.
                                        % This is because there are four
                                        % different categories of matrices
                                        % defined in the .mat file.

dim = size(dy001);                  % Finds the dimension of the
                                    % matrices.

imagesc(dy001)      % Displays the first matrix so that the points from
                    % where the displacement is to be found can be found

% The for loop below loads a longitudinal displacement matrix and then two
% locations in this matrix is defined. These locations agree with the two
% points from where the deformation was to be found.
for m = 1:NumFrame
    for n = 1:dim(1,1)
        My = eval([sprintf('dy%.3d',m)]); % Loads the deformation matrix
    end
    BotCirc(m) = mmPp*mean(My(47,53:63)); % Stores the deformation at the
                                          % top of the circle

    dyI(m) = mmPp*mean(My(1,55:60));      % Stores the deformation 25 mm
                                          % above the circle
end

% These two lines write the vectors to the Excel sheet "testnumber" in the
% Excel document dy.xlsx
% xlswrite('dy.xlsx',dyI',testnumber,'A2')
% xlswrite('dy.xlsx',BotCirc',testnumber,'C2')
```

Appendix C

LS-DYNA input files

This appendix contains input files for LS-DYNA. One representative input file is presented for each of the problems that were modelled. All the applied material cards are shown. The part of the geometry file defining the sets and sections are given for the respective analyses.

C.1 Material cards

C.1.1 ppFinal.k, E=400 MPa

```
$$$$$$$$$$$$$$$$$$$$$$$$$$$$$$$$$$$$$$$$$$$$$$$$$$$$$$$$$$$$$$$$$$$$$$$$$$$$$$$$
$                              MATERIAL MODEL DEFINITIONS                      $
$$$$$$$$$$$$$$$$$$$$$$$$$$$$$$$$$$$$$$$$$$$$$$$$$$$$$$$$$$$$$$$$$$$$$$$$$$$$$$$$
$
*MAT_USER_DEFINED_MATERIAL_MODELS
$      MID       rho    User mat #    LMC    # Hist var            IBULK      IG
         1 1.000E-04        49        16        50         0        15        16
$---+----1----+----2----+----3----+----4----+----5----+----6----+----7----+----8
$      IVECT      IFAIL     ITHERM   IHYPER     IEOS
         0         0         0         1         0
$---+----1----+----2----+----3----+----4----+----5----+----6----+----7----+----8
$ E         Poisson     eps0         C   sigma_T        Cr N (lamda_L)    alfa
       400      0.24     0.001  0.057163   19.3671  3.788897 50.426718     1.062
$---+----1----+----2----+----3----+----4----+----5----+----6----+----7----+----8
$ beta        kappa    sigma_ss     H                             K          G
   1.56410      0.00  12.48980   2.19287                      258.60  160.9994
$---+----1----+----2----+----3----+----4----+----5----+----6----+----7----+----8
*END
```

C.1.2 ppFinalE700.k, E=700 MPa

```
$$$$$$$$$$$$$$$$$$$$$$$$$$$$$$$$$$$$$$$$$$$$$$$$$$$$$$$$$$$$$$$$$$$$$$$$$$$$$$$$
$                              MATERIAL MODEL DEFINITIONS                      $
$$$$$$$$$$$$$$$$$$$$$$$$$$$$$$$$$$$$$$$$$$$$$$$$$$$$$$$$$$$$$$$$$$$$$$$$$$$$$$$$
$
*MAT_USER_DEFINED_MATERIAL_MODELS
$      MID       rho    User mat #    LMC    # Hist var            IBULK      IG
         1 1.000E-04        49        16        50         0        15        16
$---+----1----+----2----+----3----+----4----+----5----+----6----+----7----+----8
$      IVECT      IFAIL     ITHERM   IHYPER     IEOS
         0         0         0         1         0
$---+----1----+----2----+----3----+----4----+----5----+----6----+----7----+----8
$ E         Poisson     eps0         C   sigma_T        Cr N (lamda_L)    alfa
       700      0.24     0.001  0.057163   19.3671  3.788897 50.426718     1.062
$---+----1----+----2----+----3----+----4----+----5----+----6----+----7----+----8
$ beta        kappa    sigma_ss     H                             K          G
   1.56410      0.00  12.48980   2.19287                      448.72  282.2580
```

```
$---+----1----+----2----+----3----+----4----+----5----+----6----+----7----+----8
*END
```

C.1.3 ppFinalE750.k, E=750 MPa

```
$$$$$$$$$$$$$$$$$$$$$$$$$$$$$$$$$$$$$$$$$$$$$$$$$$$$$$$$$$$$$$$$$$$$$$$$$$$$$$$
$                              MATERIAL MODEL DEFINITIONS                       $
$$$$$$$$$$$$$$$$$$$$$$$$$$$$$$$$$$$$$$$$$$$$$$$$$$$$$$$$$$$$$$$$$$$$$$$$$$$$$$$
$
*MAT_USER_DEFINED_MATERIAL_MODELS
$      MID      rho    User mat #    LMC    # Hist var            IBULK      IG
         1 1.000E-04        49        16        50         0        15        16
$---+----1----+----2----+----3----+----4----+----5----+----6----+----7----+----8
$      IVECT      IFAIL     ITHERM   IHYPER     IEOS
         0          0         0         1         0
$---+----1----+----2----+----3----+----4----+----5----+----6----+----7----+----8
$ E         Poisson     eps0         C   sigma_T        Cr N (lamda_L)    alfa
       750      0.24     0.001  0.057163   19.3671  3.788897 50.426718     1.062
$---+----1----+----2----+----3----+----4----+----5----+----6----+----7----+----8
$ beta        kappa    sigma_ss     H                              K          G
   1.56410      0.00  12.48980   2.19287                        480.77  302.4194
$---+----1----+----2----+----3----+----4----+----5----+----6----+----7----+----8
*END
```

C.1.4 ppFinalDTOPT.k, E=700 MPa and C=0.07

```
$$$$$$$$$$$$$$$$$$$$$$$$$$$$$$$$$$$$$$$$$$$$$$$$$$$$$$$$$$$$$$$$$$$$$$$$$$$$$$$
$                              MATERIAL MODEL DEFINITIONS                       $
$$$$$$$$$$$$$$$$$$$$$$$$$$$$$$$$$$$$$$$$$$$$$$$$$$$$$$$$$$$$$$$$$$$$$$$$$$$$$$$
$
*MAT_USER_DEFINED_MATERIAL_MODELS
$      MID      rho    User mat #    LMC    # Hist var            IBULK      IG
         1 1.000E-09        49        16        50         0        15        16
$---+----1----+----2----+----3----+----4----+----5----+----6----+----7----+----8
$      IVECT      IFAIL     ITHERM   IHYPER     IEOS
         0          0         0         1         0
$---+----1----+----2----+----3----+----4----+----5----+----6----+----7----+----8
$ E         Poisson     eps0         C   sigma_T        Cr N (lamda_L)    alfa
       700      0.24     0.001  0.070000   19.3671  3.788897 50.426718     1.062
$---+----1----+----2----+----3----+----4----+----5----+----6----+----7----+----8
$ beta        kappa    sigma_ss     H                              K          G
```

```
   1.56410      0.00  12.48980   2.19287                       448.7179 282.25806
$---+----1----+----2----+----3----+----4----+----5----+----6----+----7----+----8
*END
```

C.1.5 ppFinalDTOPT_075.k, E=700 MPa and C=0.070

```
$$$$$$$$$$$$$$$$$$$$$$$$$$$$$$$$$$$$$$$$$$$$$$$$$$$$$$$$$$$$$$$$$$$$$$$$$$$$$$$$
$                              MATERIAL MODEL DEFINITIONS                       $
$$$$$$$$$$$$$$$$$$$$$$$$$$$$$$$$$$$$$$$$$$$$$$$$$$$$$$$$$$$$$$$$$$$$$$$$$$$$$$$$
$
*MAT_USER_DEFINED_MATERIAL_MODELS
$      MID      rho    User mat #    LMC    # Hist var            IBULK      IG
         1 1.000E-09        49        16        50         0        15        16
$---+----1----+----2----+----3----+----4----+----5----+----6----+----7----+----8
$      IVECT      IFAIL     ITHERM    IHYPER     IEOS
         0          0          0          1          0
$---+----1----+----2----+----3----+----4----+----5----+----6----+----7----+----8
$ E         Poisson     eps0         C   sigma_T        Cr N (lamda_L)    alfa
       700      0.24     0.001  0.075000   19.3671  3.788897 50.426718     1.062
$---+----1----+----2----+----3----+----4----+----5----+----6----+----7----+----8
$ beta        kappa    sigma_ss     H                             K          G
   1.56410      0.00  12.48980   2.19287                       448.7179 282.25806
$---+----1----+----2----+----3----+----4----+----5----+----6----+----7----+----8
*END
```

C.1.6 ppFinalDTOPT_08.k, E=700 MPa and C=0.08

```
$$$$$$$$$$$$$$$$$$$$$$$$$$$$$$$$$$$$$$$$$$$$$$$$$$$$$$$$$$$$$$$$$$$$$$$$$$$$$$$$
$                              MATERIAL MODEL DEFINITIONS                       $
$$$$$$$$$$$$$$$$$$$$$$$$$$$$$$$$$$$$$$$$$$$$$$$$$$$$$$$$$$$$$$$$$$$$$$$$$$$$$$$$
$
*MAT_USER_DEFINED_MATERIAL_MODELS
$      MID      rho    User mat #    LMC    # Hist var            IBULK      IG
         1 1.000E-09        49        16        50         0        15        16
$---+----1----+----2----+----3----+----4----+----5----+----6----+----7----+----8
$      IVECT      IFAIL     ITHERM    IHYPER     IEOS
         0          0          0          1          0
$---+----1----+----2----+----3----+----4----+----5----+----6----+----7----+----8
$ E         Poisson     eps0         C   sigma_T        Cr N (lamda_L)    alfa
       700      0.24     0.001  0.080000   19.3671  3.788897 50.426718     1.062
$---+----1----+----2----+----3----+----4----+----5----+----6----+----7----+----8
```

```
$ beta         kappa     sigma_ss      H                              K           G
   1.56410       0.00   12.48980    2.19287                       448.7179 282.25806
$---+----1----+----2----+----3----+----4----+----5----+----6----+----7----+----8
*END
```

C.2 Finite element analyses of the calibration tests

C.2.1 Input file

```
$# LS-DYNA Keyword file created by LS-PrePost 3.2 - 16Jan2012(01:28)
$# Created on Mar-22-2012 (12:50:14)
*KEYWORD
*TITLE
$# title
LS-DYNA keyword deck by LS-PrePost
*INCLUDE
ppFinal.k
*INCLUDE
geomHalf.k
*CONTROL_ENERGY
         2         2         1         1
*CONTROL_TERMINATION
 200.00000         0     0.000     0.000     0.000
*CONTROL_TIMESTEP
     0.000  0.500000         0     0.000     0.000         0         0         0
     0.000         0         0
*DATABASE_BINARY_D3PLOT
   4.00000
*DATABASE_EXTENT_BINARY
        59         0         3         1         0         0         0         0
         0         0         4         0         0         0
$---+----1----+----2----+----3----+----4----+----5----+----6----+----7----+----8
*DATABASE_GLSTAT
  0.400000         0         0         0
*DATABASE_MATSUM
  0.400000         0         0         0
*DATABASE_NODOUT
  0.400000         0         0         0     0.000         0
*DATABASE_ELOUT
  0.400000         0         0         0     0.000         0
*DATABASE_SECFORC
  0.400000         0         0         0
*DATABASE_SPCFORC
  0.400000         0         0         0
*DATABASE_HISTORY_SOLID_SET
         1         0         0         0         0         0         0         0
```

```
*DATABASE_CROSS_SECTION_SET_ID
         1ReadSet
         3         1         0         0         0         0         0         0
*DATABASE_HISTORY_NODE_SET
         4         0         0         0         0         0         0         0
*BOUNDARY_PRESCRIBED_MOTION_SET_ID
         0Moving
         2         1         0         1  0.330000         01.0000E+28     0.000
*BOUNDARY_SPC_SET_BIRTH_DEATH
         1         0         1         1         1         0         0         0
     0.0001.0000E+20
*PART

         2         1         1         0         0         0         0         0
*SECTION_SOLID_TITLE
Section ONE
         1         2         0
*DEFINE_CURVE_SMOOTH_TITLE
Smooooooooooth
         1         0 500.00000     0.000     0.000 1.0000E-4  1.000000
*END
```

C.2.2 Excerpt from the geometry file geomHalf.k

```
$# LS-DYNA Keyword file created by LS-PrePost 3.2 - 16Jan2012(01:28)
$# Created on May-19-2012 (14:18:37)
*KEYWORD
*TITLE
$# title
LS-DYNA keyword deck by LS-PrePost
*BOUNDARY_SPC_SET_BIRTH_DEATH
         5         0         0         1         0         1         1         1
     0.0001.0000E+20
*SET_NODE_LIST_TITLE
Rigid
$#     sid       da1       da2       da3       da4    solver
         1     0.000     0.000     0.000     0.000MECH
$#    nid1      nid2      nid3      nid4      nid5      nid6      nid7      nid8
        44        45        46        47        48        49        51        52
        53        54        55        56        58        59        60        61
        62        63        65        66        67        68        69        70
        72        73        74        75        76        77        79        80
        81        82        83        84        86        87        88        89
        90        91      1036      1038      1040      1042      1043      1044
      1045      1046      1047      1048      1049      1050      1051      1052
      1053      1054      1055      1056      1057      1059      1061      1063
      1064      1065      1066      1067      1068      1069      1070      1071
      1072      1073      1074      1075      1076      1077      1078      1080
      1082      1084      1085      1086      1087      1088      1089      1090
      1091      1092      1093      1094      1095      1096      1097      1098
      1099      1101      1103      1105      1106      1107      1108      1109
      1110      1111      1112      1113      1114      1115      1116      1117
      1118      1119      1120      1122      1124      1126      1127      1128
      1129      1130      1131      1132      1133      1134      1135      1136
      1137      1138      1139      1140      1141      1143      1145      1147
      1148      1149      1150      1151      1152      1153      1154      1155
      1156      1157      1158      1159      1160      1161      1162      1164
      1166      1168      1169      1170      1171      1172      1173      1174
      1175      1176      1177      1178      1179      1180      1181      1182
*SET_NODE_LIST_TITLE
Move
$#     sid       da1       da2       da3       da4    solver
         2     0.000     0.000     0.000     0.000MECH
$#    nid1      nid2      nid3      nid4      nid5      nid6      nid7      nid8
       134       135       136       137       138       139       141       142
```

```
       143       144       145       146       148       149       150       151
       152       153       155       156       157       158       159       160
       162       163       164       165       166       167       169       170
       171       172       173       174       176       177       178       179
       180       181      1309      1310      1311      1312      1313      1314
      1315      1316      1317      1318      1319      1320      1321      1322
      1323      1324      1325      1326      1330      1331      1332      1333
      1334      1335      1336      1337      1338      1339      1340      1341
      1342      1343      1344      1345      1346      1347      1351      1352
      1353      1354      1355      1356      1357      1358      1359      1360
      1361      1362      1363      1364      1365      1366      1367      1368
      1372      1373      1374      1375      1376      1377      1378      1379
      1380      1381      1382      1383      1384      1385      1386      1387
      1388      1389      1393      1394      1395      1396      1397      1398
      1399      1400      1401      1402      1403      1404      1405      1406
      1407      1408      1409      1410      1414      1415      1416      1417
      1418      1419      1420      1421      1422      1423      1424      1425
      1426      1427      1428      1429      1430      1431      1435      1436
      1437      1438      1439      1440      1441      1442      1443      1444
      1445      1446      1447      1448      1449      1450      1451      1452
*SET_NODE_LIST_TITLE
RefNodes
$#     sid       da1       da2       da3       da4    solver
         3     0.000     0.000     0.000     0.000MECH
$#    nid1      nid2      nid3      nid4      nid5      nid6      nid7      nid8
       689       723       757       791       825       859       893      2857
      2858      2859      2953      2954      2955      3049      3050      3051
      3145      3146      3147      3241      3242      3243      3337      3338
      3339      3433      3434      3435         0         0         0         0
*SET_NODE_LIST_TITLE
Tracker
$#     sid       da1       da2       da3       da4    solver
         4     0.000     0.000     0.000     0.000MECH
$#    nid1      nid2      nid3      nid4      nid5      nid6      nid7      nid8
      1310         0         0         0         0         0         0         0
*SET_NODE_LIST_TITLE
SymNodes
$#     sid       da1       da2       da3       da4    solver
         5     0.000     0.000     0.000     0.000MECH
$#    nid1      nid2      nid3      nid4      nid5      nid6      nid7      nid8
        43        44        45        46        47        48        49       134
       135       136       137       138       139       140       250       251
       252       253       254       255       256       257       258       259
```

```
       392       393       394       395       396       397       398       399
       400       401       674       675       676       677       678       679
       680       681       682       683       684       685       686       687
       688       689       690       691       692       693       694       695
       696       697       698       699       700       701       702       703
       704       705      1036      1037      1038      1039      1040      1041
      1042      1043      1044      1045      1046      1047      1048      1049
      1050      1051      1052      1053      1054      1055      1056      1309
      1310      1311      1312      1313      1314      1315      1316      1317
      1318      1319      1320      1321      1322      1323      1324      1325
      1326      1327      1328      1329      1636      1637      1638      1639
      1640      1641      1642      1643      1644      1645      1646      1647
      1648      1649      1650      1651      1652      1653      1654      1655
      1656      1657      1658      1659      1660      1661      1662      1663
      1664      1665      2026      2027      2028      2029      2030      2031
      2032      2033      2034      2035      2036      2037      2038      2039
      2040      2041      2042      2043      2044      2045      2046      2047
      2048      2049      2050      2051      2052      2053      2054      2055
      2812      2813      2814      2815      2816      2817      2818      2819
      2820      2821      2822      2823      2824      2825      2826      2827
      2828      2829      2830      2831      2832      2833      2834      2835
      2836      2837      2838      2839      2840      2841      2842      2843
      2844      2845      2846      2847      2848      2849      2850      2851
      2852      2853      2854      2855      2856      2857      2858      2859
      2860      2861      2862      2863      2864      2865      2866      2867
      2868      2869      2870      2871      2872      2873      2874      2875
      2876      2877      2878      2879      2880      2881      2882      2883
      2884      2885      2886      2887      2888      2889      2890      2891
      2892      2893      2894      2895      2896      2897      2898      2899
      2900      2901      2902      2903      2904      2905      2906      2907
*SET_SOLID_TITLE
RefEl
$#     sid    solver
         1MECH
$#      k1        k2        k3        k4        k5        k6        k7        k8
      2575      2576      2577      2674      2675      2676      2773      2774
      2775      2872      2873      2874      2971      2972      2973      3070
      3071      3072         0         0         0         0         0         0
*ELEMENT_SOLID
$#   eid     pid      n1      n2      n3      n4      n5      n6      n7      n8
     889       2      43      44      51      50    1037    1036    1057    1058
     890       2    1037    1036    1057    1058    1039    1038    1059    1060
     891       2    1039    1038    1059    1060    1041    1040    1061    1062
```

892	2	44	45	52	51	1036	1042	1063	1057
.	.	.	.	.	.	.	.	.	.
.	.	.	.	.	.	.	.	.	.
.	.	.	.	.	.	.	.	.	.

C.3 Finite element analyses of the plate with a centric hole

C.3.1 Input file

```
$# LS-DYNA Keyword file created by LS-PrePost 3.2 - 16Jan2012(01:28)
$# Created on Mar-22-2012 (12:50:14)
*KEYWORD
*TITLE
$# title
LS-DYNA keyword deck by LS-PrePost
*INCLUDE
ppFinal.k
*INCLUDE
geomTFV2_4thick.k
*CONTROL_ENERGY
         2         2         1         1
*CONTROL_TERMINATION
 25.000000         0     0.000     0.000     0.000
*CONTROL_TIMESTEP
     0.000  0.500000         0     0.000     0.000         0         0         0
     0.000         0         0
*DATABASE_BINARY_D3PLOT
      0.25
*DATABASE_EXTENT_BINARY
        59         0         3         1         0         0         0         0
         0         0         4         0         0         0
$---+----1----+----2----+----3----+----4----+----5----+----6----+----7----+----8
*DATABASE_GLSTAT
  0.050000         0         0         0
*DATABASE_MATSUM
  0.050000         0         0         0
*DATABASE_NODOUT
  0.050000         0         0         0     0.000         0
*DATABASE_ELOUT
  0.050000         0         0         0     0.000         0
*DATABASE_SECFORC
  0.050000         0         0         0
*DATABASE_SPCFORC
  0.050000         0         0         0
*DATABASE_CROSS_SECTION_SET_ID
         1ReadSet
```

```
         4         1         0         0         0         0         0         0
*DATABASE_HISTORY_NODE_SET
         6         0         0         0         0         0         0         0
*DATABASE_HISTORY_NODE_SET
         5         0         0         0         0         0         0         0
*DATABASE_HISTORY_SOLID_SET
         1         0         0         0         0         0         0         0
*BOUNDARY_PRESCRIBED_MOTION_SET_ID
         0Moving
         1         1         0         1 -0.239000         01.0000E+28     0.000
*BOUNDARY_SPC_SET_BIRTH_DEATH
         2         0         1         0         1         1         1         1
     0.0001.0000E+20
*BOUNDARY_SPC_SET_BIRTH_DEATH
         3         0         1         0         0         1         1         1
     0.0001.0000E+20
*PART

         2         1         1         0         0         0         0         0
*SECTION_SOLID_TITLE
Section ONE
         1         2         0
*DEFINE_CURVE_SMOOTH_TITLE
Smooooooooooth
         1         0 500.00000     0.000     0.000 1.0000E-4  1.000000
*END
```

C.3.2 Excerpt from the geometry file geomTFV2_4thick.k

```
$# LS-DYNA Keyword file created by LS-PrePost 3.2 - 16Jan2012(01:28)
$# Created on May-24-2012 (16:30:36)
*KEYWORD
*SET_NODE_LIST_TITLE
Move
$#     sid       da1       da2       da3       da4    solver
         1     0.000     0.000     0.000     0.000MECH
$#    nid1      nid2      nid3      nid4      nid5      nid6      nid7      nid8
         1         2         4         7        11        16        22        29
        37        46        56        67        78        89       100       111
       122       133       144       155       166       177       188       199
       210       569       572       573       576       577       580       581
       584       610       612       614       616       650       652       654
```

```
       656       686       688       690       692       726       728       730
       732       774       776       778       780       862       864       866
       868       938       940       942       944      1018      1020      1022
      1024      1102      1104      1106      1108      1194      1196      1198
      1200      1290      1292      1294      1296      1386      1388      1390
      1392      1474      1476      1478      1480      1558      1560      1562
      1564      1634      1636      1638      1640      1718      1720      1722
      1724      1790      1792      1794      1796      1882      1884      1886
      1888      1982      1984      1986      1988      2070      2072      2074
      2076      2158      2160      2162      2164      2242      2244      2246
      2248      2330      2332      2334      2336         0         0         0
*SET_NODE_LIST_TITLE
SymZ
$#     sid       da1       da2       da3       da4    solver
         2     0.000     0.000     0.000     0.000MECH
$#    nid1      nid2      nid3      nid4      nid5      nid6      nid7      nid8
      1375      1376      1394      1470      1486      1554      1626      1667
      1668      1678      1710      1738      1750      2087      2088      2166
      2238      2326      2422      2471      2472      2498      2530      2554
      2570      2578         0         0         0         0         0         0
*SET_NODE_LIST_TITLE
SymY
$#     sid       da1       da2       da3       da4    solver
         3     0.000     0.000     0.000     0.000MECH
$#    nid1      nid2      nid3      nid4      nid5      nid6      nid7      nid8
      1377      1378      1379      1380      1395      1396      1471      1472
      1487      1488      1555      1556      1627      1628      1669      1670
      1671      1672      1679      1680      1711      1712      1739      1740
      1751      1752      2089      2090      2091      2092      2167      2168
      2239      2240      2327      2328      2423      2424      2473      2474
      2475      2476      2499      2500      2531      2532      2555      2556
      2571      2572      2579      2580       359       369       371       380
       381       389       395       396       400       401       404       406
       407       456       467       478       490       505       518       519
       524       529       531       535       538       540      1373      1374
      1393      1469      1485      1553      1625      1665      1666      1677
      1709      1737      1749      2085      2086      2165      2237      2325
      2421      2469      2470      2497      2529      2553      2569      2577
*SET_NODE_LIST_TITLE
RefNodes
$#     sid       da1       da2       da3       da4    solver
         4     0.000     0.000     0.000     0.000MECH
$#    nid1      nid2      nid3      nid4      nid5      nid6      nid7      nid8
```

```
       359       369       371       380       381       389       395       396
       400       401       404       406       407       456       467       478
       490       505       518       519       524       529       531       535
       538       540      1373      1374      1375      1376      1377      1378
      1379      1380      1393      1394      1395      1396      1469      1470
      1471      1472      1485      1486      1487      1488      1553      1554
      1555      1556      1625      1626      1627      1628      1665      1666
      1667      1668      1669      1670      1671      1672      1677      1678
      1679      1680      1709      1710      1711      1712      1737      1738
      1739      1740      1749      1750      1751      1752      2085      2086
      2087      2088      2089      2090      2091      2092      2165      2166
      2167      2168      2237      2238      2239      2240      2325      2326
      2327      2328      2421      2422      2423      2424      2469      2470
      2471      2472      2473      2474      2475      2476      2497      2498
      2499      2500      2529      2530      2531      2532      2553      2554
      2555      2556      2569      2570      2571      2572      2577      2578
      2579      2580         0         0         0         0         0         0
*SET_NODE_LIST_TITLE
BotCirc
$#     sid       da1       da2       da3       da4    solver
         5     0.000     0.000     0.000     0.000MECH
$#    nid1      nid2      nid3      nid4      nid5      nid6      nid7      nid8
       871         0         0         0         0         0         0         0
*SET_NODE_LIST_TITLE
Tracker
$#     sid       da1       da2       da3       da4    solver
         6     0.000     0.000     0.000     0.000MECH
$#    nid1      nid2      nid3      nid4      nid5      nid6      nid7      nid8
      1400         0         0         0         0         0         0         0
*SET_SOLID_TITLE
RefEl
$#     sid    solver
         1MECH
$#      k1        k2        k3        k4        k5        k6        k7        k8
      1082      1083      1084      1085      1094      1095      1096      1097
      1170      1171      1172      1173      1182      1183      1184      1185
      1250      1251      1252      1253      1318      1319      1320      1321
      1354      1355      1356      1357      1362      1363      1364      1365
      1366      1367      1368      1369      1398      1399      1400      1401
      1422      1423      1424      1425      1434      1435      1436      1437
      1726      1727      1728      1729      1802      1803      1804      1805
      1874      1875      1876      1877      1966      1967      1968      1969
      2066      2067      2068      2069      2118      2119      2120      2121
```

```
      2142      2143      2144      2145      2146      2147      2148      2149
      2178      2179      2180      2181      2226      2227      2228      2229
      2254      2255      2256      2257      2274      2275      2276      2277
*ELEMENT_SOLID
$#    eid     pid      n1      n2      n3      n4      n5      n6      n7      n8
     458       2     250     257     262     256     541     542     543     544
     459       2     541     542     543     544     545     546     547     548
     460       2     545     546     547     548     549     550     551     552
     461       2     549     550     551     552     553     554     555     556
     462       2     251     258     263     257     557     558     559     542
     463       2     557     558     559     542     560     561     562     546
       .       .       .       .       .       .       .       .       .       .
```

C.4 Drop tower

C.4.1 Input file

```
$# Created on Apr-24-2012 (16:50:16)
*KEYWORD
*TITLE
Droptower. High steel spear, instead of rigid material.
*INCLUDE
geommdt.k
*INCLUDE
ppFinalDTOPT.k
*CONTROL_TERMINATION
$#  endtim    endcyc     dtmin    endeng    endmas
  0.014400         0     0.000     0.000     0.000
*CONTROL_TIMESTEP
$#  dtinit    tssfac      isdo    tslimt     dt2ms      lctm     erode     ms1st
     0.000  0.500000         0     0.000     0.000         0         0         0
$#  dt2msf   dt2mslc     imscl
     0.000         0         0
*CONTROL_SHELL
 0.0000000         0         0         0         0         0         0
*CONTROL_DAMPING
         0 0.0000000 0.0000000 0.0000000 0.0000000         0 0.0000000         0
*CONTROL_CONTACT
 0.0000000 0.0000000         0         0         0         0         0
         0         0         0         0 0.0000000         0         0         0
*CONTROL_OUTPUT
         0         0         0         0 0.0000000         0         0
*CONTROL_ENERGY
         2         2         2         1
*CONTROL_CPU
 0.0000000
*DATABASE_ELOUT
$#      dt    binary      lcur     ioopt
 0.1800E-4         0         0         1
*DATABASE_GLSTAT
$#      dt    binary      lcur     ioopt
 0.1800E-4         0         0         1
*DATABASE_MATSUM
$#      dt    binary      lcur     ioopt
 0.1800E-4         0         0         1
```

```
*DATABASE_NODOUT
$#      dt    binary      lcur     ioopt      dthf     binhf
 0.1800E-4         0         0         1     0.000         0
*DATABASE_SPCFORC
$#      dt    binary      lcur     ioopt
 0.1800E-4         0         0         1
*DATABASE_SECFORC
 0.1800e-4
*DATABASE_BINARY_D3PLOT
$#      dt      lcdt      beam     npltc    psetid
 2.0000E-4         0         0         0         0
$#   ioopt
         0
*DATABASE_EXTENT_BINARY
$#   neiph     neips    maxint    strflg    sigflg    epsflg    rltflg    engflg
        59         0         3         1         1         1         1         1
$#  cmpflg    ieverp    beamip     dcomp      shge     stssz    n3thdt   ialemat
         0         0         4         1         1         1         2         0
$---+----1----+----2----+----3----+----4----+----5----+----6----+----7----+----8
$# nintsld   pkp_sen      sclp    unused     msscl     therm    intout    nodout
         0         0  1.000000         0         0         0STRESS    STRESS
*DATABASE_HISTORY_NODE_SET
         3
$ Section definitions - start
*DATABASE_HISTORY_SHELL_SET
         1
*DATABASE_CROSS_SECTION_SET_ID
         1 InnerCSedge
         2         0         0         1
*DATABASE_HISTORY_SHELL_SET
         2
*DATABASE_CROSS_SECTION_SET_ID
         2 SpearEdge
         5         0         0         2
*DATABASE_HISTORY_SHELL_SET
         3
*DATABASE_CROSS_SECTION_SET_ID
         3 TransCircToSpear
         7         0         0         3
*DATABASE_HISTORY_SHELL_SET
         4
*DATABASE_CROSS_SECTION_SET_ID
         4 SecInnerCSedge
```

```
         6         0         0         4
*DATABASE_HISTORY_SHELL_SET
         5
*DATABASE_CROSS_SECTION_SET_ID
         5 SpearSec
         8         0         0         5
$ Section definitions - end
*BOUNDARY_SPC_SET_BIRTH_DEATH
$#    nsid       cid      dofx      dofy      dofz     dofrx     dofry     dofrz
         1         0         1         1         0         1         1         1
$#   birth     death
     0.0001.0000E+20
*CONTACT_2D_AUTOMATIC_SINGLE_SURFACE
         0         0 1.5000000         1 0.2500000 0.2250000 0.0000000         0
 0.0000000 1.0000e20 1.0000000 1.0000000         0         0         0         0
*PART
$# title

$#     pid     secid       mid     eosid      hgid      grav    adpopt      tmid
         4         2         2         0         0         0         0         0
*PART
$# title

$#     pid     secid       mid     eosid      hgid      grav    adpopt      tmid
         3         1         1         0         0         0         0         0
*PART
$# title

$#     pid     secid       mid     eosid      hgid      grav    adpopt      tmid
         5         2         3         0         0         0         0         0
*SECTION_SHELL_TITLE
Section
$#   secid    elform      shrf       nip     propt   qr/irid     icomp     setyp
         1        15  1.000000         2         1         0         0         1
$#      t1        t2        t3        t4      nloc     marea      idof    edgset
  0.000000  0.000000  0.000000  0.000000     0.000     0.000     0.000         0
*SECTION_SHELL_TITLE
Section
$#   secid    elform      shrf       nip     propt   qr/irid     icomp     setyp
         2        15  1.000000         2         1         0         0         1
$#      t1        t2        t3        t4      nloc     marea      idof    edgset
  0.000000  0.000000  0.000000  0.000000     0.000     0.000     0.000         0
*HOURGLASS
```

```
         1         1
*HOURGLASS
         2         2
*MAT_ELASTIC
         27.85000E-9    210000      0.30         0         0
*MAT_ELASTIC
         31.06448e-6    210000      0.30         0         0
*INITIAL_VELOCITY
$#    nsid    nsidex     boxid    irigid      icid
         4         0         0         0         0
$#      vx        vy        vz       vxr       vyr       vzr
     0.000-4430.0000     0.000     0.000     0.000     0.000
*DEFINE_CURVE_SMOOTH_TITLE
Smooooooooth
$#    lcid      sidr      dist    tstart      tend     trise        v0
         1         0 5.0000E+6     0.000     0.000 1.0000E-6  1.000000
*END
```

C.4.2 Excerpt from the geometry file geommdt.k

```
$# LS-DYNA Keyword file created by LS-PrePost 3.2 - 16Jan2012(01:28)
$# Created on May-01-2012 (09:35:56)
*KEYWORD
*TITLE
$# title
Geometry: Droptower modelled as steel tip with extra weight.
*SET_NODE_LIST_TITLE
Rigid
$#     sid       da1       da2       da3       da4    solver
         1     0.000     0.000     0.000     0.000MECH
$#    nid1      nid2      nid3      nid4      nid5      nid6      nid7      nid8
     17093     17094     17095     17096     17097     17098     17099     17100
     17101     17102     17103     17104     17105     17106     17107         0
*SET_NODE_LIST_TITLE
InnerCSedge
$#     sid       da1       da2       da3       da4    solver
         2     0.000     0.000     0.000     0.000MECH
$#    nid1      nid2      nid3      nid4      nid5      nid6      nid7      nid8
     19151     19150     19149     19148     19147     19146     19145     19144
     19143     18986     18978     18970     18962     18954     18946     18938
     18930     18922     18897         0         0         0         0         0
*SET_NODE_LIST_TITLE
SpearTIP
$#     sid       da1       da2       da3       da4    solver
         3     0.000     0.000     0.000     0.000MECH
$#    nid1      nid2      nid3      nid4      nid5      nid6      nid7      nid8
     19171         0         0         0         0         0         0         0
*SET_NODE_LIST_TITLE
Spear
$#     sid       da1       da2       da3       da4    solver
         4     0.000     0.000     0.000     0.000MECH
$#    nid1      nid2      nid3      nid4      nid5      nid6      nid7      nid8
     18827     18828     18829     18830     18831     18832     18833     18834
     18835     18836     18837     18838     18839     18840     18841     18842
     18843     18844     18845     18846     18847     18848     18849     18850
     18851     18852     18853     18854     18855     18856     18857     18858
     18859     18860     18861     18862     18863     18864     18865     18866
     18867     18868     18869     18870     18871     18872     18873     18874
     18875     18876     18877     18878     18879     18880     18881     18882
     18883     18884     18885     18886     18887     18888     18889     18890
     18891     18892     18893     18894     18895     18896     18897     18898
```

18899	18900	18901	18902	18903	18904	18905	18906
18907	18908	18909	18910	18911	18920	18921	18922
18923	18924	18925	18926	18927	18928	18929	18930
18931	18932	18933	18934	18935	18936	18937	18938
18939	18940	18941	18942	18943	18944	18945	18946
18947	18948	18949	18950	18951	18952	18953	18954
18955	18956	18957	18958	18959	18960	18961	18962
18963	18964	18965	18966	18967	18968	18969	18970
18971	18972	18973	18974	18975	18976	18977	18978
18979	18980	18981	18982	18983	18984	18985	18986
18987	18988	18989	18990	18991	19003	19004	19005
19006	19007	19008	19009	19010	19011	19013	19014
19015	19016	19017	19018	19019	19020	19021	19023
19024	19025	19026	19027	19028	19029	19030	19031
19033	19034	19035	19036	19037	19038	19039	19040
19041	19043	19044	19045	19046	19047	19048	19049
19050	19051	19053	19054	19055	19056	19057	19058
19059	19060	19061	19063	19064	19065	19066	19067
19068	19069	19070	19071	19073	19074	19075	19076
19077	19078	19079	19080	19081	19083	19084	19085
19086	19087	19088	19089	19090	19091	19103	19104
19105	19106	19107	19108	19109	19110	19111	19113
19114	19115	19116	19117	19118	19119	19120	19121
19123	19124	19125	19126	19127	19128	19129	19130
19131	19133	19134	19135	19136	19137	19138	19139
19140	19141	19143	19144	19145	19146	19147	19148
19149	19150	19151	19153	19154	19155	19156	19157
19158	19159	19160	19161	19163	19164	19165	19166
19167	19168	19169	19170	19171	19172	19173	19174
19175	19176	19177	19178	19179	19180	19181	19182
19183	19184	19185	19186	19187	19188	19189	19190
19191	19192	19193	19194	19195	19196	19197	19198
19199	19200	19201	19202	19203	19204	19205	19206
19207	19208	19209	19210	19211	19212	19213	19214
19215	19216	19217	19218	19219	19220	19221	19222
19223	19224	19225	19226	19227	19228	19229	19230
19231	19232	19233	19234	19235	19236	19237	19238
19239	19240	19241	19242	19243	19244	19245	19246
19247	19248	19249	19250	19251	19252	19253	19254
19255	19256	19257	19258	19259	19260	19261	19262
19263	19264	19265	19266	19267	19268	19269	19270
19271	19272	19273	19274	19275	19276	19277	19278
19279	19280	19281	19282	19283	19284	19285	19286

```
     19287     19288     19289     19290     19291     19292     19293     19294
     19295     19296     19297     19298     19299     19300     19301     19302
     19303     19304     19305     19306     19307     19308     19309     19310
     19311     19312     19313     19314     19315     19316     19317     19318
     19319     19320     19321     19322     19323     19324     19325     19326
     19327     19328     19329     19330     19331     19332     19333     19334
     19335     19336     19337     19338     19339     19340     19341     19342
     19343     19344     19345     19346     19347     19348     19349     19350
     19351     19352     19353     19354     19355     19356     19357     19358
     19359     19360     19361     19362     19363     19364     19365     19366
     19367     19368     19369     19370     19371     19372     19373     19374
     19375         0         0         0         0         0         0         0
*SET_NODE_LIST_TITLE
SpearEdge
$#     sid       da1       da2       da3       da4    solver
         5     0.000     0.000     0.000     0.000MECH
$#    nid1      nid2      nid3      nid4      nid5      nid6      nid7      nid8
     19170     19171     19169     19168     19167     19166     19165     19164
     19163     18984     18976     18968     18960     18952     18944     18936
     18928     18920     18895         0         0         0         0         0
*SET_NODE_LIST_TITLE
secondInnerCSedge
$#     sid       da1       da2       da3       da4    solver
         6     0.000     0.000     0.000     0.000MECH
$#    nid1      nid2      nid3      nid4      nid5      nid6      nid7      nid8
     19161     19160     19159     19158     19157     19156     19155     19154
     19153     18985     18977     18969     18961     18953     18945     18937
     18929     18921     18896         0         0         0         0         0
*SET_NODE_LIST_TITLE
TopCircleSection
$#     sid       da1       da2       da3       da4    solver
         7     0.000     0.000     0.000     0.000MECH
$#    nid1      nid2      nid3      nid4      nid5      nid6      nid7      nid8
     18923     18924     18925     18926     18927     19003     19004     19005
     19006     19007     19008     19009     19010     19011         0         0
*SET_NODE_LIST_TITLE
CSspear
$#     sid       da1       da2       da3       da4    solver
         8     0.000     0.000     0.000     0.000MECH
$#    nid1      nid2      nid3      nid4      nid5      nid6      nid7      nid8
     18844     18845     18846     18847     18848     18849     18850     18851
     18852     18853     18854     18855     18856     18857     18858     18859
     18860         0         0         0         0         0         0         0
```

```
*SET_PART_LIST_TITLE
Plate
$#     sid       da1       da2       da3       da4    solver
         1     0.000     0.000     0.000     0.000MECH
$#    pid1      pid2      pid3      pid4      pid5      pid6      pid7      pid8
         3         0         0         0         0         0         0         0
*SET_PART_LIST_TITLE
Spear
$#     sid       da1       da2       da3       da4    solver
         2     0.000     0.000     0.000     0.000MECH
$#    pid1      pid2      pid3      pid4      pid5      pid6      pid7      pid8
         4         5         0         0         0         0         0         0
*SET_SHELL_LIST_TITLE
RefEl
$#     sid       da1       da2       da3       da4
         1     0.000     0.000     0.000     0.000
$#    eid1      eid2      eid3      eid4      eid5      eid6      eid7      eid8
      8124      8123      8122      8121      8120      8119      8118      8117
      8116      7994      7987      7973      7980      7966      7952      7959
      7945      7938         0         0         0         0         0         0
*SET_SHELL_LIST_TITLE
SpearEdge
$#     sid       da1       da2       da3       da4
         2     0.000     0.000     0.000     0.000
$#    eid1      eid2      eid3      eid4      eid5      eid6      eid7      eid8
      8142      8141      8140      8139      8138      8137      8136      8135
      7992      8134      7985      7978      7971      7957      7964      7950
      7943      7936         0         0         0         0         0         0
*SET_SHELL_LIST_TITLE
SpearLowEL
$#     sid       da1       da2       da3       da4
         3     0.000     0.000     0.000     0.000
$#    eid1      eid2      eid3      eid4      eid5      eid6      eid7      eid8
      7939      7940      7941      7942      7999      8000      8001      8002
      8003      8004      8005      8006      8007         0         0         0
*SET_SHELL_LIST_TITLE
VerEl
$#     sid       da1       da2       da3       da4
         4     0.000     0.000     0.000     0.000
$#    eid1      eid2      eid3      eid4      eid5      eid6      eid7      eid8
      8133      8131      8132      8130      8129      8128      8127      8126
      8125      7993      7986      7979      7972      7965      7958      7951
      7944      7937         0         0         0         0         0         0
```

```
*SET_SHELL_LIST_TITLE
ElSpear
$#     sid       da1       da2       da3       da4
         5     0.000     0.000     0.000     0.000
$#    eid1      eid2      eid3      eid4      eid5      eid6      eid7      eid8
      7872      7873      7874      7875      7876      7877      7878      7879
      7880      7881      7882      7883      7884      7885      7886      7887
*ELEMENT_SHELL
$#   eid     pid      n1      n2      n3      n4      n5      n6      n7      n8
    6280       3   17108   17109   17210   17209       0       0       0       0
       .       .       .       .       .       .       .       .       .       .
       .       .       .       .       .       .       .       .       .       .
```